

# PROJECT ALLEGRO

## A STUDY OF ADAPTIVE MULTIMODE SYSTEMS (U)

by: John R. Cummings

April 1968

Distribution of this report is provided in the interest of information exchange and should not be construed as endorsement by NASA of the material presented. Responsibility for the contents resides with the organization that prepared it.

GPO PRICE	\$	_____
CSFTI PRICE(S)	\$	_____
Hard copy (HC)		3.00
Microfiche (MF)		.65

ff 653 July 65

N 68-29547  
 (ACCESSION NUMBER)  
 1/16  
 (PAGES)  
 CR-86065  
 (NASA CR OR TMX OR AD NUMBER)

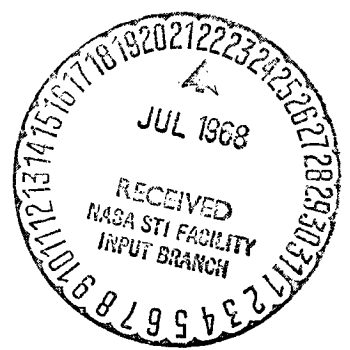
1  
 (THRU)  
 30  
 (CODE)  
 (CATEGORY)

FACILITY FORM 602

### Final Technical Report

Prepared under Contract No. NAS12-530 by  
**CORNELL AERONAUTICAL LABORATORY, INC.**  
 Buffalo, New York 14221

ELECTRONICS RESEARCH CENTER  
 NATIONAL AERONAUTICS AND SPACE ADMINISTRATION



**DR. JOHN D. OBERHOLTZER  
TECHNICAL MONITOR  
NAS 12-530  
ELECTRONICS RESEARCH CENTER  
575 TECHNOLOGY SQUARE  
CAMBRIDGE, MASSACHUSETTS 02139**

**REQUESTS FOR COPIES OF THIS REPORT SHOULD BE REFERRED TO:  
NASA SCIENTIFIC AND TECHNICAL INFORMATION FACILITY  
P.O. BOX 33, COLLEGE PARK, MARYLAND 20740**

**A STUDY OF ADAPTIVE  
MULTIMODE SYSTEMS (U)**

**By:**

**JOHN R. CUMMINGS**

**April 1968**

**FINAL TECHNICAL REPORT**

**PREPARED UNDER CONTRACT NO. NAS12-530 BY  
CORNELL AERONAUTICAL LABORATORY, INC.  
BUFFALO, NEW YORK 14221**

**ELECTRONICS RESEARCH CENTER  
NATIONAL AERONAUTICS AND SPACE ADMINISTRATION**

PRECEDING PAGE BLANK NOT FILMED.

CONTENTS

	<u>Page</u>
SUMMARY . . . . .	1
INTRODUCTION . . . . .	2
Objectives of the Study . . . . .	2
Scope of the Study . . . . .	2
Approach . . . . .	3
Summary of Results . . . . .	4
Acknowledgment . . . . .	4
DESIGN OF NEUTRON EXCITATION EXPERIMENT . . . . .	5
Objectives of Experiment . . . . .	5
Design Ground Rules . . . . .	5
Element Identification Procedures . . . . .	7
Radiative Capture of Thermal Neutrons . . . . .	11
Thermal Neutron Activation Experiment . . . . .	30
Fast Neutron Prompt Gamma Experiment . . . . .	39
Fast Neutron Activation Experiment . . . . .	43
Miscellaneous Considerations . . . . .	50
Calibration of the Neutron Excitation Experiment . . . . .	53
Instrumentation Requirements . . . . .	56
Summary of Identification Modes . . . . .	60
ADAPTIVE MULTIMODE CONTROLLER . . . . .	62
Control Philosophy of Demonstration Model . . . . .	62
Adaptive Features . . . . .	64
Operating Modes, Procedures and Flow Diagrams . . . . .	66
SUMMARY OF SPACE RESEARCH AREAS SURVEY. . . . .	93
Planetary Experiments . . . . .	93
Solar Flare Experiments . . . . .	98
Interplanetary Experiment . . . . .	102
Rank-Scoring of Experiments . . . . .	105
Suitability of Neutron Excitation for AMS . . . . .	107
RESULTS AND RECOMMENDATIONS . . . . .	108
Results . . . . .	108
Recommendations . . . . .	108
REFERENCES . . . . .	110

## ILLUSTRATIONS

<u>Figure</u>		<u>Page</u>
1	General Experiment Configuration . . . . .	6
2	Neutron Excitation Experiment Block Diagram . . . . .	8
3	Timing Diagram for Fast Neutron Mode . . . . .	9
4	Timing Diagram for Thermal Neutron Mode . . . . .	10
5	Low Energy Capture Gamma Ray Spectrum of Fe . . . . .	12
6	Low Energy Capture Gamma Ray Spectrum of Al . . . . .	13
7	Low Energy Capture Gamma Ray Spectrum of Si . . . . .	14
8	Low Energy Capture Gamma Ray Spectrum of Mg . . . . .	15
9	Composite Low Energy Capture Gamma Spectrum . . . . .	16
10	Composite Low Energy Capture Gamma Ray Spectrum . . . . .	17
11	Composite Low Energy Capture Gamma Ray Spectrum . . . . .	18
12	High Energy Capture Gamma Ray Spectrum of Fe . . . . .	21
13	High Energy Capture Gamma Ray Spectrum of Al . . . . .	22
14	High Energy Capture Gamma Ray Spectrum of Si . . . . .	23
15	High Energy Capture Gamma Ray Spectrum of Mg . . . . .	24
16	Composite High Energy Capture Gamma Ray Spectrum . . . . .	25
17	Composite High Energy Capture Gamma Ray Spectrum . . . . .	26
18	Composite High Energy Capture Gamma Ray Spectrum . . . . .	27
19	Composite Photopeak Gamma Spectrum for Thermal Activation of Sample Matrix Taken 5 Minutes After Irradiation, Spectrum Recorded for 1 Minute . . . . .	33
20	Composite Photopeak Gamma Spectrum from Thermal Activation of Sample Matrix Taken 15 Minutes After Irradiation, Spectrum Recorded for 2 Minutes . . . . .	34
21	Composite Photopeak Gamma Spectrum from Thermal Activation of Sample Matrix Taken 30 Minutes After Irradiation, Spectrum Recorded for 5 Minutes . . . . .	35
22	Calibration Curve Energy (MeV) vs Channel Number . . . . .	36
23	Calibration Spectrum for Thermal Neutron Activation . . . . .	37
24	Prompt Gamma Spectrum of Fe . . . . .	41
25	Prompt Gamma Spectrum of Si . . . . .	41
26	Prompt Gamma Spectrum of Mg . . . . .	42
27	Prompt Gamma Spectrum of Al . . . . .	42
28	Prompt Gamma Spectrum of 0 . . . . .	43
29	Half Life Determination for Mn <sup>56</sup> Used to Detect Presence of Fe <sup>56</sup> Activity of .834 MeV Photopeak . . . . .	49
30	Energy Resolution for 3"x3" Na(Tl) Scintillation Detectors . . . . .	52
31	Total Absolute Efficiency . . . . .	55
32	Functional Flowgram of Neutron Excitation Experiment . . . . .	63
33	Functional Flowgram of Pre-Calibration Mode *See Fig. 34 for Flowgram of Calibration with Known Source . . . . .	67
34	Functional Flowgram: Calibration with Known Sample . . . . .	68
35	Spectral Peaks Detected by Peak-Picking Algorithm . . . . .	69
36	Spectral Peaks Detected by Peak-Picking Algorithm . . . . .	70
37	Functional Flowgram of Test for Presence of Hydrogenous Material . . . . .	72

**ILLUSTRATIONS (Cont.)**

<u>Figure</u>		<u>Page</u>
38	Timing for the Measurement of the Capture Spectrum in the Thermal Mode . . . . .	73
39	Timing for the Measurement of the Prompt Spectrum in the Fast Mose . . . . .	74
40	Composite Low Energy Gamma Ray Spectrum Element Mass . . . . .	79
41	Stripped Low Energy Spectrum Iron Completely Removed (1gm) . . . . .	80
42	Stripped Low Energy Spectrum Iron Partially Removed . . . . .	81
43	Composite High Energy Gamma Ray Spectrum Element Mass . . . . .	82
44	Stripped High Energy Spectrum Excess Iron Removed . . . . .	83
45	Stripped High Energy Spectrum Iron Partially Removed . . . . .	84
46	Functional Flowgram of Fast-Prompt Procedure . . . . .	86
47	Functional Flowgram for Thermal-Activation Procedure . . . . .	87
48	Functional Flowgram for Fast-Activation Procedure . . . . .	88
49	Functional Flowgram for Thermal-Capture Procedure . . . . .	89
50	Trapped-Radiation Detector Functional Schematic-Adaptive Control Signals Indicated . . . . .	94
51	Schematic Arrangement for XRFA . . . . .	95
52a	Monoaxial Flux-Gate Magnetometer System Used on IMP-1 . . . . .	97
52b	Rubidium-Vapor Magnetometer Used on IMP-1 . . . . .	97
53	Solar Proton Monitoring Experiment . . . . .	99
54	Cosmic-Ray Experiment . . . . .	99
55	A Block Diagram of the UV Spectrometer . . . . .	101
56	The OGO-1 Micrometeoroid Sensor Which Determines Particle Mass and Velocity . . . . .	103

## TABLES

Table		Page
I	Experiment Scoring . . . . .	4
II	Summary of Low Energy Capture Gamma Ray Energies for Thermal Neutron Capture . . . . .	20
III	Summary of High Energy Capture Gamma Ray Energies for Thermal Neutron Capture . . . . .	28
IV	Thermal Activation Summary . . . . .	38
V	Computed Activities for Separate Irradiations . . . . .	46
VI	Summary of Reactions and Detector Schemes for Al <sup>27</sup> , Si <sup>28</sup> , Mg <sup>25</sup> , Fe <sup>56</sup> , and O <sup>16</sup> . . . . .	47
VII	Summary of Times to Record Spectrum . . . . .	50
VIII	Summary of Identification Modes . . . . .	61
IX	Example of an Identification Matrix . . . . .	75
X	Description of PDP-8/8 Computer . . . . .	91
XI	Description of SCC-655 Computer . . . . .	92
XII	Scientific Micrometeoroid Sensors . . . . .	104
XIII	Rank Scoring of Experiments . . . . .	106

# RESEARCH AND DESIGN STUDY FOR ADAPTIVE MULTIMODE SYSTEMS (U)

By John R. Cummings

Cornell Aeronautical Laboratory, Inc.  
Buffalo, New York 14221

## SUMMARY

This final report summarizes the work accomplished from March, 1967, to April, 1968. The objective of this program was to design a laboratory demonstration model of an experiment which demonstrates the feasibility of applying the concept of adaptive multimode systems to scientific spacecraft instrumentation. The study included a survey of experiments suitable for the demonstration model and the design of an adaptive multimode neutron excitation experiment.

A survey of spacecraft experiments for application of adaptive multimode systems research was carried out. Twelve scientific experiments drawn from planetary, solar, and interplanetary missions were considered and analyzed in terms of scientific interest, suitability for adaptive control, and feasibility of a laboratory demonstration model. In particular, analysis of each experiment included a description of the experiment; discussion of instrumentation including detectors and functional and physical characteristics; identification of operating modes and adaptable features pertaining to sensors and data compression; and an evaluation of the feasibility of a laboratory model. The experiments were rank-ordered according to suitability for adaptation and laboratory model feasibility and candidates were recommended for the laboratory demonstration model.

A laboratory demonstration model of an adaptive multimode neutron excitation experiment was designed. This experiment is designed to identify and weigh the elements silicon, magnesium, aluminum, iron and oxygen in a sample containing any one or all of these elements. Identification is achieved by analysis of the gamma ray spectra produced by irradiation of a sample with fast and thermal neutrons. Element mass is estimated as an absolute or relative abundance. The experiment operates autonomously and adaptively copes with high background radiation, hydrogenous materials dominating elemental responses and small temperature variations. The analytical basis for the identification and weighing procedures was established and recommendations for instrumentation hardware made. Also procedures and functional flow diagrams for the adaptive multimode controller were developed.



## **INTRODUCTION**

This report summarizes the results of a one year study performed by Cornell Aeronautical Laboratory, Inc. (CAL) for the NASA Electronics Research Center under Contract NAS 12-530. The study was performed to investigate application of adaptive multimode systems to spacecraft instrumentation.

### **Objectives of the Study**

The long term objective of this study was application of adaptive multimode systems research to future scientific spacecraft instrumentation. The specific objective of the present contract is design of a laboratory model of an experiment instrumentation which incorporates adaptive multimode features. In this context an adaptive system is one which performs sufficient data analysis to adapt sensors to conditions of sensitivity, response, sensor combination, etc. to achieve optimum mission performance. As scientific experiments in space become more sophisticated and missions are flown to greater distances, it is desirable and more effective to perform operations such as calibration, analysis, and parameter estimation onboard the spacecraft. Also because some of the greatest discoveries in science have been found where least expected, it is desirable to incorporate flexibility in the spacecraft in order to take advantage of unforeseen opportunities. That is, inclusion of adaptivity in experiments permits modification of procedures depending upon circumstances and experimental outcomes encountered. In a spacecraft, an adaptive system offers additional advantages of dynamic data compression and elimination of closed loop spacecraft-earth-spacecraft transmission delays associated with control commands. Data compression can be achieved by an adaptive system which records experimental data only during those intervals when something "interesting" occurs so that transmission capacity can be traded-off among several experiments and/or by distillation of raw data to a few characteristic numbers such as statistical moments. Closed loop transmission delays can be partially eliminated by an adaptive system which automatically accommodates changes in its environment without necessitating earth-commanded instructions. The specific objective, therefore, was the design of a laboratory model which would autonomously take measurements, calibrate sensors, process data, estimate critical parameters, and adapt the sensor system for optimum results in the face of a hostile environment.

### **Scope of the Study**

The study consisted of two phases. The first phase, completed during the first quarter, comprised a survey of spacecraft experiments suitable for application of adaptive multimode systems research. Based upon the results of this survey, the NASA chose two experiments for design of laboratory models to demonstrate adaptive control. The chosen experiments were neutron excitation and X-ray fluorescence. Design of the neutron excitation laboratory model

commenced late in the second quarter. Early in the fourth quarter, NASA directed that design of the X-ray fluorescence experiment be curtailed and that design of the instrumentation portion of the neutron excitation experiment be completed expeditiously. This decision was based upon the opinion of the several parties involved, that the program as presently constituted does not represent a significant advance in the state-of-the-art. CAL complied with this directive. Accordingly, the design of the adaptive controller described herein is incomplete.

### Approach

A survey of space research areas was made and twelve experiments suitable for adaptive multimode system research were defined. The research areas isolated in the study comprise planetary, interplanetary, and solar missions. Terrestrial missions were excluded from consideration by the expectation that adaptive techniques are most beneficial to deep space probes. Investigations of individual experiments include the following:

- definition of the experiment and assessment of scientific interest;
- determination of the feasibility of applying adaptive techniques to experiments considering adaptive sensors, adaptive data compression, and adaptable parameters unique to the experiment;
- determination of the feasibility of a laboratory demonstration model of the experimental-adaptive system;
- estimation of the physical requirements of the experimental-adaptive system with regard to scientific-spacecraft payload capability.

The experiments were thereupon rank-scored in terms of importance, suitability, feasibility, and availability of resources, and instrumentation hardware. The experiment scores are shown in Table I.

Based upon the results of the survey, the NASA designated the neutron excitation and X-ray fluorescence experiments for design of adaptive multimode laboratory models. The function of these two experiments is determination of the elemental composition of an unknown material.

The laboratory model was designed in two phases. In the first phase, element identification and weighing procedures were developed, requirements of the measurement instrumentation were defined, and specific hardware components were recommended. In the second phase, the adaptive multimode controller's function, modes of operation, and methods of adapting to various environmental conditions were defined and the computational capacity of the digital controller was estimated.

**TABLE I**  
**EXPERIMENT SCORING**

EXPERIMENT		RANK SCORE
TRAPPED RADIATION	ELECTRONS	46
	PROTONS	42
	ALPHAS	40
	DEUTERONS	40
ACTIVATION ANALYSIS		61
X-RAY FLUORESCENCE		54
MAGNETOMETER		38
SOLAR FLARES	PROTONS	44
	COSMIC RAYS	44
	ULTRAVIOLET	52
	X-RAYS	52
MICROMETEORITES		35

**Summary of Results**

The main results of research performed in this study are:

- designation of a set of scientific spacecraft experiments amenable to application of adaptive multimode control;
- delineation of parameters unique to these experiments which are suitable for adaptivity; and
- design of a laboratory model for the neutron excitation experiment which exhibits adaptive multimode behavior.

**Acknowledgment**

Major contributors to the study were: Mr. J. Beyer, Mr. R. O. Breault, Mr. V. A. DePalma, Dr. D. J. Gawlowicz and Dr. D. P. Malone. Mr. S. G. Keeney provided technical writing and editing assistance.

## DESIGN OF NEUTRON EXCITATION EXPERIMENT

### Objectives of Experiment

The advantages of neutron excitation analysis for determination of the composition of a surface in an on-site landing mission are, primarily, the elimination of complex sample treatment, e.g., chemical and spectrographic, and generally rapid data acquisition. Also this experiment provides significant opportunity for data processing/reduction and adaptation to environment.\*

Excitation of a sample, i.e., the production of radionuclides by nuclear reactions, can be carried out by charged particles, neutrons, or gamma rays. The products may emit alpha, beta, or gamma radiation, or they may decay by electron capture. The requirements of remote operation with minimum-sample treatment restrict, in general, the analysis to neutron irradiation and gamma detection. Since the spectral and temporal characteristics of the decay products of neutron excitation are of interest, pulsed operation of sources is desirable. In addition, higher fluxes are, in general, available if pulsed source operation is utilized.

The laboratory demonstration model of the neutron excitation experiment is designed to adaptively perform complete automatic element analysis of a sample containing the elements Si, Al, Fe, Mg and O which are to be identified and weighed. While the element identification and weighing processes are interesting in their own right, their main function is as a test vehicle for an adaptive multimode system.

### Design Ground Rules

The constraints within which the adaptive multimode neutron excitation experiment was designed are to:

- operate in a laboratory environment;
- demonstrate feasibility of adaptive operation;
- identify and weigh the elements Si, Al, Fe, Mg and O;
- adaptively compensate for background radiation, hydrogenous materials, dominating elemental responses, and, to a lesser extent, temperature variations;
- provide outputs in a form suitable for telemetry as well as printed output; and
- where practicable employ space-qualified components as well as solid-state and integrated circuitry.

---

\* Refer to page 107 for additional discussion regarding experiment suitability.

The general functioning of the experiment is as follows. The experimental arrangement is indicated in Figure 1. The detector package can be oriented parallel to or at right angles to the sample. The shield between source and detector serves to protect the detector from neutrons and bremsstrahlung from the accelerator. The general mode of operation consists of positioning the sample near the source-detector package, operating the detector to determine the radiation background, calibrating the system, and subsequently energizing the neutron source. Pulsed operation is then used to investigate the prompt and capture spectra. For prompt spectra, the neutron flux must be adjusted so that the gamma pulses are acceptable to the electronic system, that is, dead time of the analyzer imposes an upper limit to the pulse rate, and the effect of pulse overlap in the amplifier and associated circuitry must be taken into account. After termination of the desired pulse sequence, the neutron generator is operated in a mode selected to optimize activation of the target. Activation, however, requires the highest possible integrated flux, that is, the highest possible value of  $n/cm^2/sec$  at the target. Since activation cross sections generally obey a  $v^{-1}$  relation, activation products due to a fast neutron flux will probably contribute less activity than those due to a thermal flux. Consequently, operation of the generator in a "fast-activation" mode would probably precede operation in a "thermal-activation" mode. The latter would be achieved by mechanically positioning a moderator (paraffin) about the accelerator target. Insertion of a thermalizing medium reduces the thermal flux to something like two orders of magnitude less than the fast flux, so that appropriate compensation must be made.

The data analysis performed by the adaptive processor is based primarily on the output of a multichannel analyzer (MCA), which presents an intensity versus energy curve of the gamma spectrum, or, when operated as a multichannel scaler (MCS), presents a total intensity versus time curve. A reference

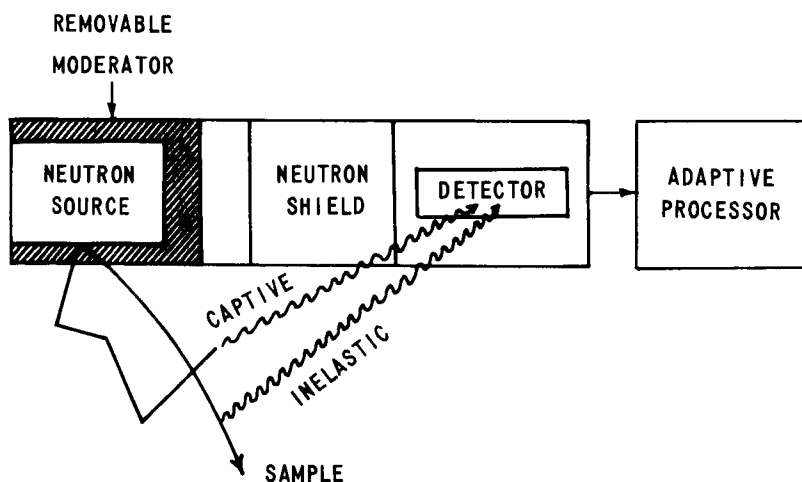


Figure 1 GENERAL EXPERIMENT CONFIGURATION

data file would be provided in the adaptive controller/processor portion of the system to facilitate the identification analysis. This file would contain:

- reference spectra for spectrum stripping purposes,
- reaction cross sections,
- half-life data,
- neutron generator data, and
- detector characteristics.

#### Element Identification Procedures

The identification of five elements in a chemical matrix by selected neutron experiments is discussed in this section. These experiments are designed to perform adaptively complete, remote element analyses in a laboratory demonstration model of an adaptive multimode system. The experimental chemical matrix to be analyzed consists of mixtures of the elements Si, Al, Fe, Mg and O. A general description of the identification procedure is presented followed by detailed discussion of each of the several measurement techniques involved. A block diagram of the adaptive neutron excitation experiment is shown in Figure 2.

The element identification process is based on the detection of gamma rays produced by the interaction of the elemental nuclei with either thermal ( $< .0250$  eV) or fast (14.7 MeV) neutrons. Each of these modes provides two sets of gamma rays which are characteristic of the excited nuclei. In the thermal neutron mode it is possible to produce:

- 1) characteristic capture gamma rays from radiative capture of thermal neutrons,  $(n, \gamma)$  reactions producing an isotope of the original nucleus; and
- 2) characteristic photopeak gamma rays produced by the decay of radioactive compound nuclei,  $(n, \gamma)$  reactions producing an isotope of the original nucleus which is radioactive.

In the fast neutron mode it is possible to produce:

- 1) characteristic prompt gamma rays from inelastically scattered neutrons,  $(n, n)$  reactions produced from the bombarded nuclei; and
- 2) characteristic photopeak gamma rays from the decay of radioactive compound nuclei produced from  $(n, \alpha)$   $(n, p)$  or  $(n, 2n)$  reactions.

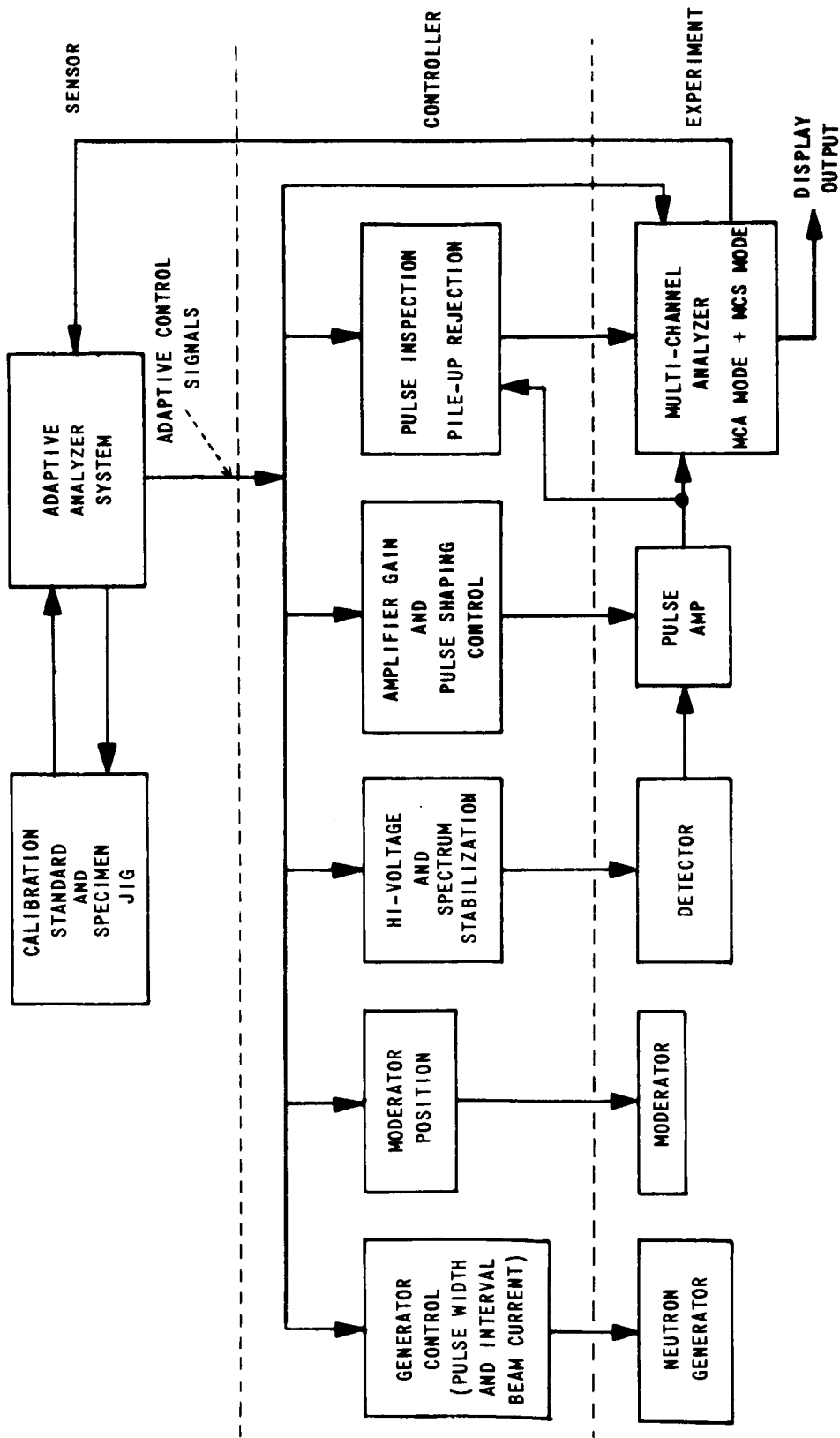


Figure 2 NEUTRON EXCITATION EXPERIMENT BLOCK DIAGRAM

The identification modes which will be used are listed below in the order in which they will be performed by the laboratory model:

- |                      |                      |
|----------------------|----------------------|
| Thermal neutron mode | 1) Capture gammas    |
|                      | 2) Activation gammas |
| Fast neutron mode    | 1) Prompt gammas     |
|                      | 2) Activation gammas |

Each of these modes is discussed in detail in subsequent sections.

Analysis of capture gammas from fast neutrons has not been included in the identification scheme because of ambiguities which can result from multiple capture reactions of epithermal neutrons.

Terrestrial natural abundances are assumed in determinations of the elements present when the detection scheme provides information on the least abundant isotope.

**Fast Neutron Mode** -- After the fast-neutron burst all prompt gamma production ceases, hence prompt gammas must be detected during the neutron pulse. Gating on of the MCA at the start of the  $1\mu$  sec neutron pulse for  $3\mu$  sec allows detection of the prompt gammas produced. Furthermore, this procedure affords time discrimination necessary to isolate the prompt gammas from capture gammas emitted. Each successive fast-neutron burst gives rise to an increasing activation gamma activity as illustrated in Figure 3. Between neutron bursts those neutrons which have been thermalized also produce capture gammas as illustrated in Figure 3. Therefore, each time the neutron generator and MCA are turned on two distinct sets of gamma rays are simultaneously recorded; prompt and activation gammas. Capture gammas do not interfere since they appear some  $10\mu$  sec after the neutron pulse and last for approximately  $500\mu$  sec.

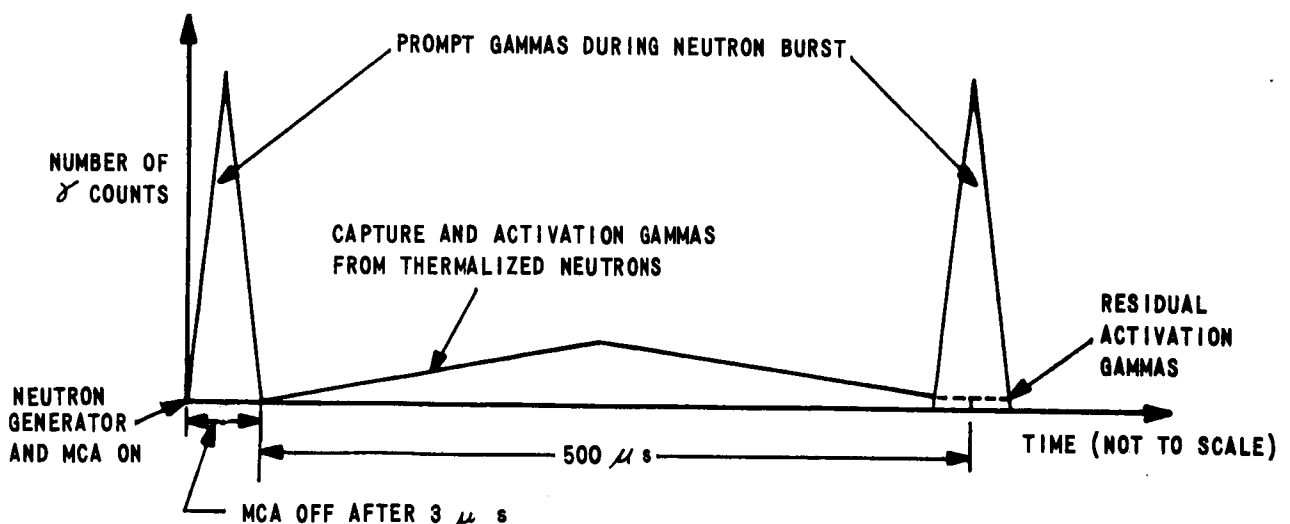


Figure 3 TIMING DIAGRAM FOR FAST NEUTRON MODE



If the activation component is strong relative to the prompt gamma spectrum, it will be necessary to subtract it from the prompt spectrum prior to identification analysis. This can be done by using a sufficiently large time interval between pulses ( $500 \mu\text{sec}$ ) so that only activation gammas are recorded if the MCA is turned on immediately prior to a neutron pulse. The proper sequence of events is, then, to record the prompt and activation spectra during the  $3 \mu\text{sec}$  neutron pulse. Then, prior to the next neutron pulse and  $500 \mu\text{sec}$  after the previous pulse, record the activation spectrum in the subtract mode of the MCA for  $3 \mu\text{sec}$  by gating on the MCA. In this way a nearly pure prompt spectrum will be obtained. The exact gating times are best determined experimentally since system geometry plays an important role in the timing sequence. Figure 3 illustrates the relative number of gamma counts emitted during a pulse cycle. The relative number of counts from inelastically scattered neutrons is greater since it is approximately six times (1) the number from capture and activation neutron reactions. In the event the activation component of the spectrum is small it would not be necessary to perform any subtraction process. Necessity of this refinement can be determined by experiment.

After the prompt spectrum has been accumulated and analyzed, the MCA can be cleared and the activation spectrum recorded after all neutron bombardment has been stopped. The appropriate recording times and irradiation time are given in a later section of this report.

**Thermal Neutron Mode** -- In this mode of operation capture and thermal activation gammas are produced and detected. With successive pulses, the activation gammas increase in intensity.

During the capture gamma-ray mode of analysis it is necessary to remove the activation component from measured spectra to recover the capture spectrum. To do this the MCA can be gated on shortly after the neutron pulse to record the capture and activation gammas, shown dashed in Figure 4, and between pulses the MCA can be gated on in the subtract mode to remove the activation component from the spectrum. The resultant spectrum will be representative of the capture gamma rays emitted.

The activation spectrum can be recorded after all neutron bombardment has stopped. For purposes of mass determination it will be necessary to record

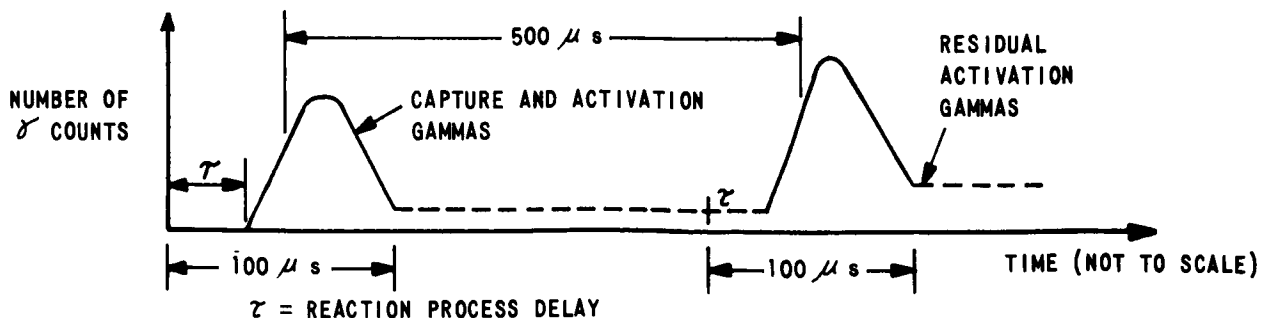


Figure 4 TIMING DIAGRAM FOR THERMAL NEUTRON MODE

the total neutron irradiation time and the time lapse before recording of the activation spectrum; that lapse is commonly called the cooling time.

Neutron activation from the pulsed source will proceed for a time equal to the activation time produced by a continuous neutron flux of  $10^9$  n/cm<sup>2</sup>/sec. These values were chosen from experimental results\* obtained from thermal activation of a sample matrix. A higher neutron flux is necessary in the pulsed mode in order to obtain equivalent activation for equal irradiation times. This point is discussed later in this report. The activation spectrum is recorded for a preset time, beginning one minute after all neutron pulsing has stopped. Five minutes later another activation spectrum is recorded for a live-count of one minute in order to detect the radioactive decay of activation gammas. This information can then be used to compute half lives of the elements producing the activation gammas to further aid identification.

### Radiative Capture of Thermal Neutrons

The nucleus formed by the capture of a thermal neutron in an ( $n, \gamma$ ) reaction is in an excited state for approximately  $10^{-14}$  seconds. De-excitation to the ground state occurs by the emission of both low and high energy gamma rays, these gammas being characteristic of the compound nucleus formed. It is the detection of these capture gammas and the association of their observed energies with elements in the matrix which forms the basis for the identification scheme of this section. The use of capture gamma rays for elemental identification is not a new concept (2,3). However, only recently has sufficient experimental information been made available to determine precise capture gamma ray spectra (4) of a composite matrix of elements. Furthermore, it is fortuitous that this data has been accumulated by using standard scintillation--instead of the more exotic Compton--spectrometer detector. Greenwood (4) has also published digital data for each of his spectra, thereby facilitating construction of the composite spectrum of a chemical matrix under standard experimental conditions. In the following sections both low and high energy capture spectra are presented for an elemental matrix. Oxygen is not detectable, consequently the composite spectrum is for Al, Si, Mg and Fe only.

Composite Low Energy Spectra - - Three composite low energy spectra have been compiled in order to reveal the characteristic gamma ray energies of four of the five elements present in a sample matrix. Information about oxygen cannot be obtained from the capture process due to its low thermal capture cross section. The elemental spectra of Fe, Al, Si and Mg were reproduced from the digital data<sup>(6)</sup> and appear, normalized, for 1.0 gm samples of each element for a neutron flux of  $10^6$  n/cm<sup>2</sup>/sec and one-minute count and irradiation times in Figures 5 through 8. Figures 5 through 8 have not been fitted with a smooth curve; consequently, many of the peaks in these figures are not real but result from connecting the data points rather than smoothing the curve. The actual spectral peaks which will be used have been labeled with their appropriate energies in Figures 5 - 8. The composite spectra of various amounts of the four elements appear in Figures 9, 10 and 11 as cases 1, 2 and 3. Figure 9

---

\* Experiment conducted at Western N.Y. Research Center.

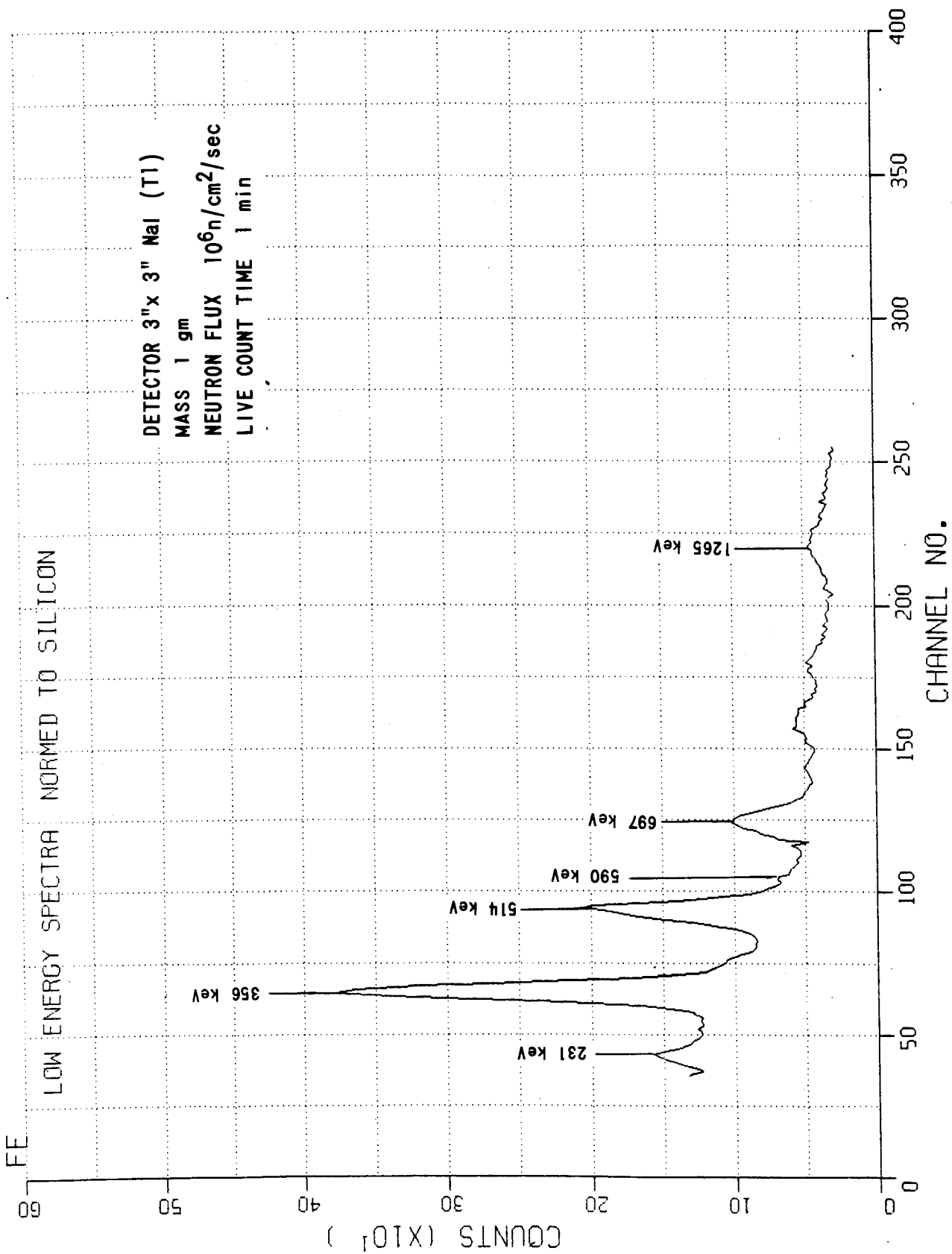


Figure 5 LOW ENERGY CAPTURE GAMMA RAY SPECTRUM OF Fe

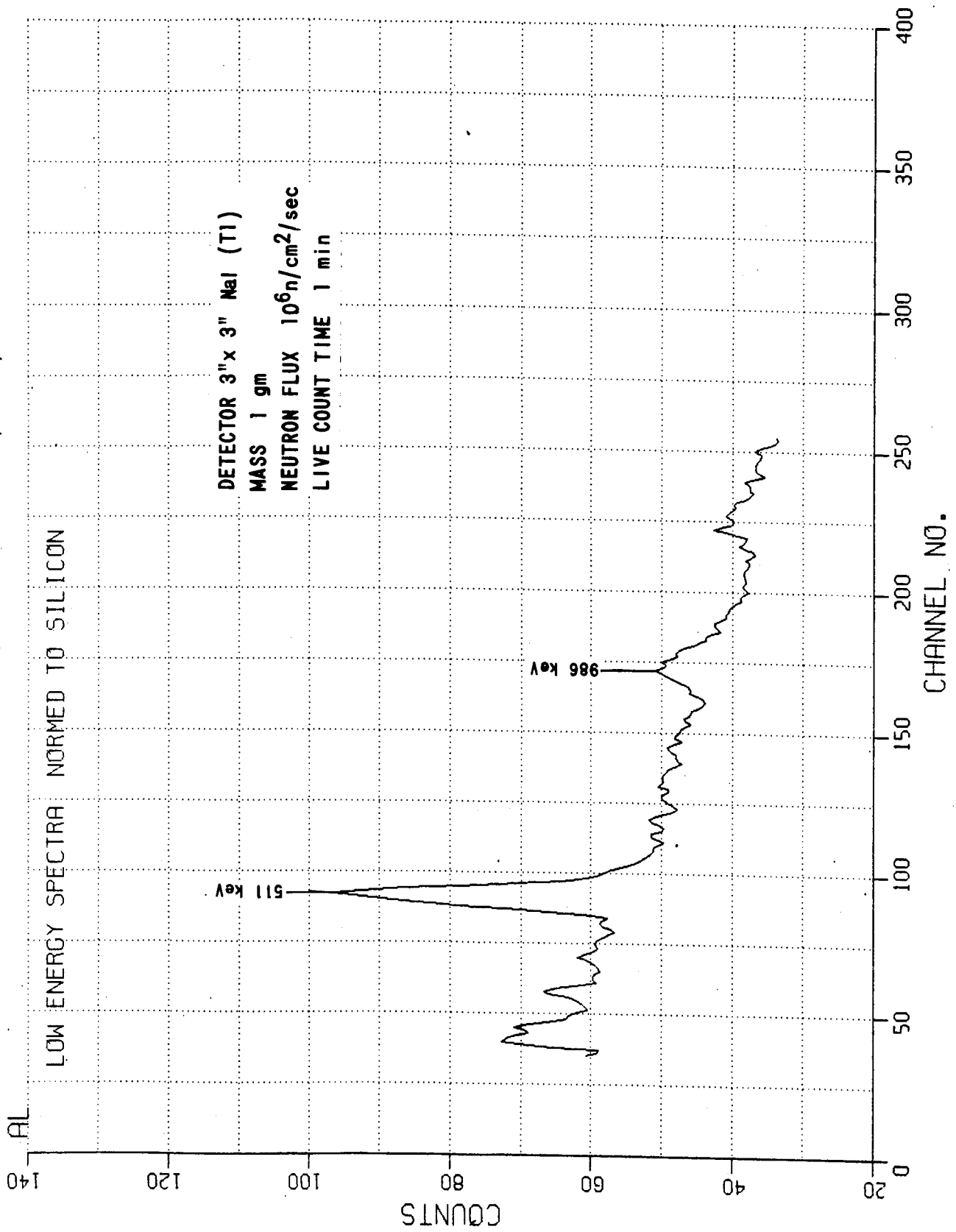


Figure 6 LOW ENERGY CAPTURE GAMMA RAY SPECTRUM OF AL A1

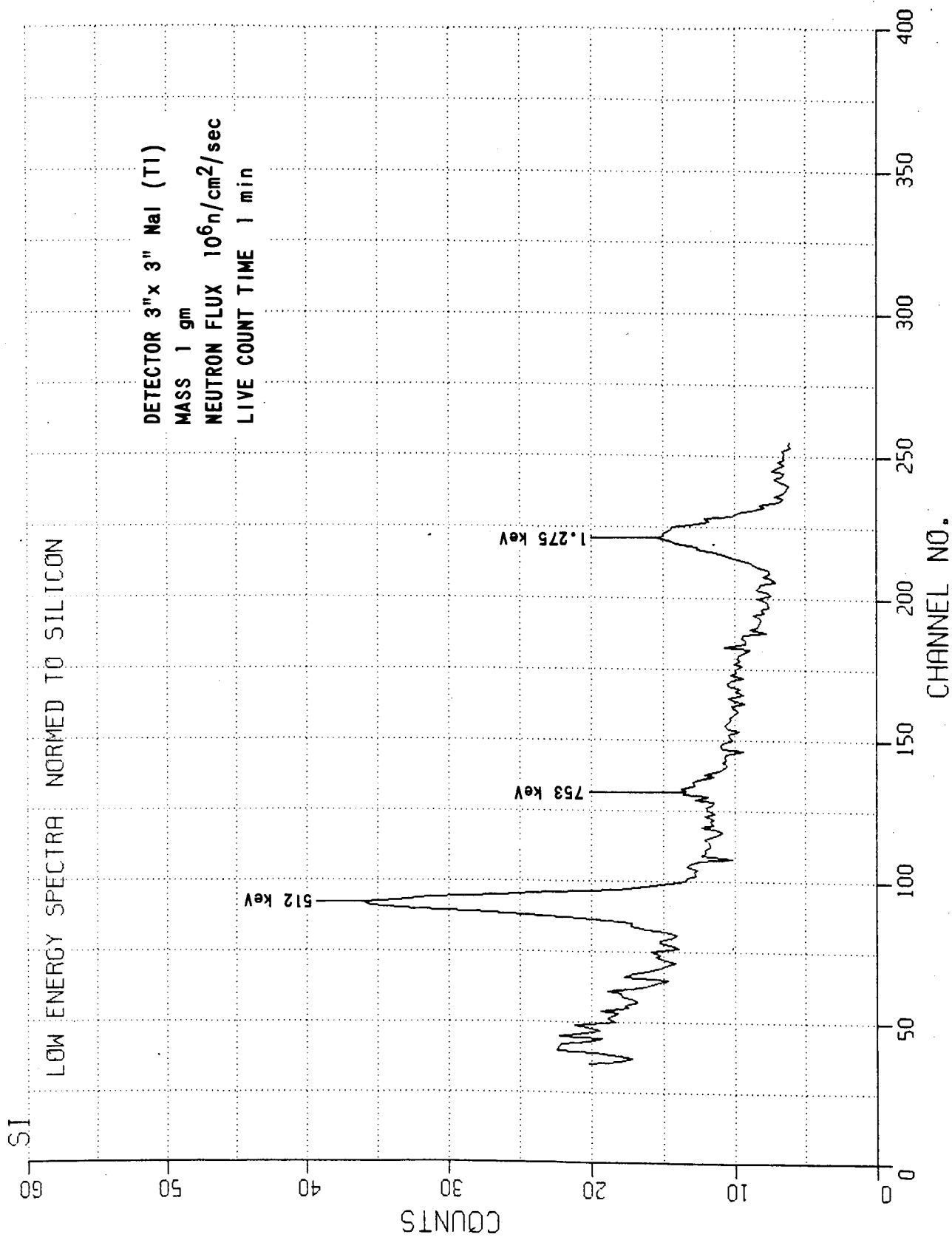


Figure 7 LOW ENERGY CAPTURE GAMMA RAY SPECTRUM OF SI

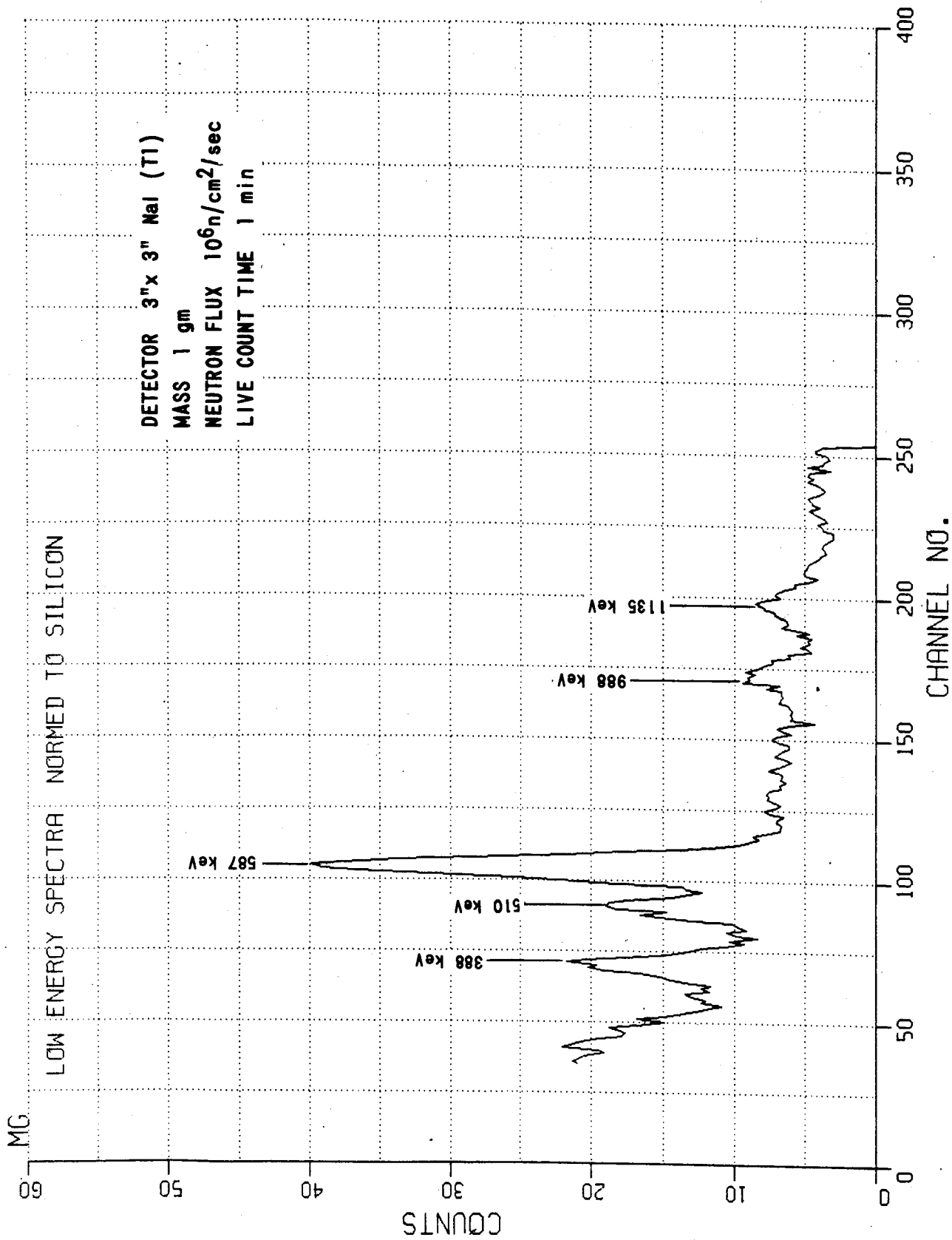


Figure 8 LOW ENERGY CAPTURE GAMMA RAY SPECTRUM OF M9

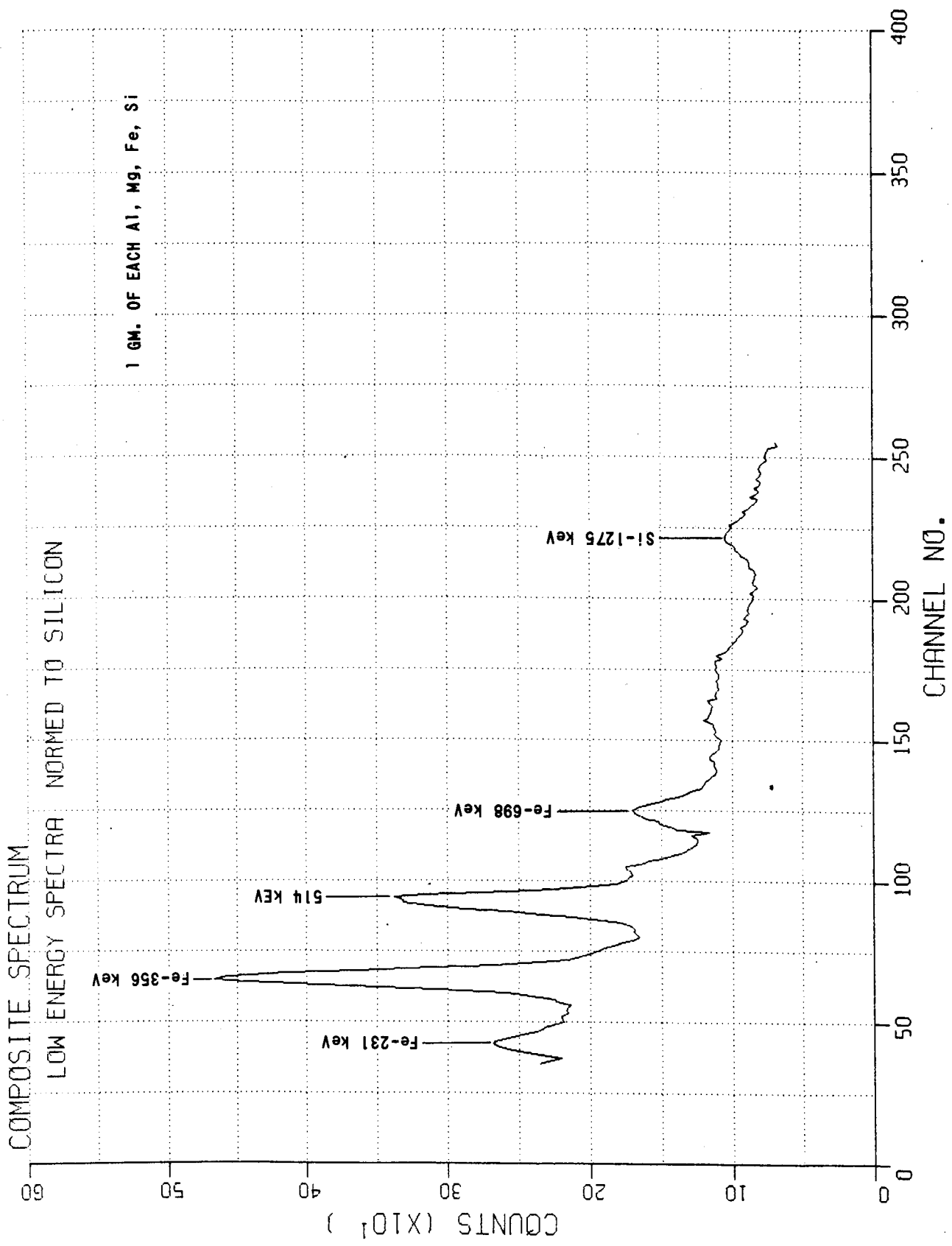


Figure 9 COMPOSITE LOW ENERGY CAPTURE GAMMA SPECTRUM

COMPOSITE SPECTRUM

LOW ENERGY SPECTRA NORMED TO SILICON 0.1 GM. IRON, 1.0GM OTHERS

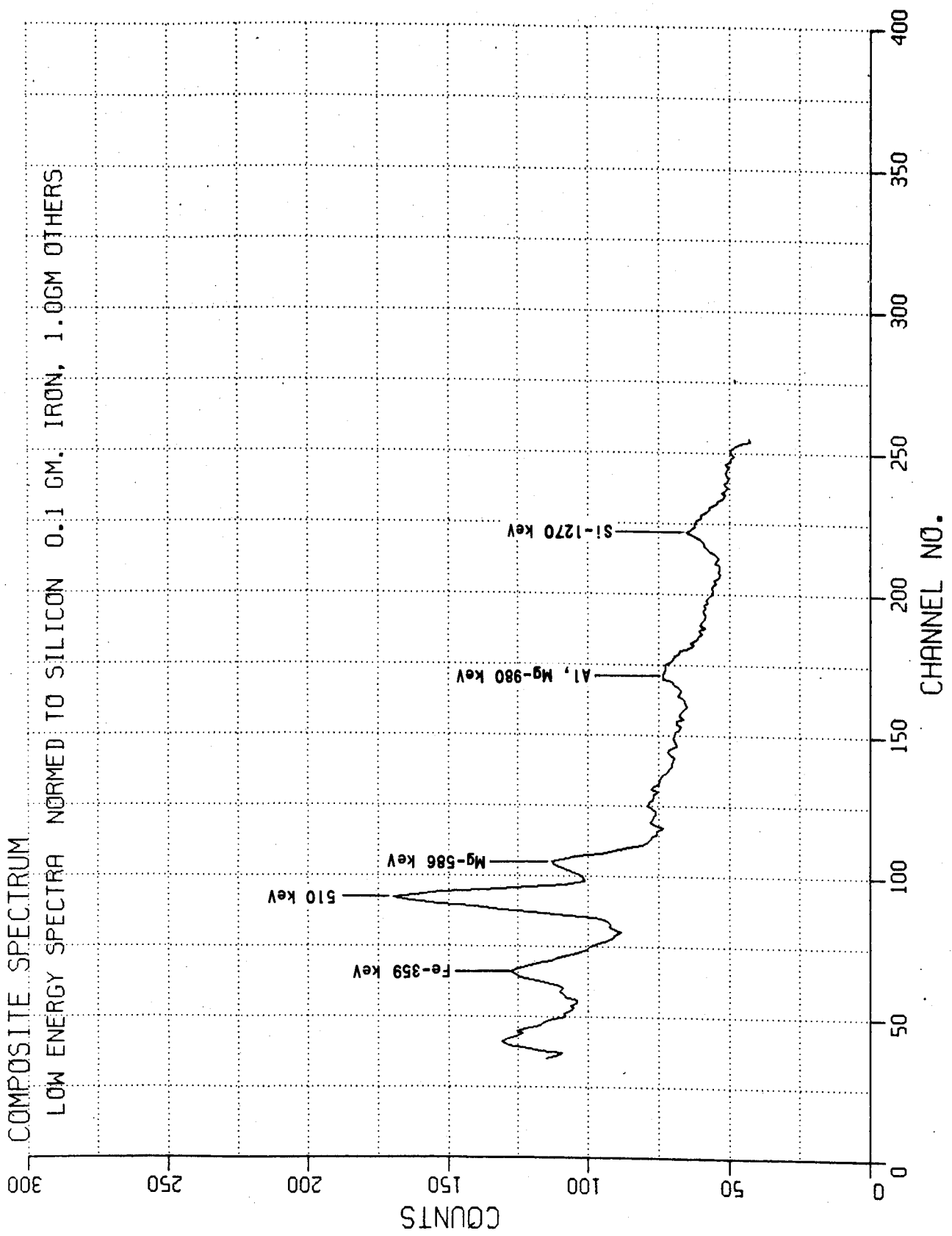


Figure 10 COMPOSITE LOW ENERGY CAPTURE GAMMA RAY SPECTRUM



COMPOSITE SPECTRUM

LOW ENERGY SPECTRA NORMED TO SI, 0.5GM AL, 0.0GM FE, 1.0 GM OTHERS

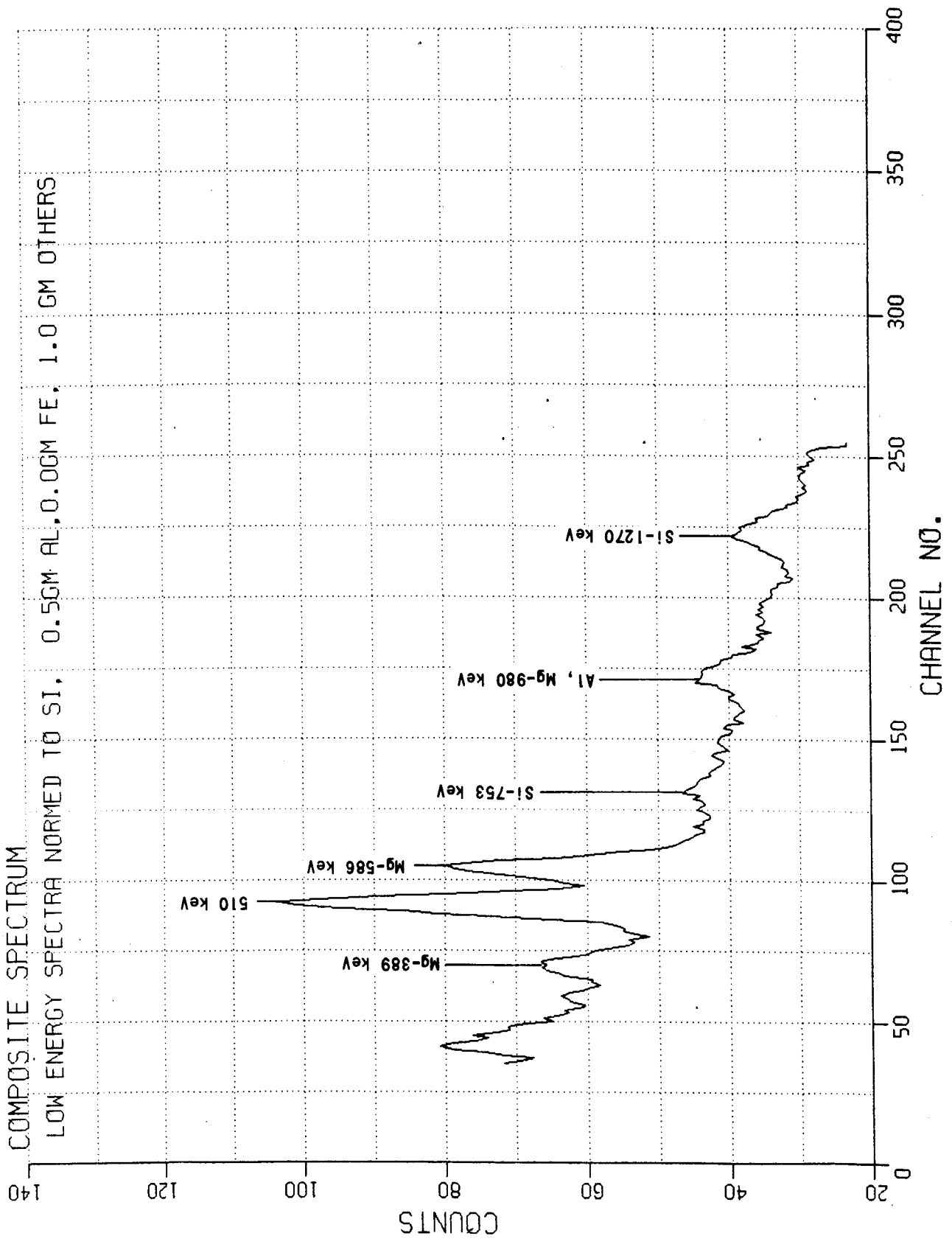


Figure 11 COMPOSITE LOW ENERGY CAPTURE GAMMA RAY SPECTRUM

results from combining the elemental spectra of 1.0 gm of each of the four elements. Figure 10 was compiled from 0.1 gm Fe and 1.0 gm each of Al, Si and Mg whereas Figure 11 was compiled from only 0.5 gm Al and 1.0 gm each of Si and Mg.

The appropriate capture gamma ray energies best suited for element identification are listed in Table II for the three composite spectra. It should be noted that the energies of the spectral peaks of the pure element may be slightly shifted as a result of adding two peaks of slightly different energies. Some degree of confusion is possible when analyzing the composite spectra for the following spectral lines: 0.590 MeV and 0.980 MeV. The first can be from iron or magnesium. Only magnesium is listed in Table II as having this line in the composite spectra of Case 2 because magnesium gives a line which is three times more intense than that of iron under identical experimental conditions and equal amounts of Mg and Fe. Since Case 2 represents a mass ratio of Mg to Fe of 10, the Mg spectral line would be 30 times more intense than that of Fe. Consequently, for positive identification of the 0.590 MeV spectral line in the presence of Fe it is first necessary to determine the ratio of Mg to Fe present. If the peak height above background for this line is greater than the peak height obtained for Fe alone, Mg is present. The 0.980 MeV spectral line can result from aluminum or magnesium with equal peak heights for equal amounts for these elements. The 0.980 MeV spectral line only begins to show if the mass ratio of Mg or Al to Fe is greater than 10. Under the conditions of Case 2, either Mg or Al would be detected from the 0.980 MeV line. However, if the presence of Mg can be determined separately, the uncertainty is reduced as to the presence of both elements. Clearly, if Mg is not present and the 0.980 line appears, then Al is present.

**Composite High Energy Spectra** - - Three composite high-energy spectra covering the energy range 0 - 8.0 MeV have been compiled in Figures 16, 17 and 18. These spectra were compiled from the elemental spectra of Fe, Al, Si and Mg which were produced from the digital data (4). These spectra appear in Figures 12, 13, 14 and 15 and are for 1.0 gm samples of each element for a neutron flux of  $10^6$  n/cm<sup>2</sup>/sec and one-minute count and irradiation times. Not all the capture gamma rays are labeled in the elemental spectra since only those elements are used in the identification of an element. Table III was constructed from an analysis of the three composite spectra. The three

cases given in Table III are for: one gram of each element taken together - Case 1; 0.1 gm iron with 1.0 gm of Al, Mg and Si - Case 2; 0.1 gm Fe, 0.1 gm Al, 1.0 gm Mg and 1.0 gm Si - Case 4. In cases 2 and 4 all four elements can be identified as shown in Table III, which lists the gamma ray energies used in identifying the four elements. The gamma ray energies listed in Table III may be different from the pure spectral energy due to interference of two peaks of slightly different energy or addition of a peak to background, which increases with decreasing gamma ray energy. This should not affect the identification of a given element since the appropriate detection energy is obtained from a composite spectrum. In general, the detection energy for a given spectral line is within one channel width of the true gamma ray energy as obtained from the pure elemental spectra.



FE  
HIGH ENERGY SPECTRA NORMED TO SILICON

DETECTOR 3" X 3" NaI (TI)  
MASS 1 gm  
NEUTRON FLUX  $10^6$  n/cm<sup>2</sup>/sec  
LIVE COUNT TIME 1 min.

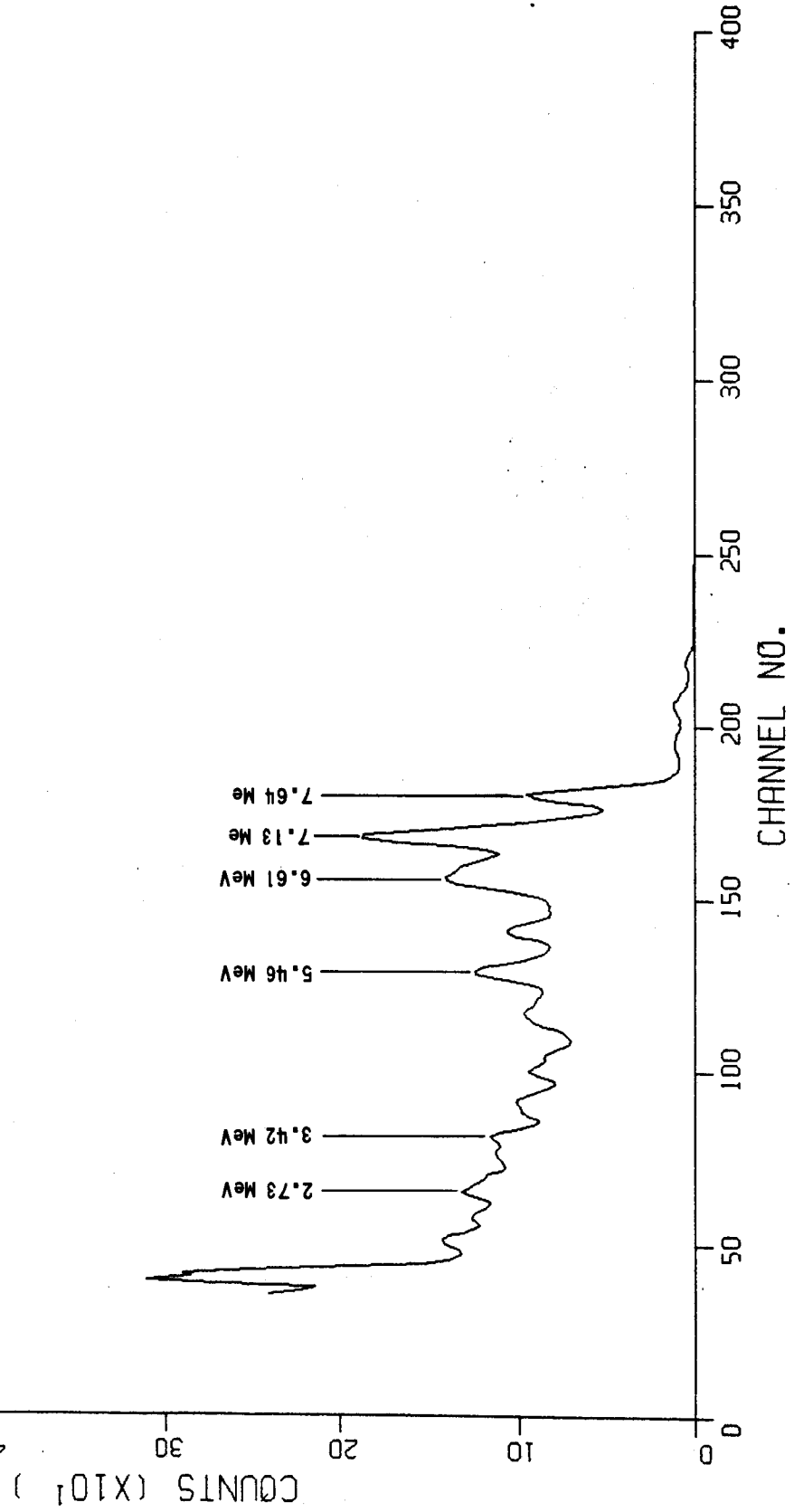


Figure 12 HIGH ENERGY CAPTURE GAMMA RAY SPECTRUM OF Fe

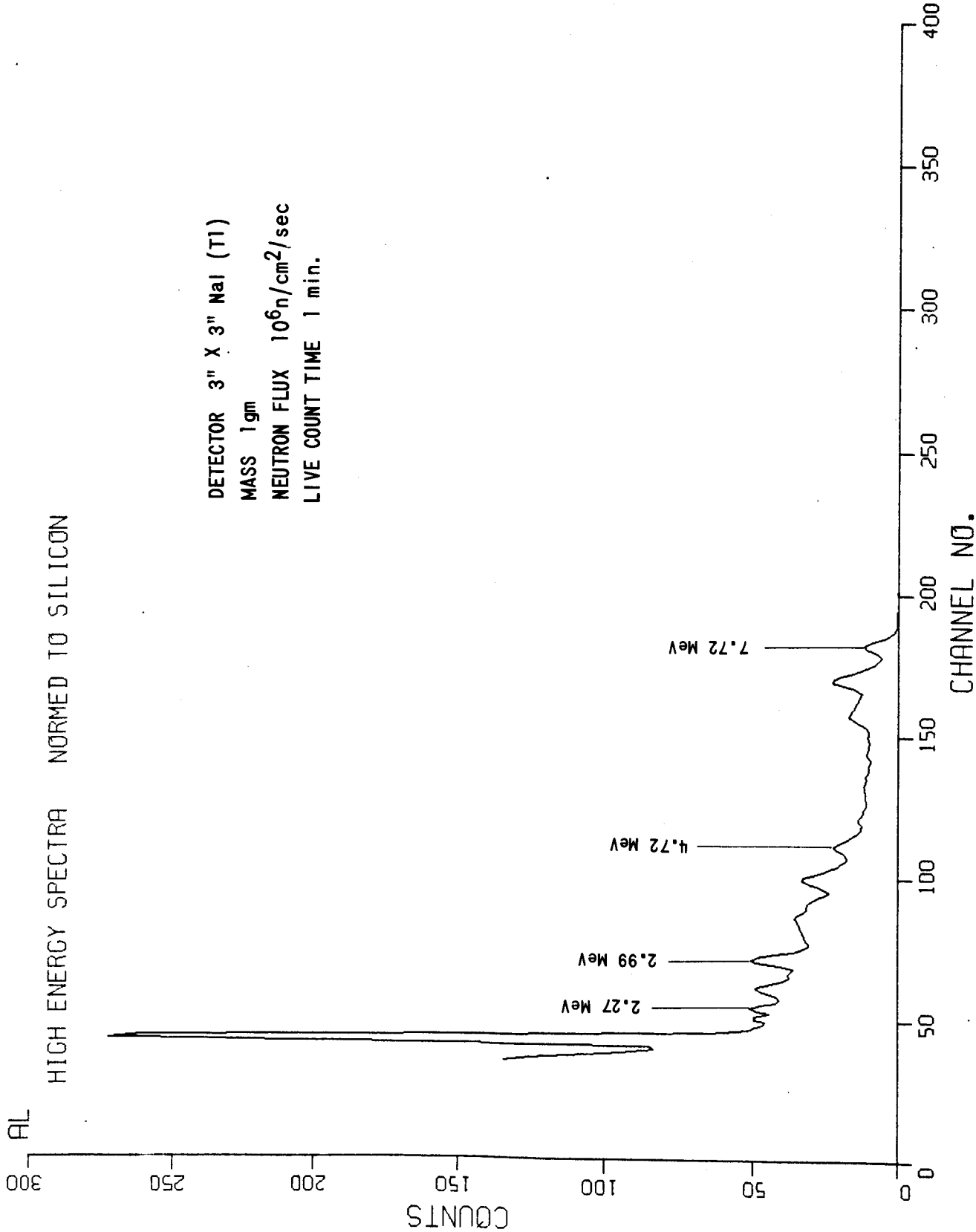


Figure 13 HIGH ENERGY CAPTURE GAMMA RAY SPECTRUM OF AL

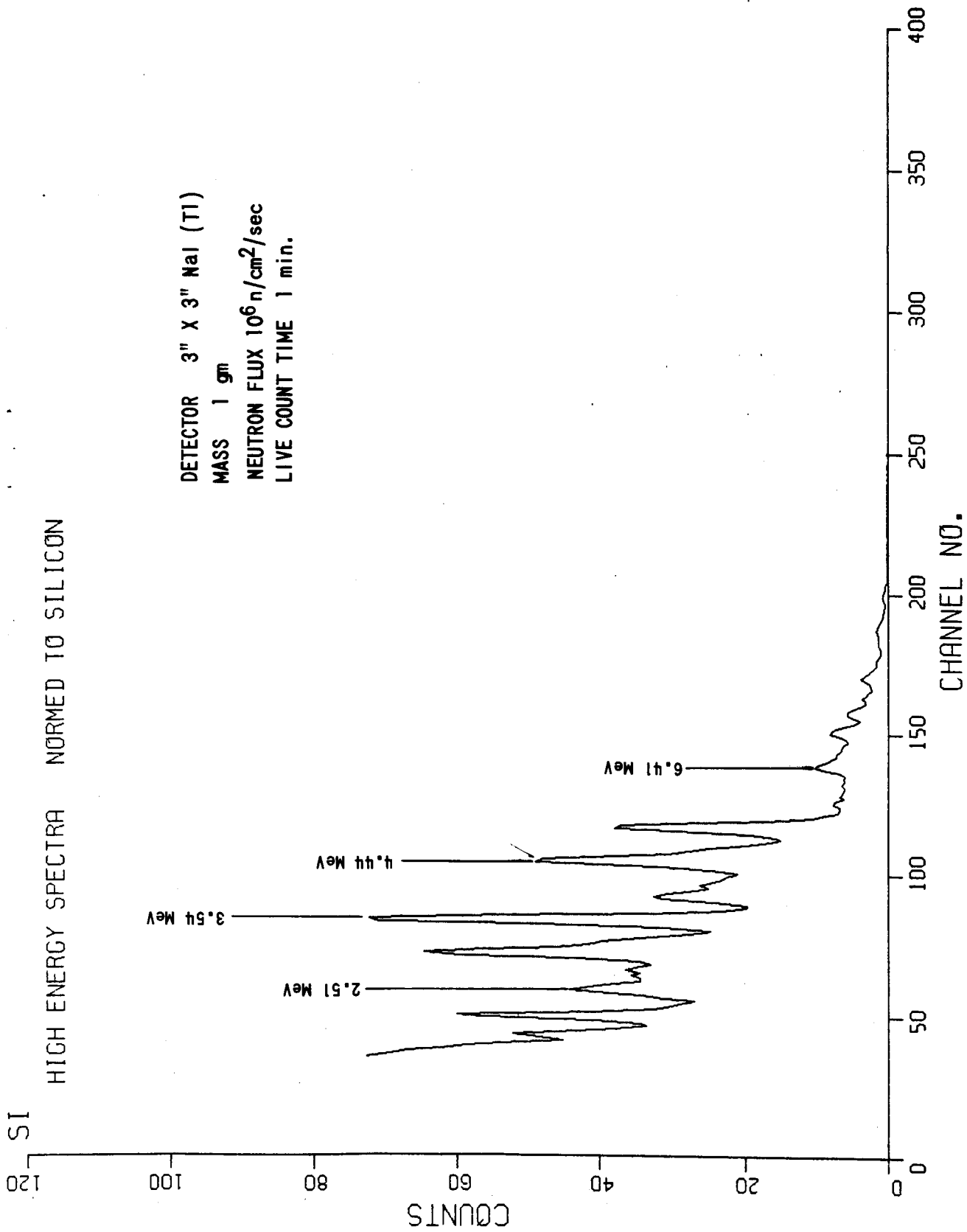


Figure 14 HIGH ENERGY CAPTURE GAMMA RAY SPECTRUM OF Si

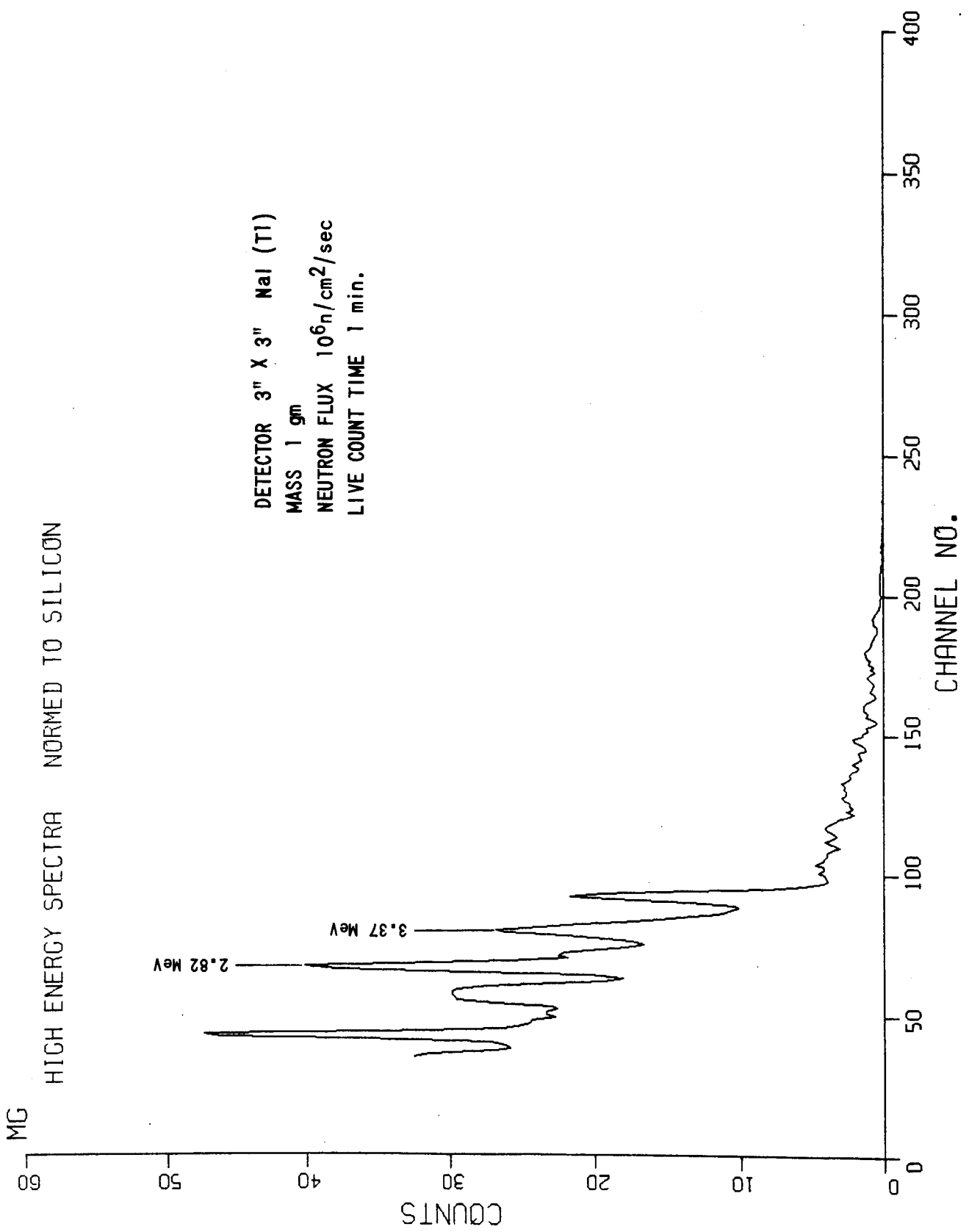


Figure 15 HIGH ENERGY CAPTURE GAMMA RAY SPECTRUM OF Mg

COMPOSITE SPECTRUM  
HIGH ENERGY SPECTRA NORMED TO SILICON

1 GM OF EACH Al, Mg, Fe, Si

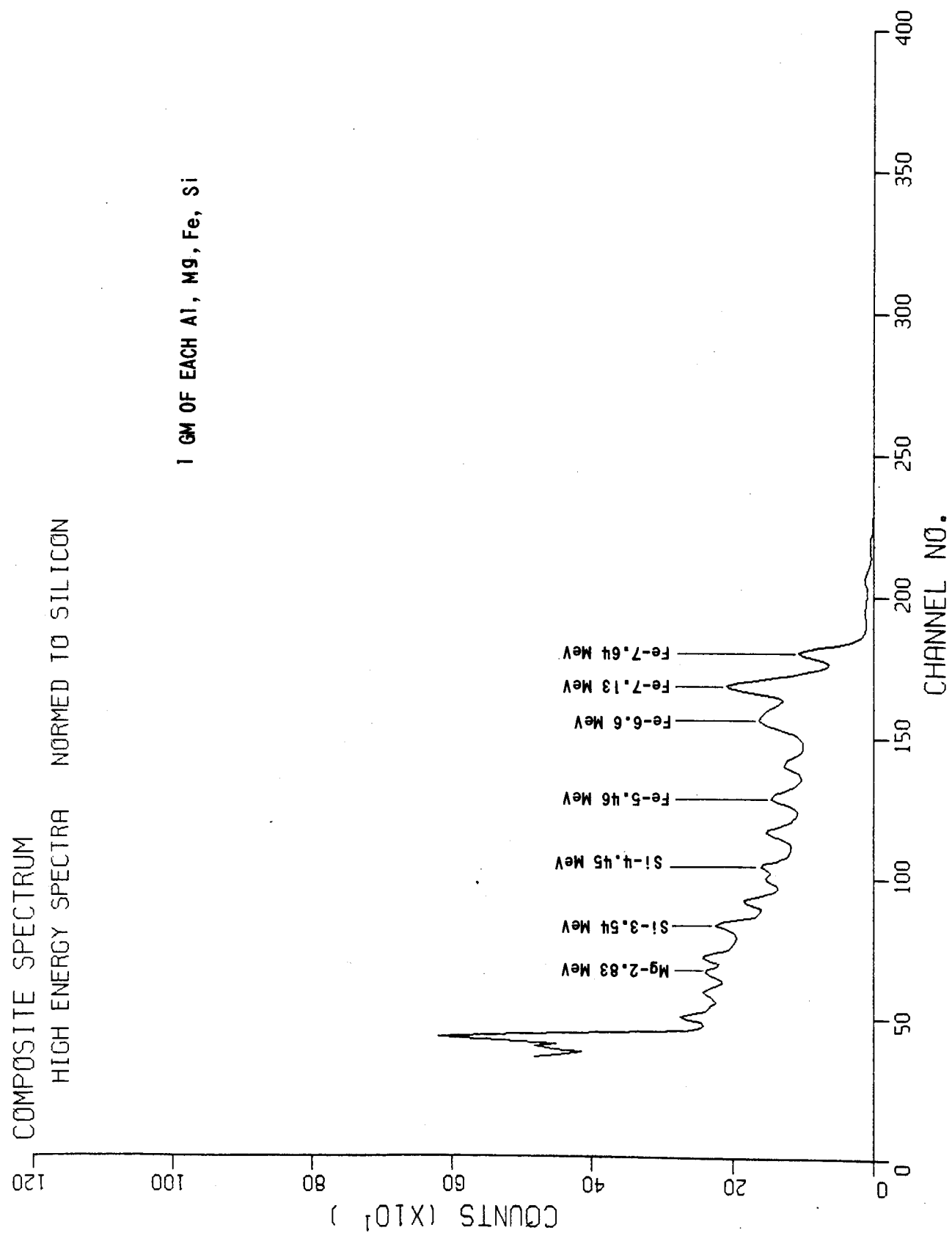


Figure 16 COMPOSITE HIGH ENERGY CAPTURE GAMMA RAY SPECTRUM



COMPOSITE SPECTRUM

HIGH ENERGY SPECTRA NORMED TO SILICON 0.1GM FE, 1.0GM OTHERS

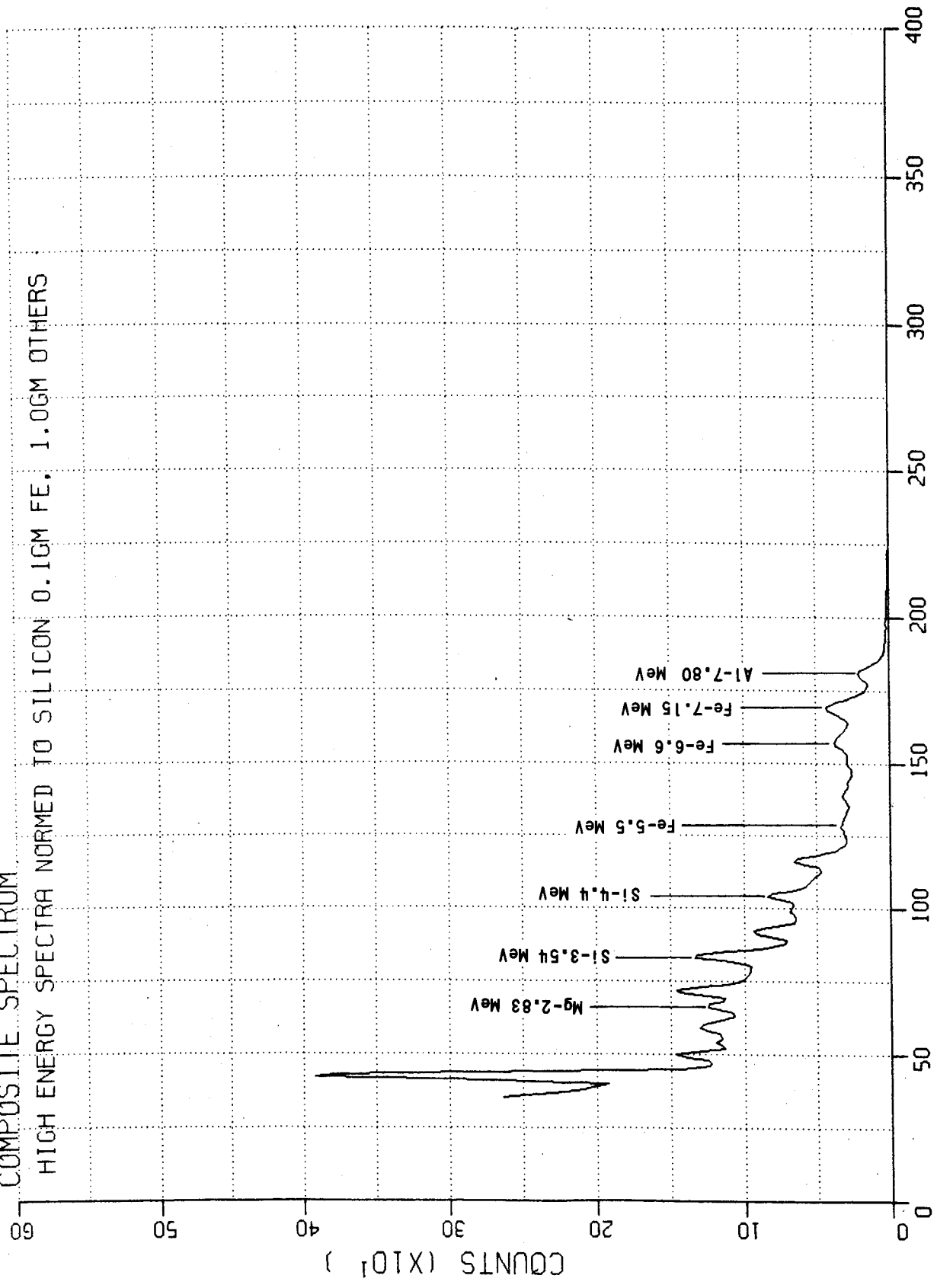


Figure 17 COMPOSITE HIGH ENERGY CAPTURE GAMMA RAY SPECTRUM

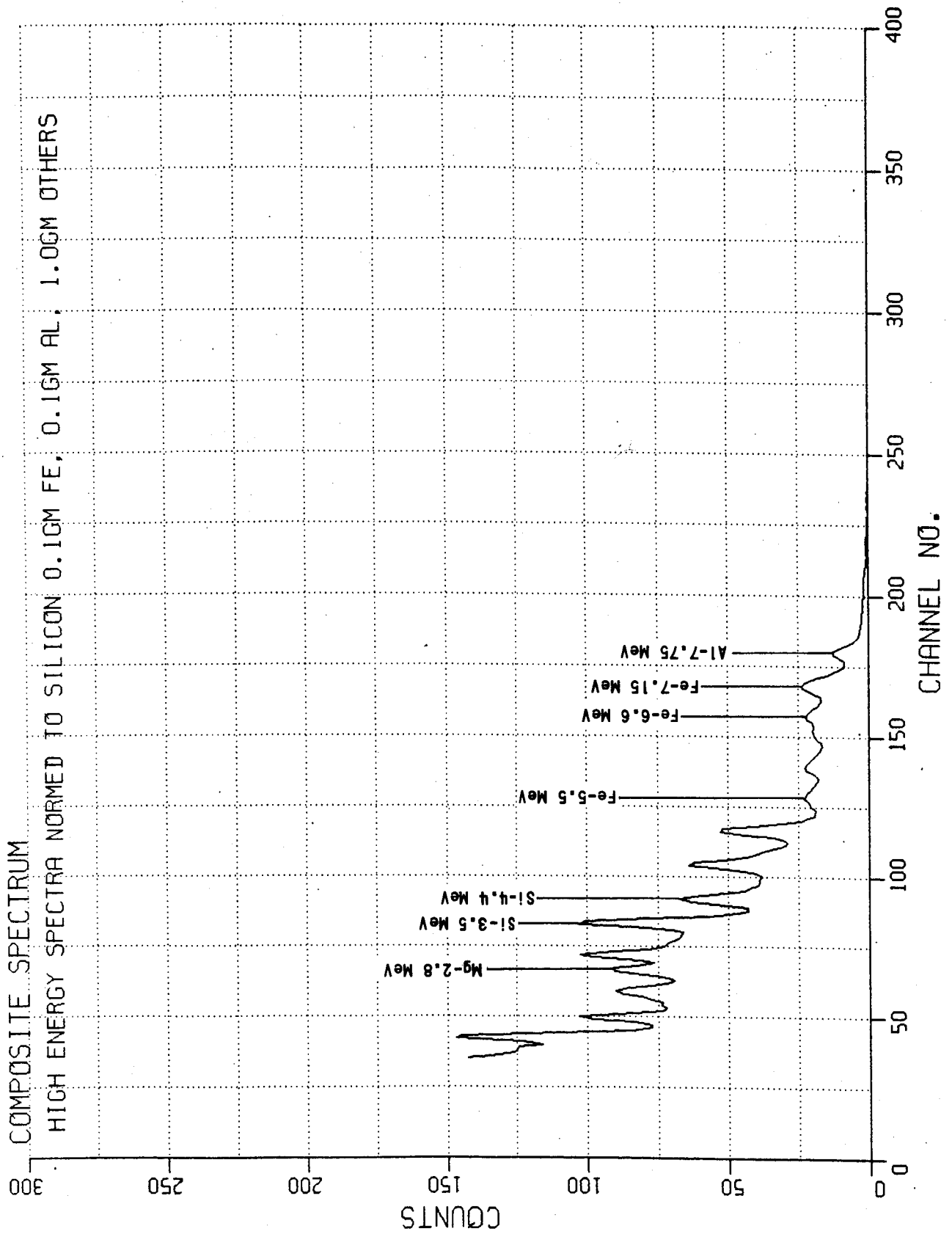


Figure 18 COMPOSITE HIGH ENERGY CAPTURE GAMMA RAY SPECTRUM

Table III  
SUMMARY OF HIGH ENERGY CAPTURE GAMMA RAY  
ENERGIES FOR THERMAL NEUTRON CAPTURE

REACTION AND ABUNDANCE	UNIQUE COMPOSITE SPECTRUM LINES WITH APPROPRIATE DETECTION ENERGY IN MeV			SIGNIFICANT CAPTURE GAMMA RAY ENERGY FROM SINGLE ELEMENT MeV	PERCENT OF DECAY Ki	ATOMIC THERMAL CAPTURE CROSS SECTION BARNS
	CASE 1	CASE 2	CASE 4			
Al <sup>27</sup> (100%) n,γ				2.27	5.1	0.235
				2.99	*	
				4.72	8.0	
		X (7.80)	X (7.75)	7.72	24.0	
Si <sup>28</sup> (92.2%) n,γ				2.51	*	0.16
	X	X	X (3.50)	3.54	48.7	
	X (4.45)	X	X (4.40)	4.44	*	
				6.41	*	
Mg <sup>24</sup> (78.7%) n,γ	X (2.83)	X (2.88)	X (2.80)	2.82	65.0	0.63
				3.37	13.0	
Fe <sup>56</sup> (96.6%) n,γ				2.73	*	2.62
				3.42	3.9	
	X	X (5.50)	X (5.50)	5.46	*	
	X	X	X	6.61	*	
	X	X (7.15)	X (7.15)	7.13	*	
	X		7.64	29.0		

CASE 1 1 gm OF EACH ELEMENT Al, Si AND Mg

CASE 2 0.1 gm Fe, 1 gm OF EACH Al, Si AND Mg

CASE 4 0.1 gm Fe, 0.1 gm Al AND 1 gm OF EACH Si, AND Mg

X POSITIVE ELEMENT IDENTIFICATION

\* DATA NOT AVAILABLE

### Elemental Analysis Procedure for Capture Mode

Two experiments must be performed in the capture mode in order to record the low and high energy capture spectra with sufficient accuracy to enable subsequent evaluation. Initial calibration is made by requiring the 348th channel of the MCA to contain the Am<sup>241</sup> (5.44 MeV) peak. By a linear gain change of 5X from this pre-chosen scale it is possible to convert the initial 512 channels, spanning 0 - 8.0 MeV, to the range 0 - 1.60 MeV. At this gain setting the low energy capture spectrum can be recorded with resolution corresponding to 3.12 keV per channel. The neutron generator will be set to yield  $5 \times 10^6$  neutrons/cm<sup>2</sup>/sec with a pulse length of 100  $\mu$  sec and a pulse rate of  $2 \times 10^3$  sec<sup>-1</sup>. During the irradiation time of 100  $\mu$ sec the MCA will be gated on in the add mode in order to record the low-energy capture spectrum. Then, prior to the next neutron pulse, the analyzer will be gated on in the subtract mode in order to remove the activation spectrum from the low-energy capture spectrum. Neutron pulsing and recording will be stopped and the spectrum analyzed when a counting standard deviation of 10% is reached or when 100 counts/min. are registered for the capture peaks of interest. The low-energy capture peaks will then be analyzed as discussed in a later section. After the low-energy capture spectrum has been analyzed the high energy capture spectrum will be recorded. The gain will be set for a resolution corresponding to 15.6 keV per channel and a calibration check made using the Am<sup>241</sup> source in the detector.

After calibration, the neutron generator will be operated in the same way as for the low-energy capture gamma ray mode. The high-energy capture gamma rays will then be analyzed as discussed in a later section. Here again it is important to realize that the relative proportion of the elements in the chemical matrix is a variable in the analysis. In the various chemical matrices chosen, i.e., Cases 1, 2, 3 and 4, it is possible to identify Si<sup>28</sup> and Fe<sup>56</sup> in the low-energy spectrum and Si<sup>28</sup>, Mg<sup>24</sup> and Fe<sup>56</sup> in the high-energy spectrum of Case 1. The other cases are summarized in Tables II and III.

Minimum detectable limits for these elements under conditions of different amounts of the four elements cannot be worked out with the experimental information on hand. This is because spectra resulting from 1000 total counts for 1.0 gm of material and one-minute live count cannot be used directly to obtain spectra of equivalent counting statistics for 0.1 gm of material and a one-minute live count. The counting statistics of a real experiment have a standard deviation which is proportional to the square root of the number of gammas recorded. On the other hand, the number of counts recorded is proportional to the mass of the element present. Consequently:

$$\sigma \propto N^{1/2} \propto M^{1/2}$$

$\sigma$  = standard deviation of the measurement

$N$  = total number of gammas recorded

$M$  = mass of element present

Hence, counting statistics for a normalized elemental spectrum are scaled improperly and inferences made therefrom can be erroneous.

The detectability of the four elements in a composite matrix depends on the relative amounts of the elements present. Tables II and III only serve as a guide to which elements can be detected for specific quantities of the elements. At this point it is not fruitful to extend these conditions to exact minimum detectable limits of the four elements since this would require experimental information obtained from the laboratory model of this experiment.

#### Thermal Neutron Activation Experiment

In thermal neutron activation, neutrons having an energy less than .0250 eV are captured by target nuclei. Both capture and photopeak gamma rays can be produced, the latter deriving only from radioactive decay of a compound nucleus. The reaction can be written as:

target nuclei ( $n, \gamma$ ) product nucleus.

The gamma ray within parenthesis is the capture gamma. Activation gammas derive from the decay of the product nucleus. If thermal neutron capture produces a stable isotope, only capture gammas are observed. Capture gammas are emitted approximately  $10^{-14}$  sec after neutron capture. Activation gammas are emitted with a characteristic half life,  $T_{1/2}$ , which depends on the radioactive nucleus.

The gamma ray energies of the photopeaks are used for element identification. Once the photopeaks in the activation spectrum have been identified, it is possible to make a determination of the relative amounts of elements present. This technique is illustrated in a later section. In addition to photopeak identification, a measurement of half life can be made to augment the identification process.

Activation Reactions - - The five possible thermal neutron activation reactions of interest are listed below.

Magnesium\*  $Mg^{26} (11.2\%)(n,\gamma)Mg^{27} (\sigma = 0.036b) \frac{9.5 \text{ min}}{\beta^-} Al^{27} \text{ stable}$

photo-peak gammas:  $\gamma_1 = 1.015 \text{ MeV} (42\%)$

Aluminum  $Al^{27} (100\%)(n,\gamma)Al^{28} (\sigma = 0.24b) \frac{2.3 \text{ m}}{\beta^-} Si^{28} \text{ stable}$

$\gamma_1 = 1.782 \text{ MeV} (100\%)$

Silicon  $Si^{30} (3.1\%)(n,\gamma)Si^{31} (\sigma = 0.11b) \frac{2.6 \text{ hr}}{\beta^-} P^{31} \text{ stable}$

$\gamma_1 = 1.27 \text{ MeV} (0.07\%)$

Iron  $Fe^{58} (0.3\%)(n,\gamma)Fe^{59} (\sigma = 1.1b) \frac{49 \text{ d}}{\beta^-} Co^{59} \text{ stable}$

$\gamma_1 = 1.29 \text{ MeV} (43\%)$

$\gamma_2 = 1.10 \text{ MeV} (5\%)$

Oxygen

$O^{18} (0.20\%)(n,\gamma)O^{19} (\sigma = 0.21 \text{ mb}) \frac{29.5 \text{ s}}{\beta^-} F^{19} \text{ stable}$

$\gamma_1 = 1.6 \text{ MeV} (70\%)$

Notice that activation of  $Mg^{26}$ , whose end product nucleus is  $Al^{27}$ , could cause an interference in the detection of  $Al^{27}$  in the matrix. The detection of  $Si^{28}$  could also be ambiguous with the decay of  $Al^{28}$ . These interferences are not expected to pose any problem provided the irradiation times are kept short: for 1 gram of  $Al^{28}$  irradiated at  $10^9 \text{ n/cm}^2/\text{sec}$  for 10 minutes the production rate of  $Si^{28}$  would be too small to be detected. The same is true of  $Mg^{27}$  producing  $Al^{27}$ . It is concluded that interference will be minimal among photopeak gamma rays during neutron irradiation.

Using the activation equation with a neutron flux of  $10^9 \text{ n/cm}^2/\text{sec}$ , an irradiation time of 10 minutes, and a total absolute detector efficiency of

\* In this description of the reaction, the following identifications hold, in order from left to right:

- 1) original nucleus,
- 2) isotopic abundance of original nucleus,
- 3)  $(n,\gamma)$  reaction initiated by a neutron with a gamma ejected,
- 4) activated nucleus formed,
- 5) isotopic cross section in barns for thermal activation,
- 6) half life of activated nucleus with mode of decay,
- 7) final nucleus, stability.

\*\* Photopeak gammas and percent transitions.

4% for a source-to-detector separation of 10 cm, the following count rates have been calculated for 0.1 gm\* of each element five minutes after irradiation. Calculations are based on the most abundant gamma ray energy from decay schemes.

0.1 gm of Mg <sup>27</sup>	gives	31 counts/sec
0.1 gm of Al <sup>28</sup>	gives	1.7 x 10 <sup>3</sup> counts/sec
0.1 gm of Si <sup>31</sup>	gives	3.4 x 10 <sup>-3</sup> counts/sec
0.1 gm of Fe <sup>59</sup>	gives	10 <sup>-8</sup> counts/sec
0.1 gm of O <sup>19</sup>	gives	1.5 x 10 <sup>-5</sup> counts/sec

From these results it is clear that only Mg and Al can be detected from the decay of Mg<sup>27</sup> and Al<sup>28</sup> respectively.

Composite spectra of a chemical matrix of 0.1 gram each of the five elements of interest are reproduced in Figures 19, 20 and 21. These spectra\*\* were recorded five, fifteen, and thirty minutes after irradiation in the thermal flux of a nuclear reactor with live count of one, two and five minutes respectively. Examining the spectrum in Figure 19--taken five minutes after irradiation--a one minute live count reveals only the 1.78 MeV peak of Al<sup>28</sup>. After fifteen minutes of cooling, a two minute live count reveals three photopeaks, see Figure 20, the 1.78 MeV Al<sup>28</sup>, 1.01 MeV and 0.83 MeV Mg<sup>27</sup> photopeaks. These photopeaks were identified by channel number and then related through a calibration curve to photopeak energy. Figure 22 shows the calibration curve constructed from the calibration spectrum in Figure 23. Figures 19, 20, 21, and 23 are actual experimental plots of the data. All calculations utilized the digital spectrum data.

**Half-Life Determination** -- After the photopeaks have been detected, it is possible to make a half-life determination using the maximum activity of the photopeak. For example, in Figure 19 the Al<sup>28</sup> photopeak has a maximum disintegration rate of 1135 counts/minute. After fifteen minutes of total cooling with a two-minute live count the activity in the (peak) channel of the same photopeak is 57 counts/minute.

---

\*The results for 1 gm specimens can be obtained from these results by multiplying all calculated count rates by 10 since the count rate is directly proportional to mass.

\*\*The spectra were experimentally obtained at the Western New York Research Center after ten-minute irradiation with a flux of 10<sup>9</sup> n/cm<sup>2</sup>/sec. The spectra were recorded using a 3 x 3 NaI (Tl) detector and a 400 channel MCA.

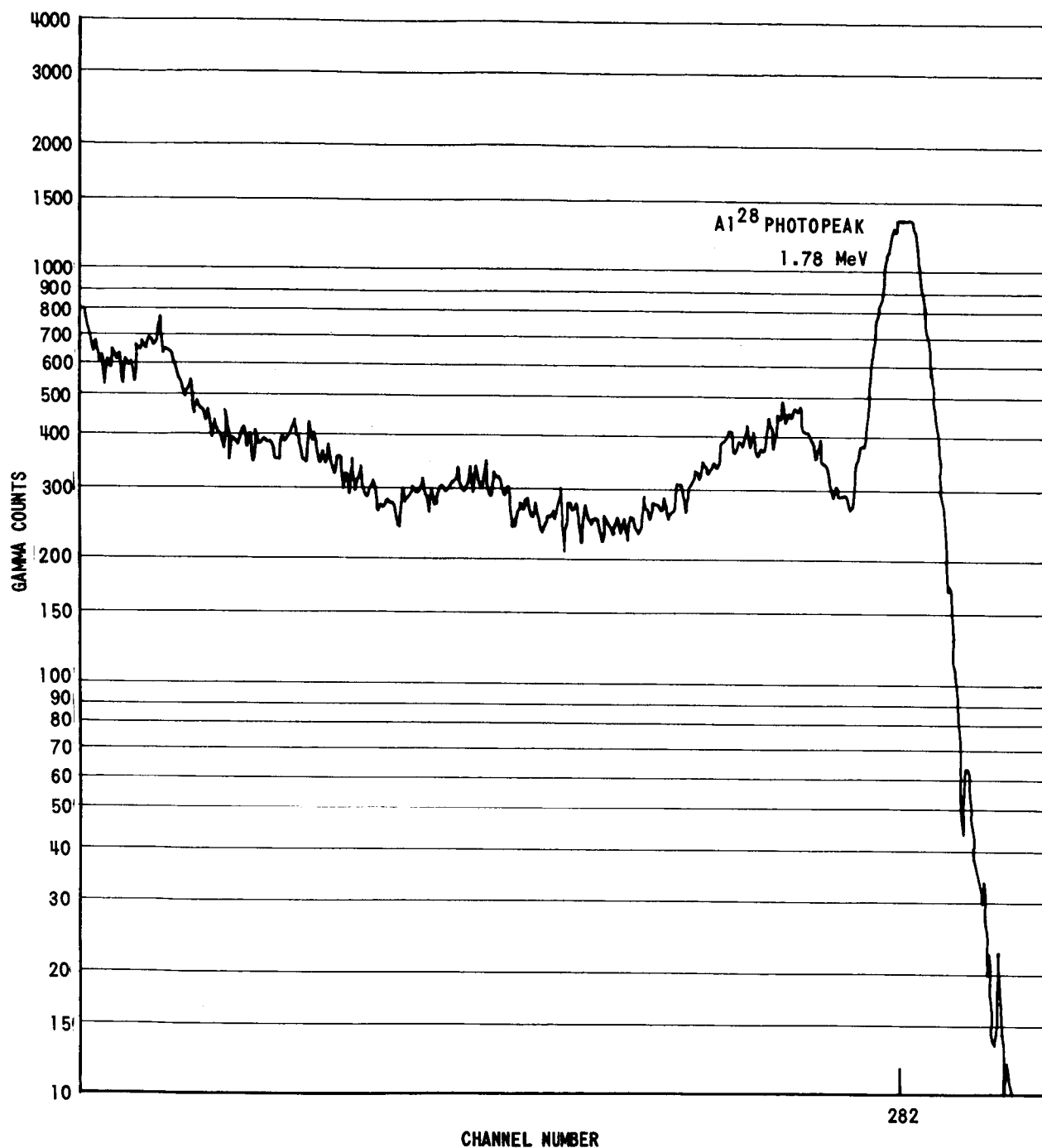


Figure 19 COMPOSITE PHOTOPEAK GAMMA SPECTRUM FOR THERMAL ACTIVATION OF SAMPLE MATRIX TAKEN 5 MINUTES AFTER IRRADIATION, SPECTRUM RECORDED FOR 1 MINUTE



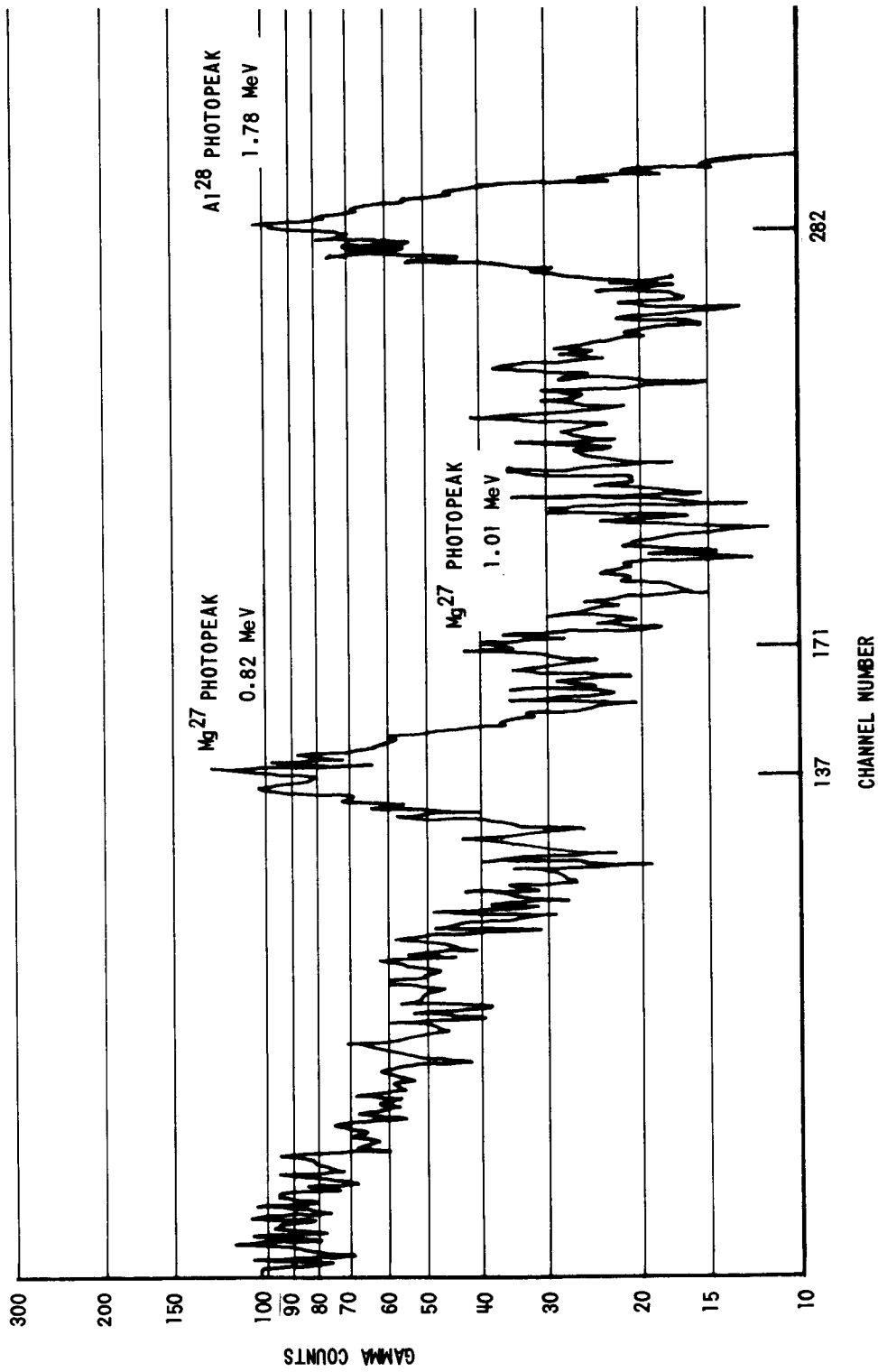


Figure 20 COMPOSITE PHOTOPEAK GAMMA SPECTRUM FROM THERMAL ACTIVATION OF SAMPLE MATRIX TAKEN 15 MINUTES AFTER IRRADIATION, SPECTRUM RECORDED FOR 2 MINUTES

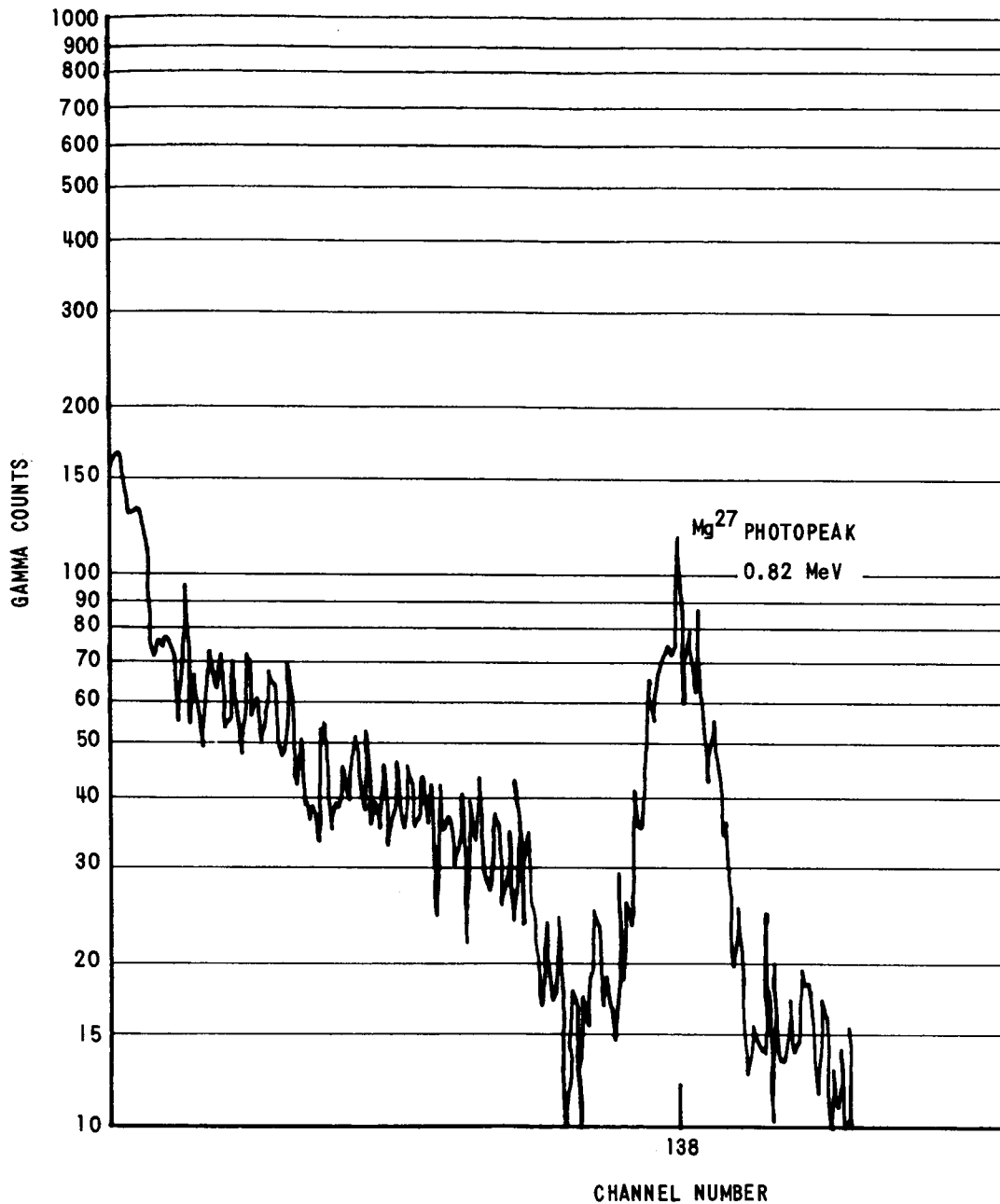


Figure 21 COMPOSITE PHOTOPEAK GAMMA SPECTRUM FROM THERMAL ACTIVATION OF SAMPLE MATRIX TAKEN 30 MINUTES AFTER IRRADIATION, SPECTRUM RECORDED FOR 5 MINUTES

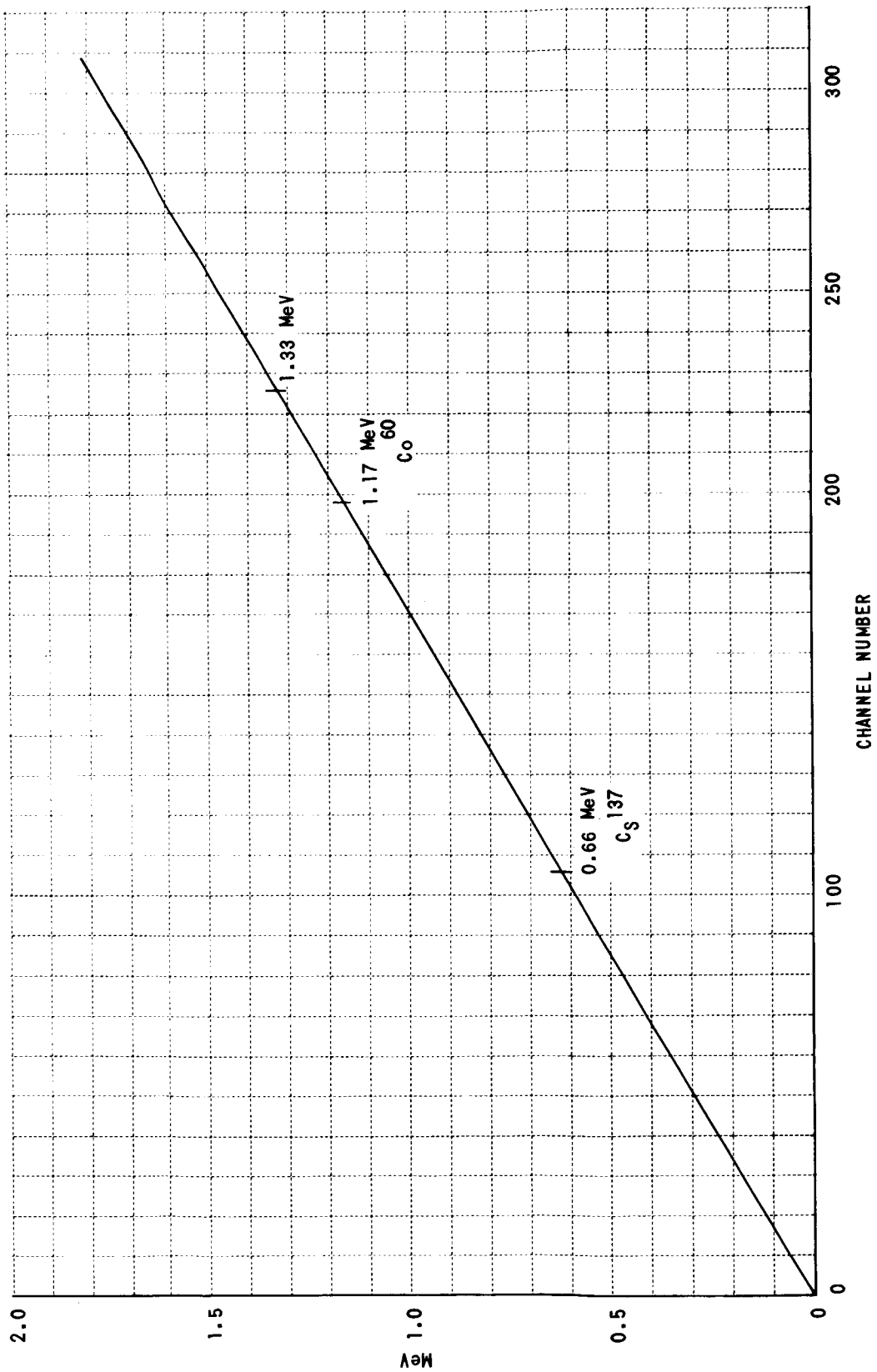


Figure 22 CALIBRATION CURVE ENERGY (MeV) vs CHANNEL NUMBER

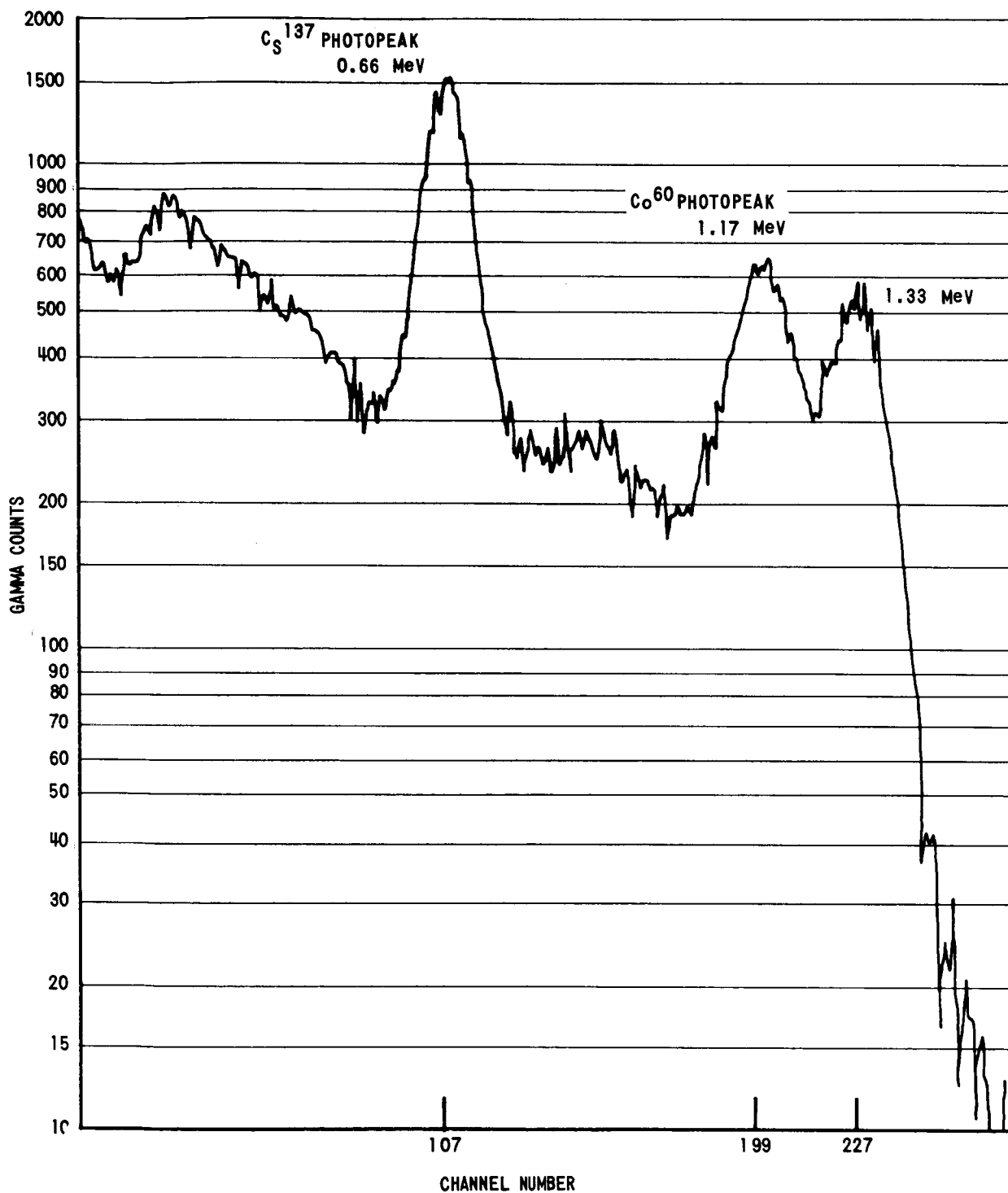


Figure 23 CALIBRATION SPECTRUM FOR THERMAL NEUTRON ACTIVATION

Cs<sup>137</sup> = 0.663 MeV

Co<sup>60</sup> = 1.17 MeV ; 1.332 MeV

Using the radioactive decay equation with  $t = 15$  minutes we have

$$A(t = 15 \text{ minutes}) = A(t = 5 \text{ min}) e^{-\frac{0.693(10)}{T_{1/2}}}$$

hence

$$57 = 1135 e^{-\frac{6.93}{T_{1/2}}}$$

$$\exp \frac{6.93}{T_{1/2}} = \frac{1135}{57} = e^{2.99}$$

$$T_{1/2} = \frac{6.93}{2.99} = 2.32 \text{ minutes}$$

The accepted half life of  $\text{Al}^{28}$  is 2.3 minutes.

Table IV summarizes the results of CW thermal neutron activation.

TABLE IV  
THERMAL ACTIVATION SUMMARY

ELEMENT	PHOTOPEAK ENERGY	PERCENT OF DECAY	HALF LIFE	DETECTABLE
$\text{Al}^{28}$	1.782 MeV	100%	2.3 MIN	YES
$\text{Mg}^{26}$	1.015 MeV	42%	9.5 MIN	YES
	0.834 MeV	58%		
$\text{Si}^{30}$	1.27 MeV	.07%	2.6 HR	NO
$\text{Fe}^{58}$	1.29 MeV	46%	49 DAYS	NO
	0.462 MeV	54%		
$\text{O}^{18}$	1.6 MeV	70%	29.5 SEC	NO

**Pulse Mode Operation for Thermal Neutron Activation** — The experimental data represented in Figures 19, 20 and 21 were obtained from a representative chemical matrix irradiated with a constant flux of  $10^9$  n/cm<sup>2</sup>/sec for 10 minutes. For the demonstration model a pulsed neutron generator will be used. Consequently, to produce an equal amount of activity, a higher neutron flux is required. Assuming 100  $\mu$ sec duration neutron pulses at a repetition rate of  $2 \times 10^3$  sec<sup>-1</sup> the total on-time is 0.2 seconds. Let  $(nt)_p$  be the product of neutron flux and live time in the pulsed mode and  $(nt)_{cw}$  be the corresponding quantity in the continuous neutron flux mode. For equal irradiation it is required that

$$(nt)_p = (nt)_{cw}$$

Hence with  $(nt)_{CW} = 10^9$  n/cm<sup>2</sup> in one second and  $t_p = 0.2$  sec.,  $n_p = 5 \times 10^9$  n/cm<sup>2</sup>/sec. This peak neutron flux rate from a pulsed neutron generator should yield the same gamma ray activity as that of the CW source.

Experimental Procedure for Thermal Activation - - Employing the calibration procedure outlined in a later section the 5.44 MeV Am<sup>241</sup> photopeak can be placed in channel 348 of a 512 channel MCA. This gain setting corresponds to resolution of 15.6 keV per channel. The neutron generator will be set to produce  $5 \times 10^9$  n/cm<sup>2</sup>/sec with a pulse duration of 100  $\mu$  sec and a pulse repetition rate of  $2 \times 10^3$  pulses/sec. Irradiation will be carried out for 10 minutes; then after a cooling time of 1 minute, the photopeak gamma ray spectrum will be recorded for 1 minute. The photopeaks will be located according to a scheme outlined in a later section. The only photopeak anticipated in this spectrum is the 1.78 MeV gamma of Al<sup>28</sup> which will fall in channel 114 for the chosen gain setting. The number of counts in the peak channel of this photopeak and the total elapsed time after irradiation will be stored in computer memory for the later half-life measurement. After a total cooling time of fifteen minutes, a new photopeak spectrum will be recorded for two minutes. In this spectrum three photopeaks will be identifiable: the Al<sup>28</sup> photopeak in channel 114 (1.78 MeV) and two Mg<sup>27</sup> photopeaks - one in channel 65 (1.01 MeV) and one in channel 53 (0.82 MeV). The count in the peak channel associated with the photopeak and the total elapsed time after irradiation will also be stored in computer memory for half life determination.

#### Fast Neutron Prompt Gamma Experiment

Prompt gammas are those arising from inelastic scattering of neutrons from the target nuclide. In the case of inelastic scattering, the compound nucleus (formed by the neutron and target nuclide) decays by neutron emission, leaving the original nuclide in an excited state. The gamma transitions, in general to the ground state, are then characteristic of the target nuclide. In principle, analysis can proceed by irradiating the target and detecting the prompt gammas arising from inelastic scatter. This is accomplished by accepting for pulse height analysis only those gammas arriving at the detector at a time determined by neutron time of flight to the target plus gamma time of flight from target to detector. Since prompt gammas are characteristic of the target nuclide, there is less concern with secondary reactions within the matrix than with the capture and activation modes. In the laboratory, samples to be analyzed are prepared to be sufficiently thin that neutron energy degradation is unlikely so that all gammas produced can be regarded as originating from 14.3 MeV neutrons from the accelerator. A remote analysis does not afford the possibility of sample control so that activation of excited levels by neutrons of other energies would have to be taken into account.

A useful treatment of fast neutron inelastic scattering utilized samples in the form of a ring, so that multiple scattering was eliminated. For this geometry, minimum detectable abundance factors were then calculated. Application of these abundance factors directly to a remote analysis is not feasible

since the geometry is markedly different. In addition, with samples of gross dimensions, effects of Compton scattering and photoelectric absorption on the gamma spectra must be taken into account. Furthermore, since many inelastically excited peaks lead to high energy transitions, pair-production absorption will also be significant. Owing to the timing electronics, and the fact that the neutron burst must be of short time duration (of the order of 5 nanoseconds) to insure differentiation of the inelastically scattered gammas from others, dead time corrections are significant. Also, neutron flux is correspondingly low, hence long data acquisition times are required. Nonetheless, inelastic scattering was thought to be a fruitful approach, but because of the significant differences between the data available and that required for the laboratory model, empirical data would have to be acquired. Because of de-emphasis of the program during the fourth quarter, acquisition of this data was not undertaken. Consequently, quantitative results are not available and a prompt gamma experimental procedure for the laboratory model is not in hand. However, available prompt spectra for the ring geometry can be utilized qualitatively as an indication of the method's applicability.

Prompt spectra for 14.3 MeV neutron activation of Fe, Si, Mg, Al and  $O^{(5)}$  are shown in Figures 24-28. These spectra were obtained for  $2.5 \times 10^{11}$  neutrons, except for O in which case  $5 \times 10^{11}$  neutrons were utilized. The line in Fe, Figure 24, at 0.84 MeV is associated with  $2^+$  first level of  $Fe^{56}$ . Estimates of sensitivity indicate that a 0.1% abundance of Fe could be detected based on this line. (These estimates do not necessarily apply to the laboratory model as mentioned previously.) The 1.78 MeV gamma in Si, Figure 25, is the  $2^+$  level of  $Si^{28}$ , the other lines are associated with  $Si^{29}$ . The abundance factor for  $Si^{28}$  is 0.5%. The first excited level of  $Mg^{24}$  is at 1.37 MeV ( $2^+$ ), and leads to the peak shown in Figure 26. Peaks at 0.88 and 1.82 MeV are due to the (5.1-4.2)  $Mg^{24}$  transition and the  $Mg^{26}$  first level transition. The 1.37 peak is smeared by the  $Si^{29}$  1.28 MeV peak, and spectrum striping would be necessary for its resolution. The 1.01 MeV peak for  $Al^{27}$  is prominent but could be masked by the  $Si^{29}$  0.98 MeV peak. Based on the 2.20 MeV peak, an abundance of 2% is determined. The O spectrum is unique in that the 6.14 MeV level plus the (6.14-1.02) MeV annihilation escape peak at 5.12 and the (6.14-1.02+.51) level at 5.63 MeV are present at high energy and can serve as an unambiguous indication of  $O^{16}$ . The cross section is low however.

These considerations lead to the conclusion that inelastic scattering could form a useful adjunct to the capture and activation modes of analysis, but that adequate empirical data must be acquired to allow reliable estimation of minimum detectable abundances.

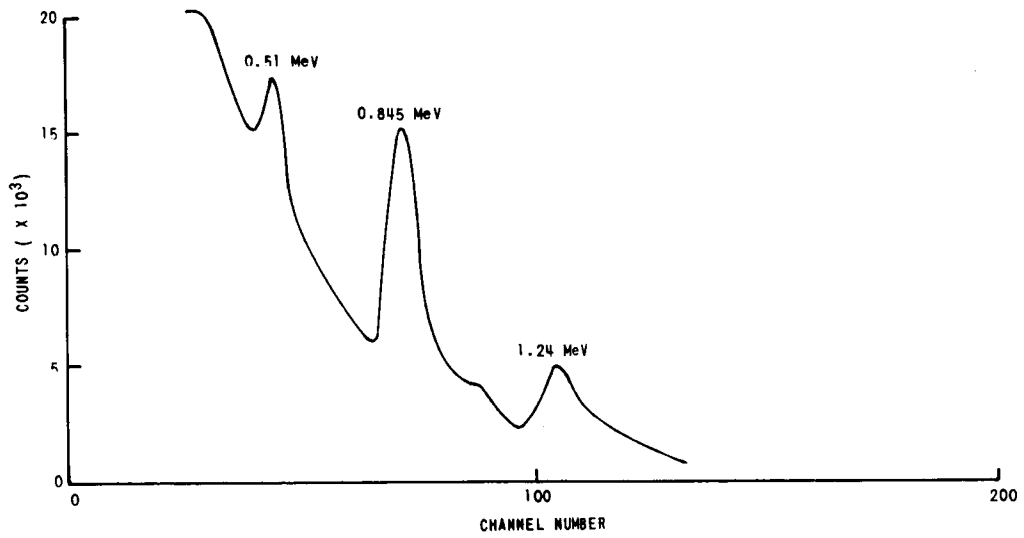


Figure 24 PROMPT GAMMA SPECTRUM OF Fe

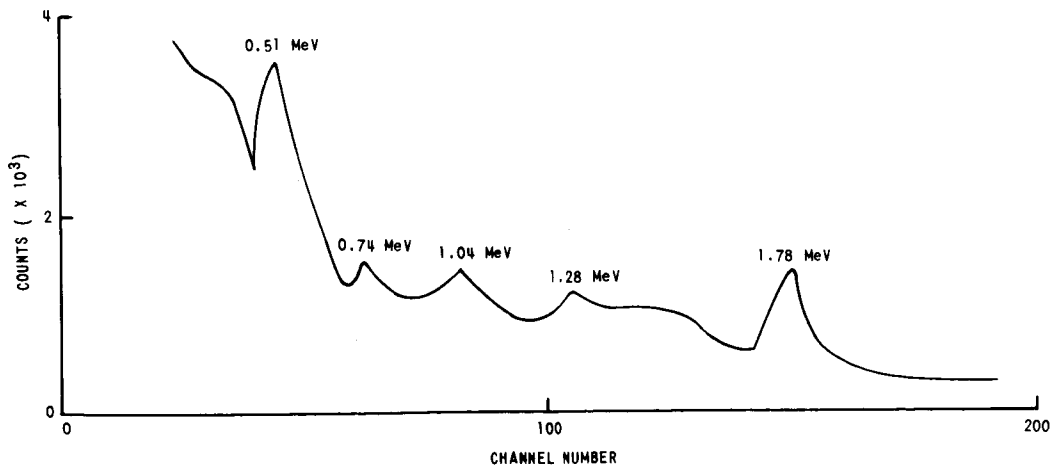


Figure 25 PROMPT GAMMA SPECTRUM OF Si



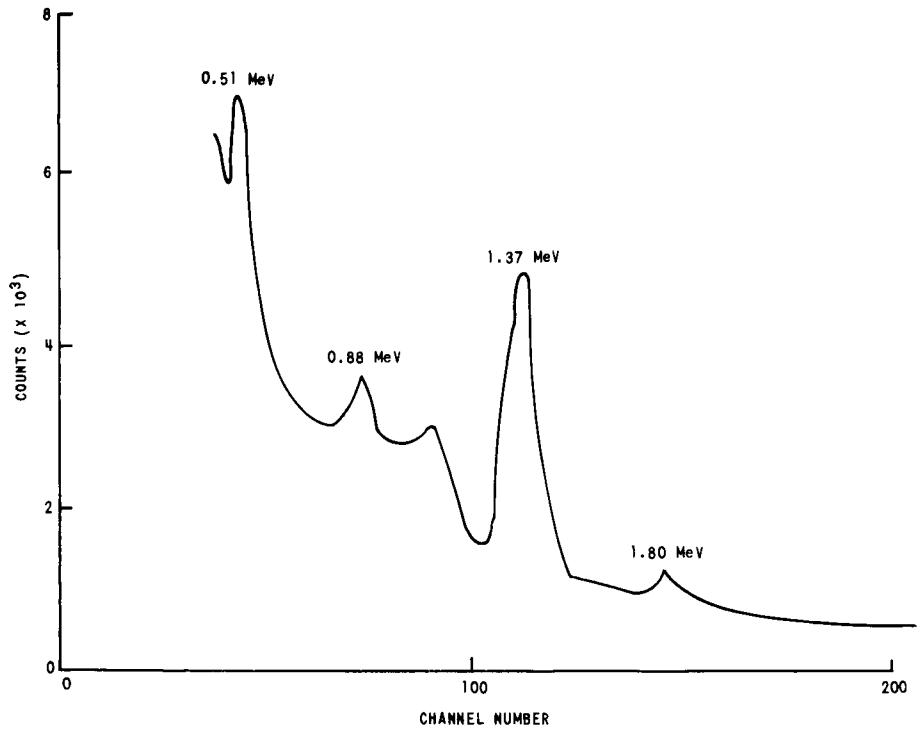


Figure 26 PROMPT GAMMA SPECTRUM OF Mg

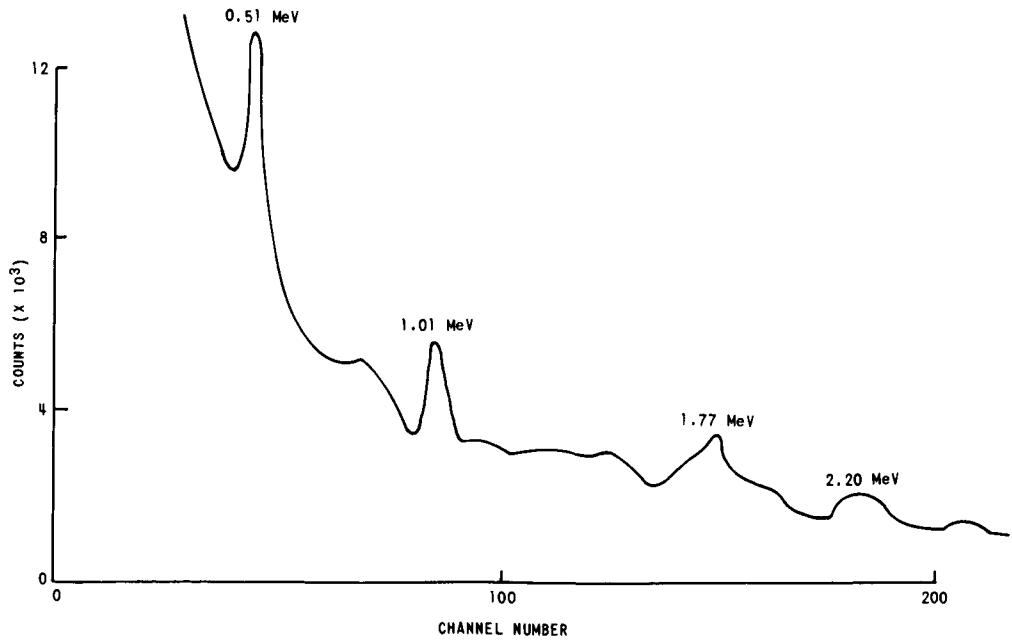


Figure 27 PROMPT GAMMA SPECTRUM OF Al

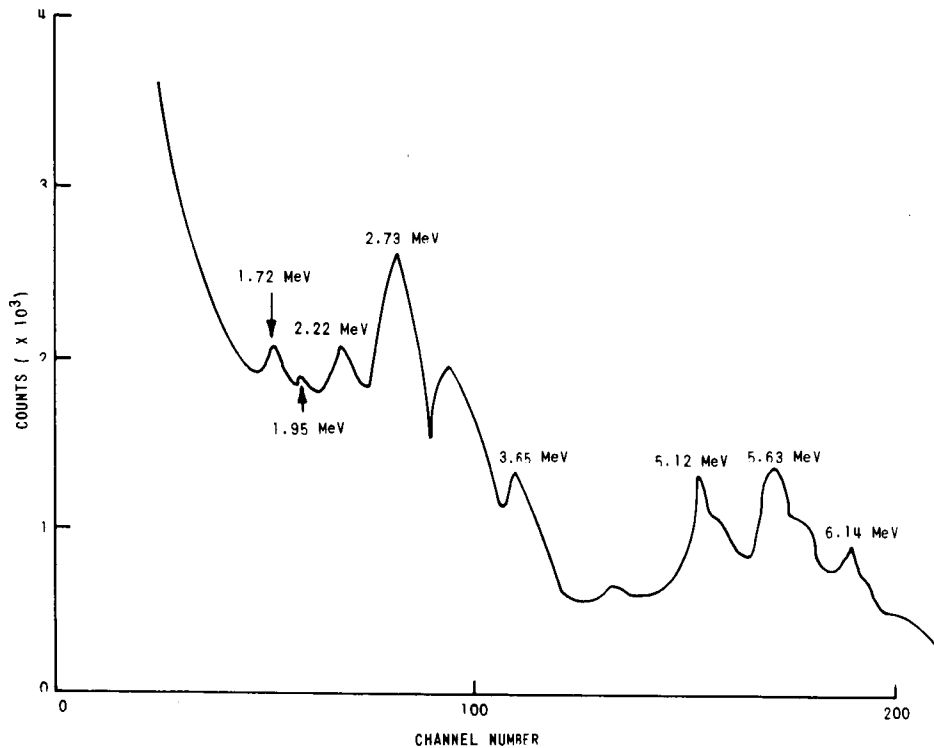
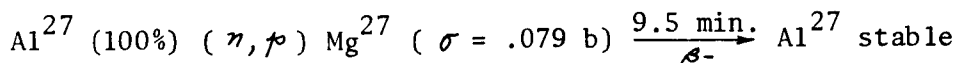


Figure 28 PROMPT GAMMA SPECTRUM OF O

#### Fast Neutron Activation Experiment

In this mode fast neutrons (14.3 MeV) from the pulsed neutron generator bombard the element matrix and undergo  $(n, p)$ ,  $(n, \alpha)$  or  $(n, 2n)$  reactions. These reactions produce nuclei which are radioactive and which emit radiations characteristic of the nucleus. The energy levels of the detected activation gammas are used to determine the elements present in the unknown matrix. It is also possible to deduce the element's identity by a half-life measurement based on the decay of the radioactive nucleus formed. Activation analysis, using fast neutrons, for the elements of interest is discussed in References (6) and (7). Activation analysis of a chemical matrix consisting of Al, Si, Mg, Fe and O in the presence of other unknown elements is extremely difficult due to the large number of interferences which are possible. Since this study is concerned primarily with the adaptive aspects of the problem, the chemical matrix consisting only of the above five elements is of concern. Interferences among these five elements then represent the only source of ambiguity. The reactions which result from the fast neutron bombardment and which yield activation gammas are listed below. Only fast neutrons are considered here; however, if the neutron beam undergoes partial thermalization then thermal activation gammas will also be produced; the extent of the interference produced by this process should be determined experimentally.

**Fast Neutron Activation Reactions** - - The possible reactions in this mode of element identification for the five elements in the matrix are listed below.\*

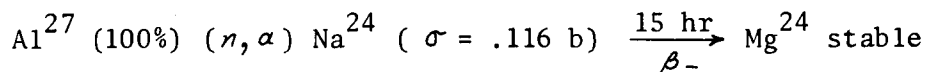


$$\gamma = 1.015 \text{ MeV (42.1\%)}$$

$$\gamma = 0.834 \text{ MeV (58.0\%)}$$

$$\gamma = 0.175 \text{ MeV (0.8\%)}$$

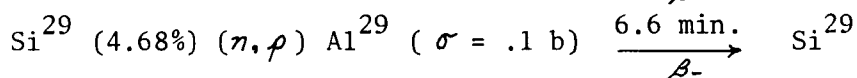
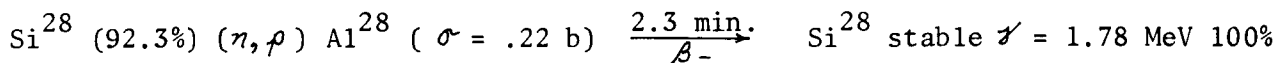
Interference from  $\text{Si}^{30} (n, \alpha) \text{Mg}^{27}$



$$\gamma = 2.75 \text{ MeV (100\%)}$$

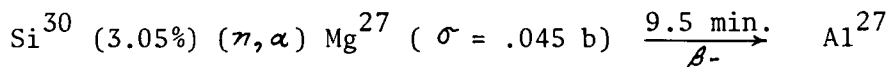
$$\gamma = 1.37 \text{ MeV (100\%)}$$

Interference from  $\text{Mg}^{24} (n, p) \text{Na}^{24}$



$$\gamma = 1.28 \text{ MeV (93.8\%)}$$

$$\gamma = 2.43 \text{ MeV (6.2\%)}$$

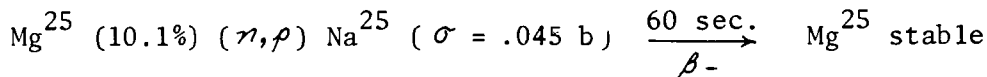


$$\gamma = 1.015 \text{ MeV (41.2\%)}$$

$$\gamma = 0.834 \text{ MeV (58\%)}$$

$$\gamma = 0.175 \text{ MeV (0.8\%)}$$

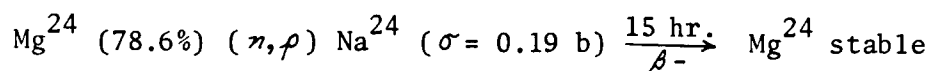
Interference from  $\text{Al}^{27} (n, p) \text{Mg}^{27}$



\* See page 31 for an explanation of the reaction format.

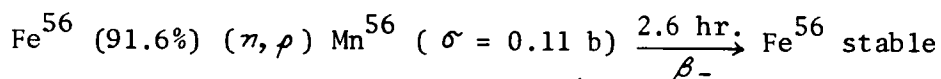
\*\* These values, for the fraction of decay producing the gamma ray given, were taken from tabulated values in Nuclear Data Sheets.

$$\begin{aligned} \gamma &= 1.60 \text{ MeV (6.5\%)}^* \\ \gamma &= 0.98 \text{ MeV (14.25\%)}^* \\ \gamma &= 0.58 \text{ MeV (14.25\%)}^* \\ \gamma &= 0.40 \text{ MeV (14.25\%)}^* \end{aligned}$$

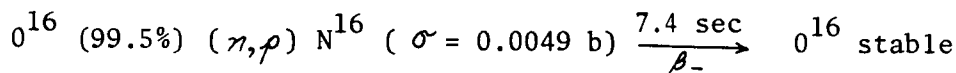


$$\begin{aligned} \gamma &= 2.75 \text{ MeV (100\%)} \\ \gamma &= 1.37 \text{ MeV (100\%)} \end{aligned}$$

Interference from  $\text{Al}^{27} (\text{n}, \alpha) \text{Na}^{24}$



$$\begin{aligned} \gamma &= 2.96 \text{ MeV (0.45\%)}^* \\ \gamma &= 2.66 \text{ MeV (0.48\%)} \\ \gamma &= 2.12 \text{ MeV (14.5\%)} \\ \gamma &= 1.81 \text{ MeV (23.5\%)} \\ \gamma &= 0.845 \text{ MeV (98.0\%)} \end{aligned}$$



$$\begin{aligned} \gamma &= 7.13 \text{ MeV (20\%)} \\ \gamma &= 6.13 \text{ MeV (55\%)} \end{aligned}$$

From these activation reactions it is possible to determine which activation photopeaks are realizable. The results of calculations of the measured activity from one gram of each element irradiated for 60 seconds by a neutron flux of  $10^8 \text{ n/cm}^2/\text{sec}$  are given in Table V.

---

\* These values, for the fraction of decay producing the gamma ray given, were taken from tabulated data in Nuclear Data Sheets.

TABLE V  
COMPUTED ACTIVITIES FOR SEPARATE IRRADIATIONS

REACTION	PHOTOPEAK GAMMA MeV	ACTIVITY IN COUNTS/SEC	INTERFERENCE
$Al^{27}(n, p)Mg^{27}$	0.834	140.0	$Si^{30}(n, \alpha)Mg^{27}$
$Al^{27}(n, \alpha)Na^{24}$	2.75	0.104	$Mg^{24}(n, p)Na^{24}$
	1.37		
$Si^{28}(n, p)Al^{28}$	1.78	2260.0	NONE
$Si^{29}(n, p)Al^{29}$	1.28	170.0	NONE
$Si^{30}(n, \alpha)Mg^{27}$	0.834	2.24	$Al^{27}(n, p)Mg^{27}$
$Mg^{25}(n, p)Na^{25}$	0.58	22.0	NONE
$Mg^{24}(n, p)Na^{24}$	2.75	0.146	$Al^{27}(n, \alpha)Na^{24}$
	1.37		
$Fe^{56}(n, p)Mn^{56}$	0.845	4.4	NONE
$O^{16}(n, p)N^{16}$	6.13	$1.58 \times 10^3$	NONE

1 GRAM OF EACH ELEMENT, FLUX =  $10^8$  NEUTRONS/CM<sup>2</sup>/SEC,  
IRRADIATION TIME 60 SEC

If the counting standard deviation ratio is 10%, it should be possible to detect those elements having a count rate of 1.6 counts/sec. Elements which have this count rate listed are  $Al^{27}$ ,  $Si^{28}$ ,  $Si^{29}$ ,  $Mg^{25}$ ,  $O^{16}$  and  $Fe^{56}$ . The interferences listed in Table V do not introduce any ambiguous results since the interferences do not have high activities for the short irradiation assumed. All the detectable elements have unique photopeaks except  $Al^{27}$  and  $Fe^{56}$  each of which has a photopeak of like energy. This interference can be eliminated, however, if the spectrum is recorded after specific cooling times, since the activities decrease in accordance with the element's half life. Since the half life for the  $Fe^{56}(n, p)Mn^{56}$  reaction is 16.4 times larger than the half life of the  $Al^{27}(n, p)Mg^{27}$  reaction it will persist longer. The measurable photopeak energies in a composite spectrum depend on the uniqueness of individual photopeaks when all are measured simultaneously. This determination can best be answered experimentally. The details of the element identification given below are based on the uniqueness of photopeaks given in Table V.

After one minute neutron irradiation and cooling time sufficient to eliminate radiation from capture gammas (approximately  $500\mu$  sec) the spectrum is recorded for two seconds live count. The spectrum is then examined, according to the technique described in a later section for the appropriate energy peaks. The photopeaks of  $\text{Si}^{28} (n, \rho) \text{Al}^{28}$  and  $0^{16} (n, \rho) \text{N}^{16}$  should be evident from this analysis. The number of counts in the peak channel is recorded for these photopeaks as well as time; this latter information is subsequently used for half life determination. A new spectrum is then recorded after a total cooling time of approximately 25 seconds for a live time of two seconds. This spectrum should indicate the presence of the following reactions:  $\text{Al}^{27} (n, \rho) \text{Mg}^{27}$ ;  $\text{Si}^{28} (n, \rho) \text{Al}^{28}$ ;  $\text{Si}^{29} (n, \rho) \text{Al}^{29}$ ;  $\text{Mg}^{25} (n, \rho) \text{Na}^{25}$  and  $0^{16} (n, \rho) \text{N}^{16}$ . Again the necessary information for half-life determination is recorded. Sufficient information should be at hand at this point to determine the presence of  $\text{Si}^{28}$  and  $0^{16}$ , both by photopeak energies and by a half-life determination. Measuring the photopeak energies and activity of a third spectrum recorded after a total cooling time of one minute with a live count of one minute should give energy levels and half-life information for  $\text{Al}^{27}$ ,  $\text{Mg}^{25}$  and  $\text{Si}^{29}$ . In order to detect  $\text{Fe}^{56}$  it is necessary to cool the specimen for one hour, after which the activity from the  $\text{Al}^{27} (n, \rho) \text{Mg}^{27}$  will have been reduced to 1.4% of its value after irradiation. On the other hand, the  $\text{Fe}^{56} (n, \rho) \text{Mn}^{56}$  activity will be at 75% of its value after irradiation. The decrease in count rate should be measurable thereby affording a half-life determination. Summary of the reactions best suited for fast neutron activation is given in Table VI.

TABLE VI  
SUMMARY OF REACTIONS AND DETECTOR SCHEMES FOR  
 $\text{Al}^{27}$ ,  $\text{Si}^{28}$ ,  $\text{Mg}^{25}$ ,  $\text{Fe}^{56}$ , AND  $0^{16}$

REACTION	PHOTOPEAK ENERGY SCHEME	HALF LIFE DETERMINATION SCHEME
$\text{Al}^{27} (n, \rho) \text{Mg}^{27}$	YES (0.834 MeV)	YES (9.5 MIN)
$\text{Si}^{28} (n, \rho) \text{Al}^{28}$	YES (1.78 MeV)	YES (2.3 MIN)
$\text{Mg}^{25} (n, \rho) \text{Na}^{25}$	YES (0.58 MeV)	YES (60 SEC)
$\text{Fe}^{56} (n, \rho) \text{Mn}^{56}$	NO (0.84 MeV)	YES (2.6 HR)
$0^{16} (n, \rho) \text{N}^{16}$	YES (6.1 MeV)	YES (7.6 SEC)

**Half-Life Determination** — — The half life measurement method discussed in pages 32-38 applies here and is extended to include the determination of half life when the same photopeak is used for two elements. Consider the activity of the  $Al^{27}$  ( $n, \rho$ )  $Mg^{27}$  reaction and the  $Fe^{56}$  ( $n, \rho$ )  $Mn^{56}$  plotted as a function of time on semi log paper, Figure 29. After a cooling period of one hour the  $Mg^{27}$  activity is 1.8 counts/sec and the  $Mn^{56}$  activity is 3.260 counts/sec. The radioactive decay of these elements is given by the following equation for  $Mg^{27}$ :

$$A_{(Mg^{27})} = 1.8 \exp \frac{-0.693 t}{9.5 (60)}, \text{ for } t \text{ in seconds,}$$

and by the

$$A_{(Mn^{56})} = 3.26 \exp \frac{-0.693 t}{2.5 (3600)}, \text{ for } Mn^{56}$$

The starting activity is given by the sum of the two equations evaluated at the start of the recording period, i.e.:

$$A = A_{(Mg^{27})} t = 0 + A_{(Mn^{56})} t = 0$$

The measured activity for  $Mg^{27}$ , after 9.5 minutes is equal to 1/2 of its starting value of 1.8; the same principle applied to  $Mn^{56}$  for its half life yields the two straight line plots shown in Figure 29. The sum of these two lines gives the total activity from the single photopeak. The slope of the best straight line fit for the straight part of the composite radioactive decay curve is given by:

$$\text{Slope} = \frac{-0.693}{T_{1/2}} \text{ from which the half life of } Fe^{56} \text{ is calculated.}$$

Any background contribution should only affect the level of the activity curve but not its slope, therefore, the method should be independent of background level. If the background activity is not constant, the first part of the composite activity curve will be different from that shown. However, the long life of  $Mn^{56}$  should dominate the activity curve after several halflives of the background material have passed.

**Pulsed Mode Operation** — — The timing diagram described earlier on page 9 utilized a  $1 \mu$  sec neutron pulse to minimize the interference by thermal and fast activation gammas with the prompt spectrum. In the fast neutron activation mode, however, it is necessary to obtain high activity in a short time; consequently, gammas produced during the irradiation are unimportant in this mode of analysis. The neutron generator will be set to give a  $100 \mu$  sec pulse at a pulse repetition rate of  $10^4$  pulses/second producing a continuous neutron flux. The specimen will be irradiated for one minute with a flux of  $10^8$  n/cm<sup>2</sup>/sec and several photopeak gamma ray spectra will be accumulated and analyzed.

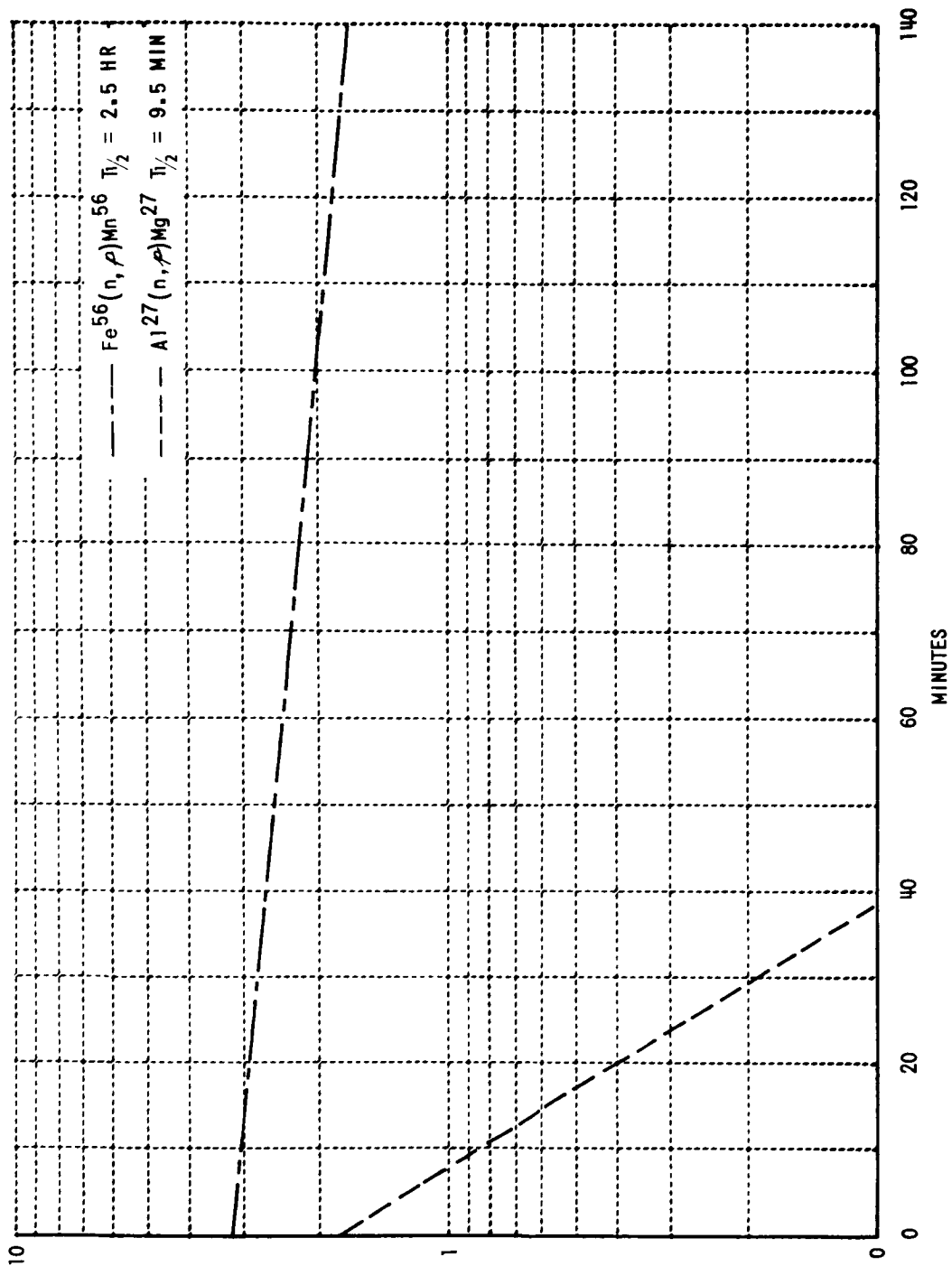


Figure 29 HALF LIFE DETERMINATION FOR  $\text{Mn}^{56}$  USED TO DETECT PRESENCE OF  $\text{Fe}^{56}$  ACTIVITY OF .834 MeV PHOTOPeAK



**Experimental Procedure for Fast Activation** - - The gain of the amplifier is set, via the calibration procedure, to record the 6.1 MeV photopeak from the  $^{16}\text{O}(\text{n},\rho)\text{N}^{16}$  reaction in channel 390. This setting corresponds to channel resolution of 15.6 keV. The 1.78 MeV photopeak from the  $\text{Si}^{28}(\text{n},\rho)\text{Al}^{28}$  will therefore be recorded in channel 114. The neutron generator is set to operate in the continuous mode with a flux of  $10^8$  neutrons/cm<sup>2</sup>/sec; the element matrix containing a sample (say) of each of the following elements, Al, Si, Mg, Fe and O is irradiated for one minute with this flux; and the spectrum is then recorded. The information obtained from subsequent recording of spectra, after specific cooling times, is given in Table VII.

TABLE VII  
SUMMARY OF TIMES TO RECORD SPECTRUM

ELEMENT DETECTED	LIFE TIME	TOTAL COOLING TIME AFTER IRRADIATION	SPECTRUM NO.	ELEMENTS IDENTIFIED BY
$\text{Al}^{27}, \text{Si}^{28}$	2 SEC	500 $\mu$ SEC	1	PHOTOPEAK ENERGIES
$\text{Al}^{27}, \text{Si}^{28}$ $\text{Si}^{29}, \text{Mg}^{25}, \text{O}^{16}$	2 SEC	25 SEC	2	PHOTOPEAK ENERGIES
$\text{Al}^{27}, \text{Mg}^{25}, \text{Si}^{29}$	1 MIN	1 MIN	3	HALF LIFE
$\text{Fe}^{56}$	2.5 HR	1 HR	4	HALF LIFE

**Miscellaneous Considerations**

Level and spectrum of background radioactivity, presence of hydrogenous material and detector characteristics are pertinent factors in performing an accurate, complete analysis of unknown elements.

**Radioactive Background** - - Both the level and spectrum of background radioactivity require adaptive schemes for accurate elemental analysis. After the electronic and source-in-detector calibration have been completed and prior to the neutron generator activation calibration, a background spectrum will be accumulated for a live count equal to the longest live count required in the proposed experiments. This spectrum will be examined to estimate level of activity and determine whether significant photopeaks exist therein. If the spectrum is uniform and activity is low, relative to the activity produced by the neutron generator, subtraction of the background spectrum from the experimental spectra will be unnecessary because photopeak locations will not be distorted. On the other hand, for half-life measurements, corrections for

background level must be made since the value of the spectral peak is used. Correction can be effected by subtracting the background count rate suitably scaled for live time, from the count rate in the channel of interest. Alternatively, the MCA can be operated in the MCS mode to obtain a plot of count rate versus time, i.e., a radioactive decay curve for the elements of interest. Half life can then be calculated from the experimental decay curve.

If the background spectrum has significant structure it will be necessary to compensate the experimental spectra for the background. Background spectra will be stored in computer memory for use as required.

In the event the background activity is high, in excess of  $10^5$  counts/sec, pulse pile-up and gain shifts will result. To cope with this, double-differentiation pulse-shaping methods may prove useful. Hence, radioactive background can be accommodated to an extent by providing a scheme to subtract it from experimental spectra or, if it is intense, by using pulse shaping techniques.

**Hydrogenous Material** -- The presence of hydrogenous material will be detected, in the thermal neutron mode, by the presence of the 2.22 MeV capture gamma ray from hydrogen. To cope with large concentrations of hydrogen some adaptive scheme must be provided. Two cases could give rise to the 2.22 MeV hydrogen capture gamma ray: a hydrogen-rich gas or liquid between the neutron generator and the sample, and/or hydrogen in the sample.

The presence of high concentrations of hydrogen between the neutron generator and the sample attenuates the neutron beam. More important, however, is thermalization of the neutron beam used in the proposed fast neutron experiments. For a flyable system these possibilities point directly to a need to measure the neutron flux and energy at the location of the sample prior to performing any experiments. Knowledge of these parameters is also important when hydrogen is present within the sample. In the latter case the 2.2 MeV capture gamma is observed, but the proposed experiments are unaffected, because the neutron beam is not thermalized.

The thermal neutron mode could be performed first to detect the presence of hydrogen and to inform the adaptive controller of the presence of hydrogen. Once hydrogen has been detected, it will be necessary to determine whether or not the beam is being thermalized. In a flyable model of the system, a solid state neutron detector could be lowered into the sample area and the neutron flux and energy measured. The thermal neutron mode can operate in the presence of hydrogenous material, but attenuation of the neutron flux by the hydrogenous material will require longer irradiation and live-count times. This condition can be ascertained by the controller after analyzing the neutron spectrum. For the laboratory model only the presence of a hydrogenous material will be ascertained.

The fast neutron mode will be seriously effected by thermalization of the neutron beam because all cross sections used in the analysis assume 14 MeV neutrons. Experimental yields will be smaller than expected if the neutron beam is attenuated. Additionally, many more reactions are possible thereby

confusing the analysis. If thermalization of the beam occurs it may be preferable to abandon the fast neutron mode; this tack is taken in the laboratory model.

In summary, the following procedure should be employed prior to experimentation:

- (1) lower neutron detector onto sample surface (flyable system);
- (2) irradiate with thermal neutrons;
- (3) check capture gamma for 2.22 MeV capture gamma ray indicative of hydrogen;
- (4) determine by analysis of neutron spectrum whether neutrons are being thermalized (flyable system);
- (5) correct irradiation and live count times for thermal mode, if neutrons are being thermalized.

**Detector Resolution** -- The pulse height resolution of a detector system is defined as its ability to discriminate between two pulses of nearly the same energy. The voltage pulses are produced when gamma rays from neutron excitation of the elemental matrix interact with the scintillation crystal. The resolution of a detector system is calculated as the ratio of the width of the photopeak at half maximum to the energy of the photopeak; resolution of a 3" x 3" NaI (Tl) detector is shown in Figure 30. The figure shows that resolution is not constant but decreases as the energy of the particles increases. The anticipated width of a spectral line is a direct function of detector resolution.

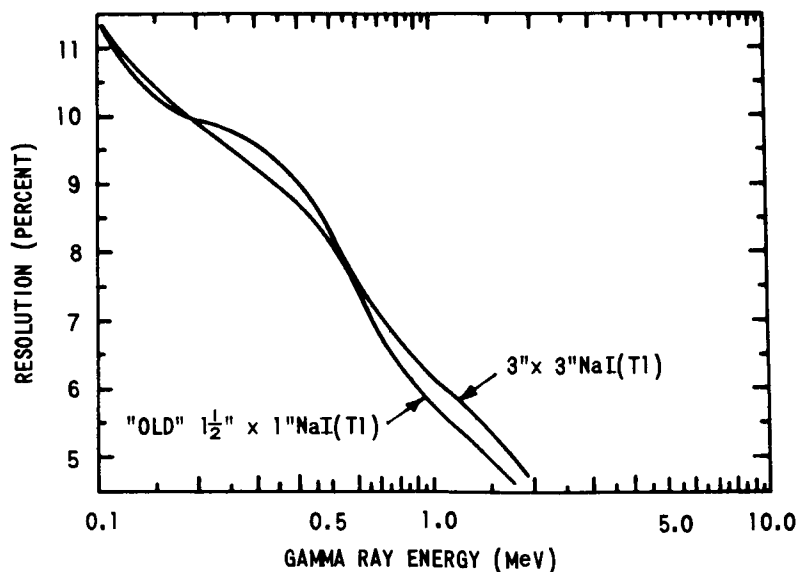


Figure 30 ENERGY RESOLUTION FOR 3" x 3" NaI(Tl) SCINTILLATION DETECTORS

Other characteristics of the detector are its stability in the long term (drift at constant count rate) and short term (gain shift with change in count rate). Both resolution and long term stability can be estimated and corrected by using a source-in-detector arrangement. Short term stability cannot be fully measured since a high count rate is not possible with the source-in-detector. Use of the chromium calibration standard to check for gain shifts produced by a count rate change may be possible. However, further study is required.

Use of a dual crystal detector assembly, Reference (6) to reduce the Compton contribution in the spectra may permit more precise analysis of the low energy gamma ray spectrum. Currently available information indicates reduction by a factor of two in the Compton background.

**Temperature Variations** -- The response of the detector is temperature dependent and will cause distortion of the spectra unless compensated. Small temperature variations about a nominal operating temperature can be compensated by the source-in-detector/digital stabilizer discussed later.

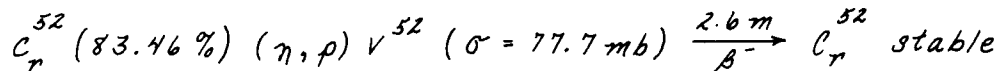
### **Calibration of the Neutron Excitation Experiment**

Prior to performing the neutron excitation experiments the multichannel analyzer (MCA), amplifier, detector and neutron generator must be calibrated. Calibration comprises adjustment of system gain so that the sensor configuration observes a prescribed energy band with prescribed resolution and estimation of the incident neutron flux. Calibration of the MCA, amplifier-detector combination is accomplished by adjusting amplifier gain and MCA analog-to-digital converter zero to force energy peaks to fall within prescribed MCA channels. The neutron generator output is estimated by measuring the activity of a known amount of a known element. Calibration is accomplished in three phases as follows.

**Preliminary Calibration** -- To simplify somewhat the demonstration model and reduce its costs, a human operator is employed to perform an equipment check and an approximate calibration. Preliminary calibration of the MCA and detector amplifier can be accomplished by applying pulses from (say) a mercury-relay pulser to the input of the detector amplifier. The pulse generator is adjusted to output pulses of amplitudes between  $V$  and  $V+\Delta V$  and the gain of the amplifier is adjusted so that these pulses are recorded in an appropriate channel. A similar measurement is made with another pulse amplitude and the MCA zero adjusted so these pulses are recorded in the appropriate channel. The operator would also verify functioning of the neutron generator.

**Calibration by Fast Neutron Activation** -- Subsequent to preliminary calibration by the operator, the instrumentation will be automatically calibrated in a fast neutron activation mode using high-purity chromium 52 as the target material. System gain and zero offset will be adjusted and neutron flux estimated.

To eliminate interferences, 100% Cr<sup>52</sup> will be employed as the calibration reference. Chromium 52 undergoes the following fast neutron reaction:



Decay of V<sup>52</sup> to Cr<sup>52</sup> occurs with the  $\beta^-$  particle in cascade with a 1.45 MeV gamma ray. System gain will be automatically adjusted to place this energy peak in a prescribed channel of the MCA. Intensity of the 1.45 MeV gamma will be used to estimate the neutron flux for subsequent mass measurements. The detector configuration will be that typical of a point source located 10 cm from the 3" x 3" NaI (Tl) detector. Since the detector does not intercept all emitted gammas, correction of the measured count rate by means of the efficiency of the detection process is necessary. Efficiency is defined as the fraction of gamma rays emitted from a point source which interacts with the detector for a given geometry. A typical total absolute detector efficiency curve (8) is shown in Figure 31. Total absolute efficiency for the 1.45 MeV gamma for the source at a distance of 10 cm from the detector is 1.6%.

Incident neutron flux can be estimated as follows, the theoretical activity of a piece of chromium foil weighing 1 mg is given by the activation equation as:

$$A_T = N\sigma\phi \left( 1 - e^{-\frac{0.693t_i}{T_{1/2}}} \right)$$

where:

$A$  = induced theoretical activity in counts/sec

$N$  = number of atoms present =  $\frac{mN_0f}{A_w}$

$\sigma$  = reaction cross section

$m$  = mass of element

$N_0$  = Avogadro's number

$f$  = isotopic fraction

$A_w$  = atomic weight of element

$\phi$  = irradiation flux n/cm<sup>2</sup>/sec

$t_i$  = irradiation duration

$T_{1/2}$  = half life of activated nucleus

For 100% Cr<sup>52</sup> the number of atoms present in 1 mg is  $1.16 \times 10^{19}$ . If the irradiation time equals the half life, the term in parentheses above equals 0.5. The theoretical count rate in terms of the neutron flux is then:

$$A_T = 41.5 \cdot 10^{-8} \phi \text{ counts/sec}$$

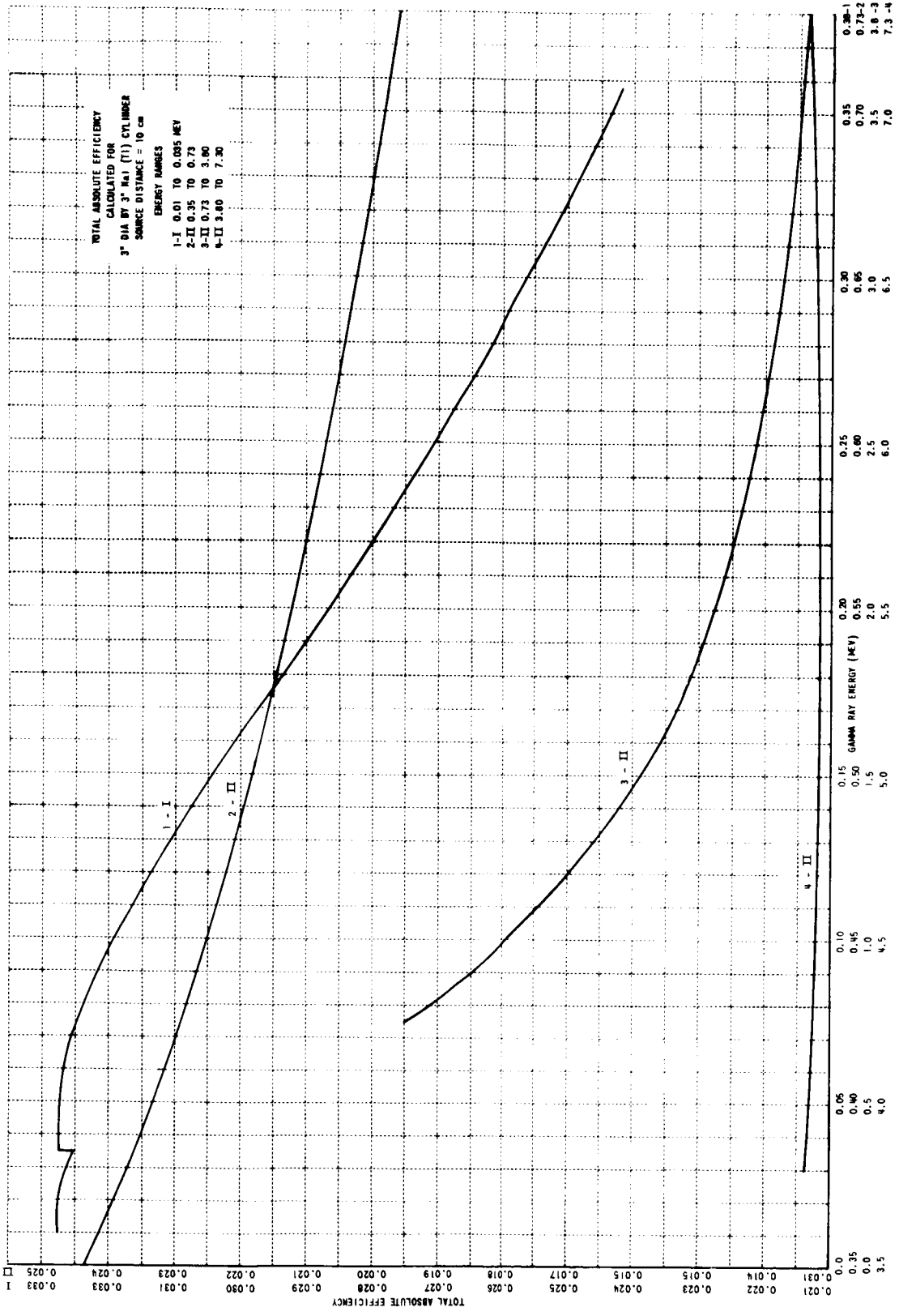


Figure 31 TOTAL ABSOLUTE EFFICIENCY (Ref. 5)

The measured count rate equals the product of theoretical rate, detector efficiency, and fractional transitions for the gamma ray of interest. The latter is 100% because the gamma ray occurs in cascade with the beta particle. Assuming a detector efficiency of 1.6%, the measured count rate is:

$$A_m = (0.016) A_T = 6.62 \cdot 10^{-9} \phi \text{ counts/sec}$$

Hence neutron flux, in terms of measured count rate, is given by:

$$\phi = 1.51 \cdot 10^8 A_m \text{ n/cm}^2/\text{sec}$$

For example, if measured rate for the 1.45 MeV gamma is found to be 100 counts/min., the incident neutron flux is calculated to be:

$$\phi = 2.52 \cdot 10^8 \text{ n/cm}^2/\text{sec}$$

After calibration is completed, the  $\text{Cr}^{52}$  standard will be removed from the vicinity of the neutron generator. Since  $\text{Cr}^{52}$  has only a 2.6 minute half life, it will decay quickly, thereby permitting its use for subsequent calibration checks.

**Continuous System Calibration** -- System gain throughout the identification process will be stabilized through use of a low-intensity radioactive source contained within the scintillator. Harshaw Chemical supplies a 3" x 3" NaI (Tl) detector with a built-in Americium 241 alpha source. This complete detector tube with photomultiplier (Model AM-12S12) has 7% resolution for  $\text{Cs}^{137}$ . The emitted alpha particles have energies of 5.44 and 5.48 MeV. These alpha particles, emitted within the scintillator, interact with the crystal in a manner similar to that of a gamma ray of the same energy. Therefore, without external activation, a photopeak can be made to appear in the MCA. A digital stabilizer within the MCA adjusts amplifier gain continuously to keep the photopeak within a prescribed channel thereby stabilizing system gain.

It may be necessary to turn off the digital stabilizer to avoid multiple-peak interference during certain of the identification measurements. If so, system gain before and after the measurement would be compared to validate the experiment. If validation fails, the experiment could be replicated or an average gain employed based on before and after experiment gains.

#### Instrumentation Requirements

The following subsections contain a discussion of the requirements of the experiment instrumentation. Specific hardware items are suggested for the multichannel analyzer, detector, amplifier and pulse shaping circuitry, and neutron generator.

The Multichannel Analyzer -- The purpose of the multichannel analyzer is to sort the pulse heights available from the detector--most probably a scintillation detector--in two ways. The first mode is that of multichannel analysis in which the analyzer computes and displays the number of counts in a given energy interval. The second mode is that of a multichannel scaler in which the analyzer totals the number of counts in each individual channel, the dwell time for each channel being set internally. The first, or multichannel, mode of analysis is the most prevalent mode and will be used for spectral analysis. The second mode (multichannel scaler mode) is most useful when utilized in a half-life determination. One of the most suitable multichannel analyzers available today is the Northern Scientific 512 Model NS-610. This analyzer contains a 512 channel memory and a linear amplifier and pulse-shaping circuitry to perform the processes of multichannel analysis and multichannel scaling. Due to the fact that we wish to employ separate control on the linear amplifier and pulse shaping modes, we will not necessarily wish to employ the internally contained amplifier of the Northern Scientific unit. The Northern analyzer also affords the option of utilizing a digital stabilizer to control system gain variations by a unique method of controlling the gain and zero level of the instrument. The performance of the entire analog-to-digital conversion (ADC) process is monitored by the stabilizer and a correction results if the digital comparison process detects an error. As a result of these compensations, virtually all baseline and gain instabilities of either short or long term variety are eliminated. The ferrite core memory is arranged for 512 addresses with a storage capacity of  $10^5$  bits per address; memory word storage is in a parallel, binary coded decimal format. For purposes of the laboratory demonstration model, the readout, which is normally either a teletype or IBM typewriter, will probably be replaced by a display oscilloscope because the information to be utilized for computation purposes will be extracted from memory and used in a separate computer. Since the operation of the multichannel analyzer in the laboratory demonstration model is meant to be entirely automatic, the functions of the manual switches on the front panel will be replaced with (say) relay-controlled switches or stepping relays. In this way one can select various time bases, change the horizontal and vertical scales, erase data, and change the memory subgroup and the display scales. The analyzer has a built-in single channel analyzer providing either an integral or differential discriminator as well as a zero level control on the ADC itself. The analyzer has four conversion gain settings which can be preselected or varied during the course of the experiment. An additional useful mode is the add-subtract mode in which background can be subtracted from previously accumulated data.

The amplifier contained within the multichannel analyzer has three inputs of which the low level input accepts inputs from zero to 100 millivolts negative with a 0.3 to 0.5 microsecond rise time. The minimum decay time of the input pulse is 30 microseconds. Through attenuators, input pulses from 0 to 100 volts positive or bipolar (from a double delay line differentiating amplifier with a 0.1 to 2 microsecond rise time and a 0.1 to 3 microsecond fall time, 1 microsecond in duration) are accepted. On the 10 volt input scale the input pulse must be 0 to 10 volts positive or bipolar with the same time characteristics as for the 100 volt input. In addition, a direct input to the analog-to-digital converter of 0 to 5 volt negative pulses, with the same time constants as before



is acceptable. Also, a coincidence input requiring 2 - 4 negative volts transcending the 2 to 4 volt range for the entire duration of the signal is available.

The Detector -- The most useful detector to use in the laboratory demonstration model of the Adaptive Multimode system is a standard scintillation detector, operated with a negative high voltage such that the signal may be taken out at ground potential, coupled to a sodium iodide crystal. The size of the crystal, in order to achieve adequate resolution and sensitivity to gamma rays in the high energy region, should be reasonably large, for instance a 3 x 3 inch crystal. Americium 241 loaded-detector crystals are ideal for the system calibration. The output pulse from a standard scintillation detector is in the range of 0 to 50 millivolts with a rise time of approximately  $2.5 \times 10^{-7}$  seconds (determined primarily by the decay time of sodium iodide phosphor). The fall time of the pulse is determined primarily by the output time constant of the scintillation detector itself and is chosen to be of the order of microseconds. The pulse is normally fed to a preamplifier of the cathode follower variety. In addition, a positive voltage pulse from the third or fourth dynode may be taken out for parallel multichannel analysis if desired. If so, the output pulse is normally taken out through a cathode follower as well. The circuitry associated with the voltage divider for the scintillation counter is standard. No modification is contemplated at this time.

The Amplifier and Pulse Shaper -- The amplifier may have either a single differentiation or double differentiation mode of operation. When the chosen pulse shaping method is that of single differentiation, the analyzed portion of the signal exists on one side of the base line, followed by an undershoot of equal area with opposite polarity. This undershoot is an undesired consequence of AC coupling in the amplifier, and it has a small amplitude of long duration in comparison with the initial portion. Since only the initial positive portion of the pulse is of interest, such pulses are termed unipolar.

On the other hand, when the pulse shaping method uses two differentiations in addition to others due to incidental AC coupling, significant portions of the signal exist both above and below the base line; hence, the term bipolar. Equal areas exist in the positive and negative portions, but the negative portion is compressed in time with return to the baseline occurring much sooner than with single differentiation. For this reason, double-differentiation pulse shaping methods are superior to single-differentiation methods in minimizing spectral distortion due to baseline shift. This form of distortion is encountered at higher count rates, and accounts for the preference of double-differentiation pulse shaping methods for high count rate applications.

Generally speaking, the single-differentiation method provides better resolution capabilities but suffers from the effects of high count rates. Similarly, double-differentiation methods have poorer resolution capability but may result in a superior net performance at count rates where the single-differentiation method is in difficulty. (One of the environmental effects for which adaptation is desired is that of a high background rate which could lead to pulse pile-up and pulse distortion problems. In this case the double differentiation technique is superior.)

In order to achieve the greatest adaptability the utilization of an amplifier such as the Ortec 410 linear amplifier appears to be indicated. This amplifier provides great flexibility of pulse shaping methods, allowing optimization of either energy or time resolution or chosen compromises as the experiment dictates. Single or double differentiation with RC or delay line shaping is provided, as well as selection of RC time constants from 0.1 to 10 microseconds. The very low input noise level is suited to high resolution spectroscopy and the excellent overload capabilities are suited to scintillation detectors. Simultaneous unipolar (singly differentiated) and bipolar (doubly differentiated) outputs allow use of the unipolar signal for optimum energy resolution with subsequent second differentiation chosen for optimum time resolution. The input polarity may be either positive or negative. Input signals of up to + 2-1/2 volts will not saturate the amplifier. Larger inputs can be attenuated, of course. Input impedance is 125 ohms and can be shunted with a pure resistance to achieve 50 ohms if desired. In the RC shaping mode gain is 0.35 to 480; in the delay line shaping mode, 0.75 to 1300. The selection of RC pulse shaping or delay line pulse shaping is accomplished by a front panel switch. In the present application (the laboratory demonstration model) the mode could be selected automatically. RC time constants, i.e.,  $e^{-1}$ , are selectable from 0.1, 0.2, 0.5, 1, 2, 5, and 10 microseconds. The delay line supplied with the amplifier provides an output pulse width of 0.08 microseconds. Pulse shaping networks can be switched to the "out" position which results in an amplifier with flat band pass from approximately 700 cycles to 4.3 megacycles. The amplifier output rise time in a unipolar output is 80 nanoseconds and the bipolar output 100 nanoseconds. The unipolar output is 0 to 10 volts positive. Since this amplifier has provisions for changing the differentiation and integration time constants, pulse shaping may be accomplished by choosing time constants appropriate to the pulse conditions encountered. Most probably there will be adaptation to the doubly delay line differentiated mode when the pulse count rate is high, otherwise the RC differentiation mode will be utilized to achieve the best pulse height resolution. A particularly useful mode of operation involves use of the Ortec 404 inspector (pileup eliminator) with fast-time derivation of the time pick-off units. This unit rejects pulse pairs whose separation is less than the resolving time of the energy channel amplifier. An associated 260-pick-off, controlled by the time pick-off control, senses detector events. Suitable circuits in the inspector then generate an inhibit pulse for the pulse height analyzer which rejects both pulses when their separation is less than 2.5 microseconds. In addition, a single output monitors the total count rate. The input signal is negative 0.3 to 1 volt and equal to or less than 20 nanoseconds in width. The input impedance is 50 ohms. The signal is positive 3 volts and 3 microseconds wide. This device accomplishes the pulse inspection and pile-up rejection functions.

**Moderator** -- The moderator will probably consist of a paraffin block which will be mounted on the end of a mechanical drive so that it may be mechanically positioned in front of the neutron generator target.

**The Neutron Generator** -- The most suitable neutron generator appears to be the Kaman Nuclear Model A711 (or A1001). This generator is a sealed-tube neutron generator producing a neutron yield of approximately  $10^{11}$  neutrons per second with a flux of  $10^9$  n/cm<sup>2</sup>/sec into a target 1/8 of an inch from the actual neutron target itself. Mean diameter is 3/4 of an inch and the tube lifetime is greater than 60 hours at  $10^{11}$  neutrons per second, where lifetime is defined as time to one-half rated yield. The pulsing characteristics of the generator are such that it may be pulsed over a range of 1 to  $10^4$  pulses per second at pulse lengths from one to approximately  $10^3$  microseconds. The pulsing signal required is a 0 to 10 volt positive signal coincident with the desired timing pulse. Alternatively, the pulse generator in the A711 control console may be used to supply timing signals for the detector or the gate on the coincidence input of the multi-channel analyzer.

**The Specimen Jig** -- The only requirements for the specimen jig are that it be movable or rotatable on an axis, presumably by a simple servo-type drive, so that the position of the particular sample at the neutron generator can be controlled. The most suitable type of jig appears to be a circular mount of a material which possesses a low activation cross section to neutrons and furthermore has a low neutron absorption cross section so that the modification of the neutron flux due to the material of which the specimen mount is composed will be negligible. A suitable material might be polystyrene although any material containing a large amount of hydrogen will, of course, contribute to the 2.2 Mev capture spectrum. There will be provision for (say) 5 to 10 samples mounted on discs which can be inserted at various positions around the table. The specimen jig will presumably be mounted in a horizontal plane so that the separate moderator may be introduced between it and the neutron generator. Individual samples of the elements to be used in the laboratory model, oxygen iron, aluminum, silicon and magnesium may be placed individually in these various sample positions as well as a sample containing a mixture of all five elements. Alternatively, if it is desirable to irradiate only one sample, i.e., a mixture of all of the elements, the specimen jig need only be able to position that target close enough to the neutron generator that it experiences an adequate flux. The only requirement would be that the sample be moved behind an appropriate material to shield it from the neutron generator if irradiation of the sample is not desired.

#### Summary of Identification Modes

The identification modes described in previous pages are summarized in Table VIII.

Table VIII  
SUMMARY OF IDENTIFICATION MODES

TECHNIQUE	NEUTRON GENERATOR MODE	NEUTRON PULSE WIDTH	GENERATOR PULSE RATE	NEUTRON FLUX $n/cm^2/s$	MCA GATE TIMING	MCA CALIBRATION AND RESOLUTION	IRRADIATION DURATION	IDENTIFIABLE ELEMENTS (Fe, Mg, Si, Al, O)
CAPTURE	THERMAL	100 $\mu$ s	$2 \times 10^3 s^{-1}$	$5 \times 10^6$	ADD DURING NEUTRON PULSE-LIVE COUNT 100 $\mu$ s; SUBTRACT PRIOR TO NEXT PULSE-LIVE COUNT 100 $\mu$ s	0-8 Mev @ 15.6 keV/ch 0-1.6 Mev @ 3.14 keV/ch	UNTIL SPECTRUM STABILIZED	Fe Si Mg* Al*
ACTIVATION	THERMAL	100 $\mu$ s	$2 \times 10^3 s^{-1}$	$5 \times 10^9$	COOL 1m. LIVE COUNT 1m. COOL 15m. LIVE COUNT 2m.	0-8 Mev @ 15.6 keV/ch.	10m.	Al Mg
ACTIVATION	FAST	100 $\mu$ s	$10^{14} s^{-1}$ (CW)	$10^8$	SEE TABLE VII	0-8 Mev @ 15.6 keV/ch	1m.	Si Al Mg O Fe
PROMPT	FAST	1 $\mu$ s	$2 \times 10^3 s^{-1}$	$10^8$	ADD DURING PULSE-LIVE COUNT 3 $\mu$ s; SUBTRACT PRIOR TO NEXT PULSE-LIVE COUNT 3 $\mu$ s.			Si** Al** Fe** Mg** O**

\* REFER TO SECTION: RADIOACTIVE CAPTURE OF THERMAL NEUTRONS FOR DISCUSSION OF LIMITATIONS

\*\* TENTATIVE

## ADAPTIVE MULTIMODE CONTROLLER

The digital controller designed to operate the neutron excitation laboratory demonstration model is described. For reference, the block diagram of the neutron excitation experiment is shown in Figure 2.

### Control Philosophy of Demonstration Model

The objective of the laboratory model is to demonstrate feasibility of the adaptive multimode concept. The essence of this concept is that of an automaton continuously monitoring the performance of an experiment to alter procedures or switch to alternative modes depending upon previous results, environmental changes or outcomes of other experiments.

The flyable system is envisioned as being free of human intervention. However, in order to minimize cost of the controller in the demonstration model, compromises in the ultimate capability of the model controller have been made. These compromises entail requiring a human operator to initially checkout equipment and to perform an approximate pre-calibration. The usefulness of the demonstration model is not believed to be severely compromised by the presence of a human operator because the functions of automatic checkout and calibration have been previously demonstrated in flyable as well as ground-based systems. Once initial checkout and pre-calibration have been completed, the laboratory model and the "flyable" system operate almost identically.

A functional flow diagram of the Neutron Excitation experiment is shown in Figure 32. Upon activation by the operator, the system performs an initial calibration using a sample of known material. First the background count is measured approximately to determine feasibility of performing the thermal activation experiment. If background is sufficiently low, the known sample is irradiated, pertinent energy peaks are located and gains are adjusted to place these peaks within prespecified channels. After calibration the unknown specimen is brought into position and a passive background spectrum is measured and stored for future use.

Assuming the calibration mode was successfully completed, a hydrogenous materials mode is entered to search for the presence of materials which could thermalize neutrons from the generator. The presence of such material is assumed to preclude operation in the fast activation mode. If hydrogenous material is not detected, then both fast and thermal modes can be utilized.

Next the measurement modes are entered. These consist of irradiating the sample with fast and thermal neutrons and determining the locations of energy spectral peaks for prompt, capture and activation gammas. Last, half-life measurements are made using activation gammas in a decay mode.

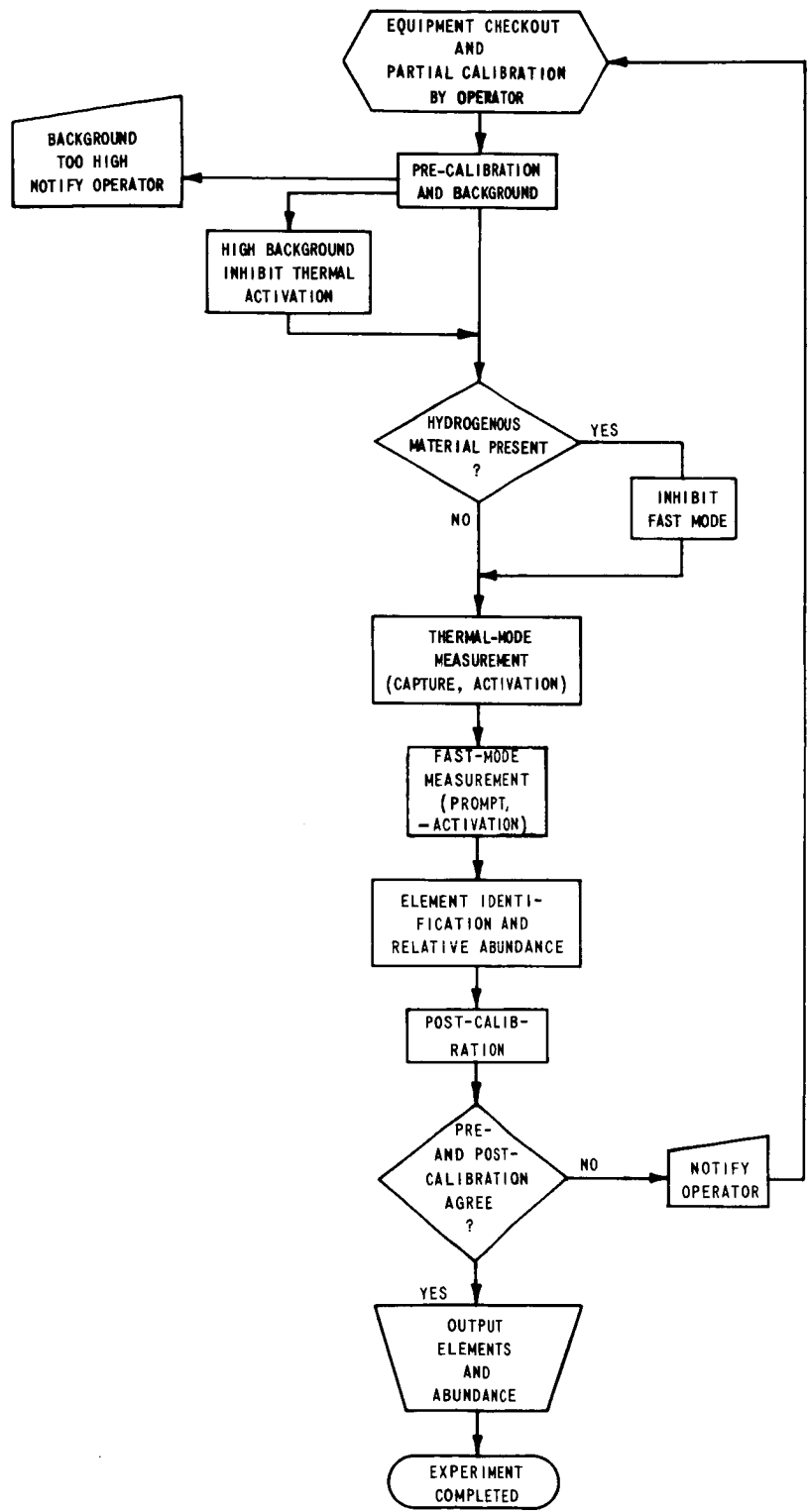


Figure 32 FUNCTIONAL FLOWGRAM OF NEUTRON EXCITATION EXPERIMENT

Subsequent to spectral measurements, an identification mode is entered in which the elements comprising the unknown sample are identified from measured spectra and their relative abundance within the sample is determined. This data is stored for future output.

Lastly, a post-calibration mode is entered. The known sample is again re-radiated and the locations of its energy peaks are compared to their locations during pre-calibration. If these locations agree within some prescribed tolerance the experiment is accepted as valid, otherwise not. (If pre- and post-calibrations do not authenticate, a self-checking mode could be entered to locate an equipment malfunction.) The demonstration model alerts the operator that the calibrations have failed to authenticate and cycles back to pre-calibration upon command.

#### **Adaptive Features**

The adaptive controller is designed to cope with high background count rates, hydrogenous materials, temperature variations within the source and/or detector, and to a lesser extent interpulse interference.

The presence of a highly radioactive material near the detector would probably preclude operation of the neutron excitation experiment. Very little can be done to render the situation tenable, e.g., stopping-down the aperture of the detector reduces the background count but reduces the count from the sample in the same proportion. If the radiation background is directional, it would be possible to reduce sensitivity of the detector to the radiation by employing movable shields or by aiming the detector in a more favorable direction. Neither of these latter schemes are implemented in the demonstration model. If the background is not so large that it precludes the entire experiment, prompt and capture spectra may be measurable because they develop within relatively short periods of time with relatively high activity compared to activation spectra. This alternative is implemented in the demonstration model. The critical background counts at which the experiment becomes untenable and partially tenable will be determined by experimentation.

The presence of a thermalizing material around the unknown sample probably precludes operation of the experiment in the fast neutron measurement mode. The presence of hydrogenous materials must be predetermined, in order to avoid erroneous inferences, and the fast mode inhibited accordingly. The procedure used in the model to detect the presence of hydrogenous material does not indicate the degree of thermalization. Accordingly, the paraffin modifier will be positioned in front of the neutron generator to ensure thermalization and the fast mode will be inhibited. The presence of thermalizing material is inferred by detecting a strong spectral line in the neighborhood of 2.2 MeV. Such a line is indicative of hydrogen, but could also derive from some other element. However, because of the strong activity of a hydrogenous material compared to an interfering reaction, a threshold criterion seems feasible. Therefore, a superthreshold count at 2.2 MeV is taken to be indicative of a hydrogenous material presence.

Inspection of the spectra in the previous section indicates that certain elements, namely iron, tend to dominate the spectra making reliable detection of other elements difficult. It is desirable to alter procedures to suppress such dominant elements once their presence is detected. An ideal, though probably unfeasible, solution is employment of an energy filter ahead of the detector to intercept gammas from the offending element. Alternatively, once the dominating element is detected and its mass determined, the input energy window of the MCA could be narrowed or translated to inhibit analysis of gammas deriving from the strong element. Increased neutron irradiation or counting times could then be used in an effort to raise weak spectral peaks above background. A second alternative is employment of "spectrum stripping" techniques in which the spectrum of the offending element is subtracted from the measured spectrum thereby revealing suppressed peaks.

The components of the experiment within the spacecraft of the flyable model are expected to be temperature stabilized. However because, as presently conceived, the neutron source and detector are lowered to the planetary surface for measurement purposes, temperature stabilization of these components presents a special problem. The demonstration model is designed to partially cope with this problem by continuously adjusting system gain to accommodate detector fluctuations due to temperature variations. This is accomplished by including an Americium 241 source within the detector, whose energy peak is automatically tracked within the MCA. (The neutron source could be temperature stabilized by providing a neutron detector to intercept neutrons from the stream and provide a control voltage to the source power supply.) Fine temperature stabilization of the neutron source may be unnecessary if fast neutrons can be guaranteed and if relative abundances of materials are determined thereby obviating need of absolute flux measurements. Of course, gross temperature variations are assumed to be compensated by a controlled-environment box surrounding the source/detector. Such a box is not included in the demonstration model design.

An additional possibility for adaptivity lies in the provision and use of several pulse shapers. Pulse shapers are generally employed to reduce the deleterious effects of interpulse interference at high pulse rates, e.g., high background, at the expense of increased noise level. Whether employment of pulse shapers of different characteristics sufficiently enhances the experiment to warrant their inclusion must be determined by experiment. It is likely that changing from one shaper to another during the course of an experiment would necessitate recalibration. A pulse shaper switching mode is tentatively included in the demonstration model design. Switching criteria would probably be based on measured pulse rates.

Also various system thresholds can be adaptively adjusted based upon (subjective) criteria such as imperativeness of data or cost/benefit.



## Operating Modes, Procedures and Flow Diagrams

The following paragraphs describe procedures for implementing the various modes of operation of the neutron excitation experiment. These modes include: pre-calibration and background measurement, detection of hydrogenous material, measurement (thermal-capture, thermal and fast-activation and fast-prompt spectra), identification and quantification, and post-calibration. Also included are functional flow diagrams which depict the functions which the controller must implement. Figure 32 depicts these modes and their relationship within the experiment.

**Pre-Calibration and Background** -- In this mode system gains are adjusted to place pertinent energy peaks of a known source material in prescribed channels of the multi-channel analyzer (MCA). This ensures that the correct energy band is observed during the experiment, that the energy vs. channel number curve of the MCA passes through the origin and is essentially straight. In addition the background radiation of the specimen is measured to determine efficacy of the experiment.

The pre-calibration mode is shown diagrammed in Figure 33. As discussed previously, it is assumed that an operator has performed an operational check of the equipment and has provided an initial, approximate calibration. Thereupon, the controller proceeds with a precise calibration. First, the unknown specimen is positioned and the total background count in a prespecified time interval is determined and compared to a threshold. If the count is super-threshold, indicating presence of active material, a message is sent to the operator and the controller idles until commanded by the operator. If the count is sub-threshold so that at least portions of the measurement procedure are feasible, calibration with a known source is initiated. The procedure is illustrated in Figure 34.

The MCA is purged of the background count, the known material is positioned between the neutron generator and detector and a fast-activation spectrum is recorded. A search for energy peaks of the calibration material is then initiated. The peaks can be located by a simple peak-picking operation or by a pseudo-crosscorrelation employing a sliding window whose width is a function of spectral resolution. Figures 35 and 36 show the results of a computer peak-picking experiment utilizing the composite capture spectrum data. The peak-picking algorithm compared the count in the channel at the center of a window, whose width equalled detector resolution, to counts in channels at each edge of the window. A peak was declared if the center channel count exceeded the channels' counts at window edges and also exceeded counts in the two channels adjacent to the center channel. An additional test must be included to distinguish true calibration peaks from the many extraneous peaks detected by the peak picker; calibration peaks are generally more symmetrical, possess narrower widths and greater amplitudes than false peaks, e.g., escape and annihilation peaks. If the peak is a legitimate calibration peak, its channel number is stored for future reference. When all calibration peaks are found, their channel numbers are compared to a prescribed set; if discrepancies exist, system gain is adjusted to place these peaks in the correct channels, the MCA is purged and the above procedure is repeated until calibration peaks fall tolerably close to the required channels.

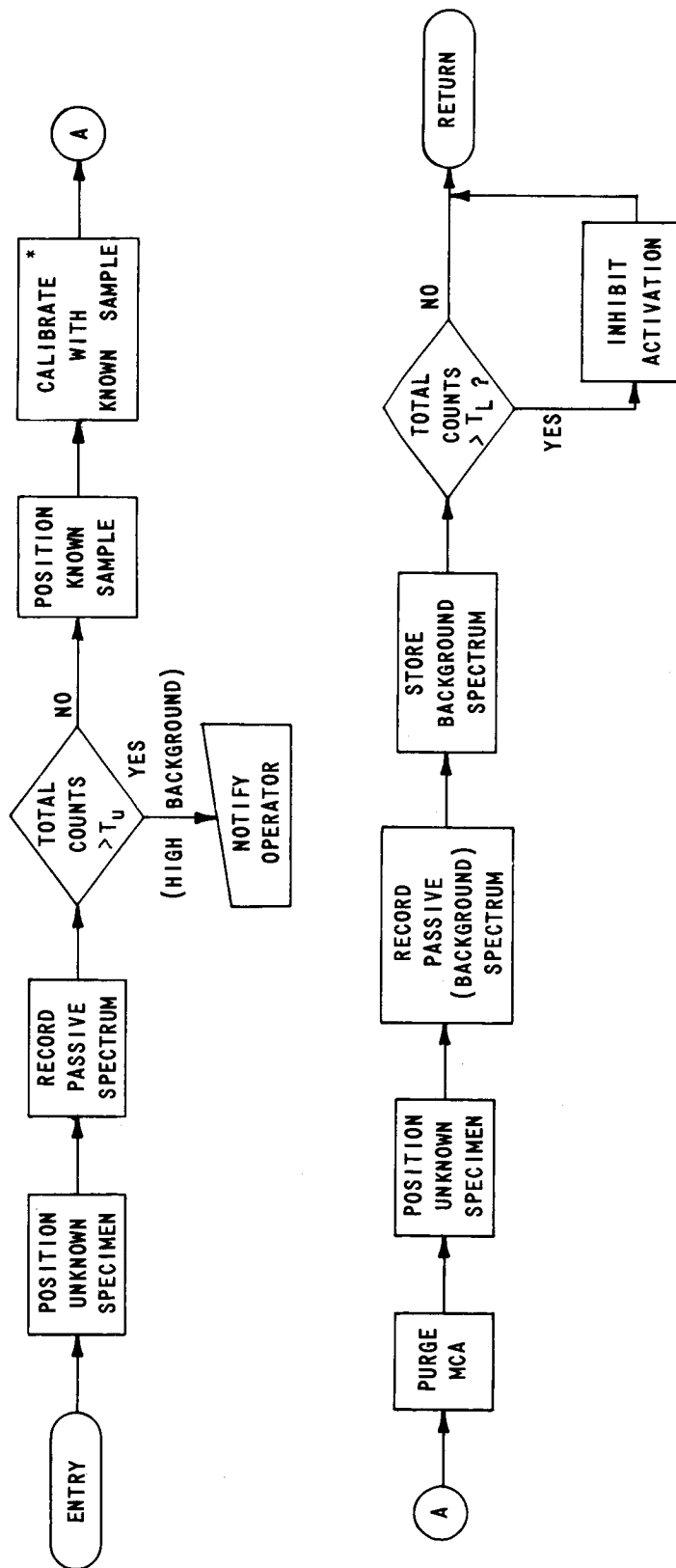


Figure 33 FUNCTIONAL FLOWGRAM OF PRE-CALIBRATION MODE  
 \* SEE FIG. 34 FOR FLOWGRAM OF CALIBRATION WITH KNOWN SOURCE

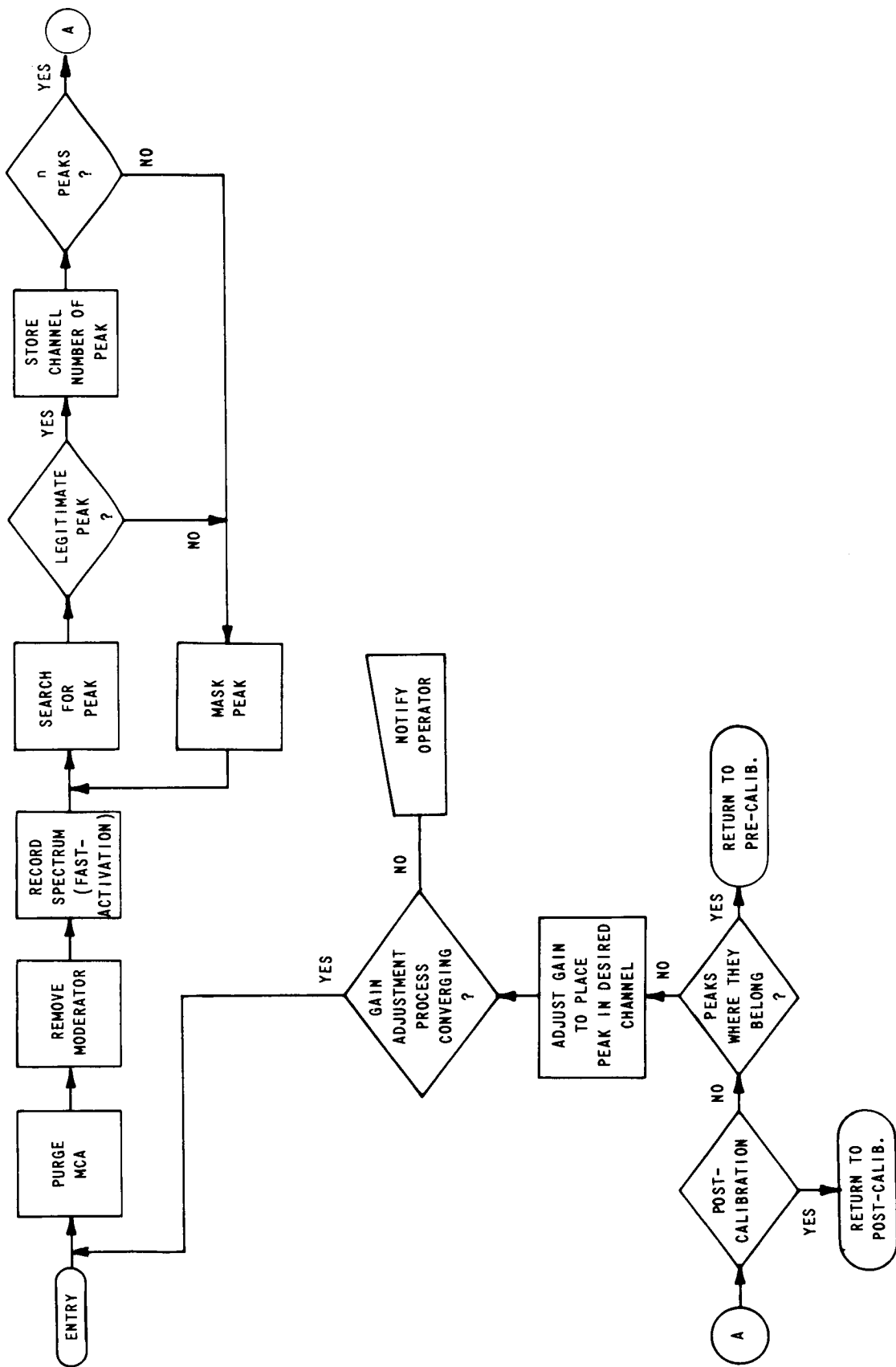


Figure 34 FUNCTIONAL FLOWGRAM: CALIBRATION WITH KNOWN SAMPLE

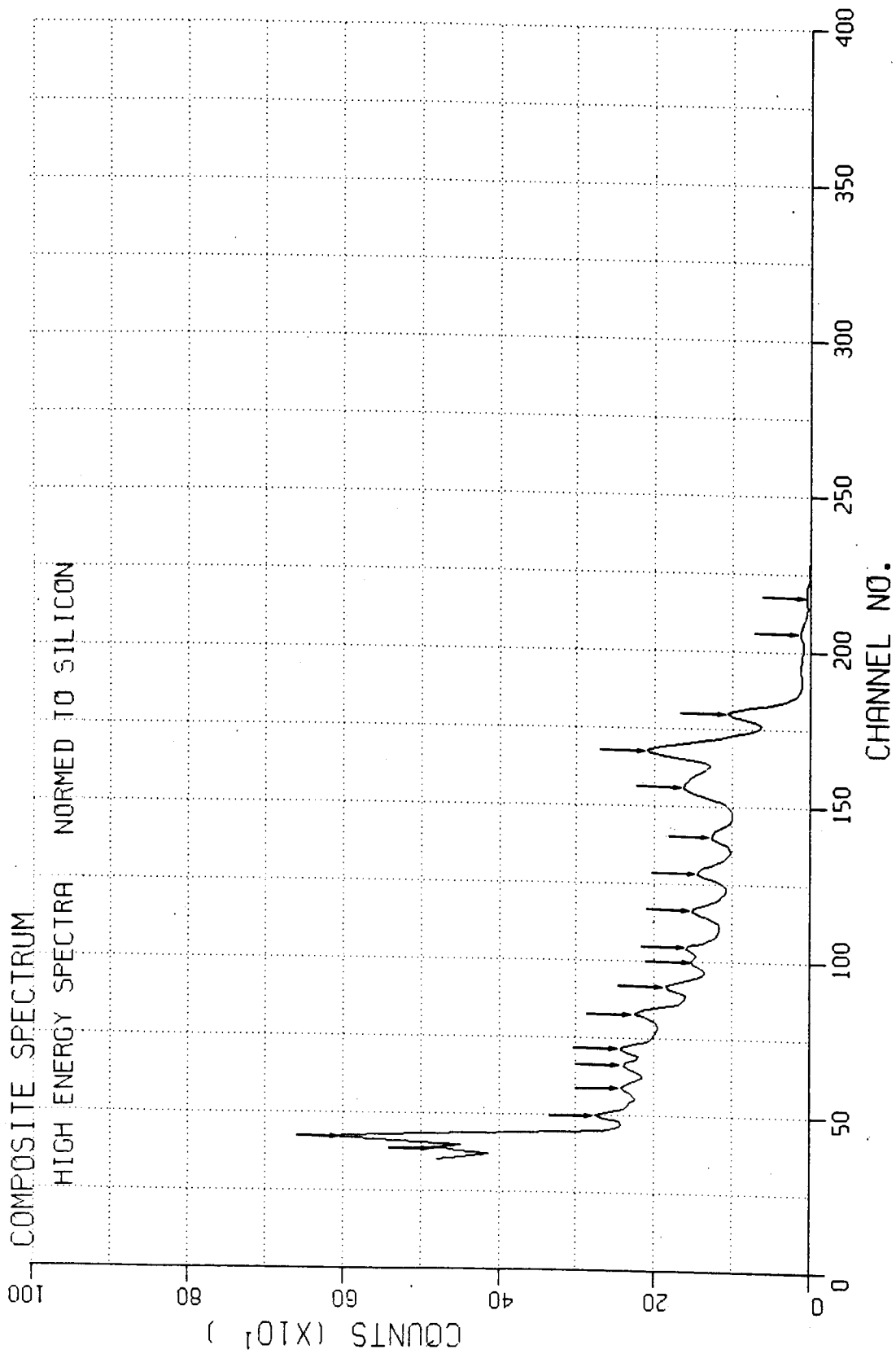


Figure 35 SPECTRAL PEAKS DETECTED BY PEAK-PICKING ALGORITHM

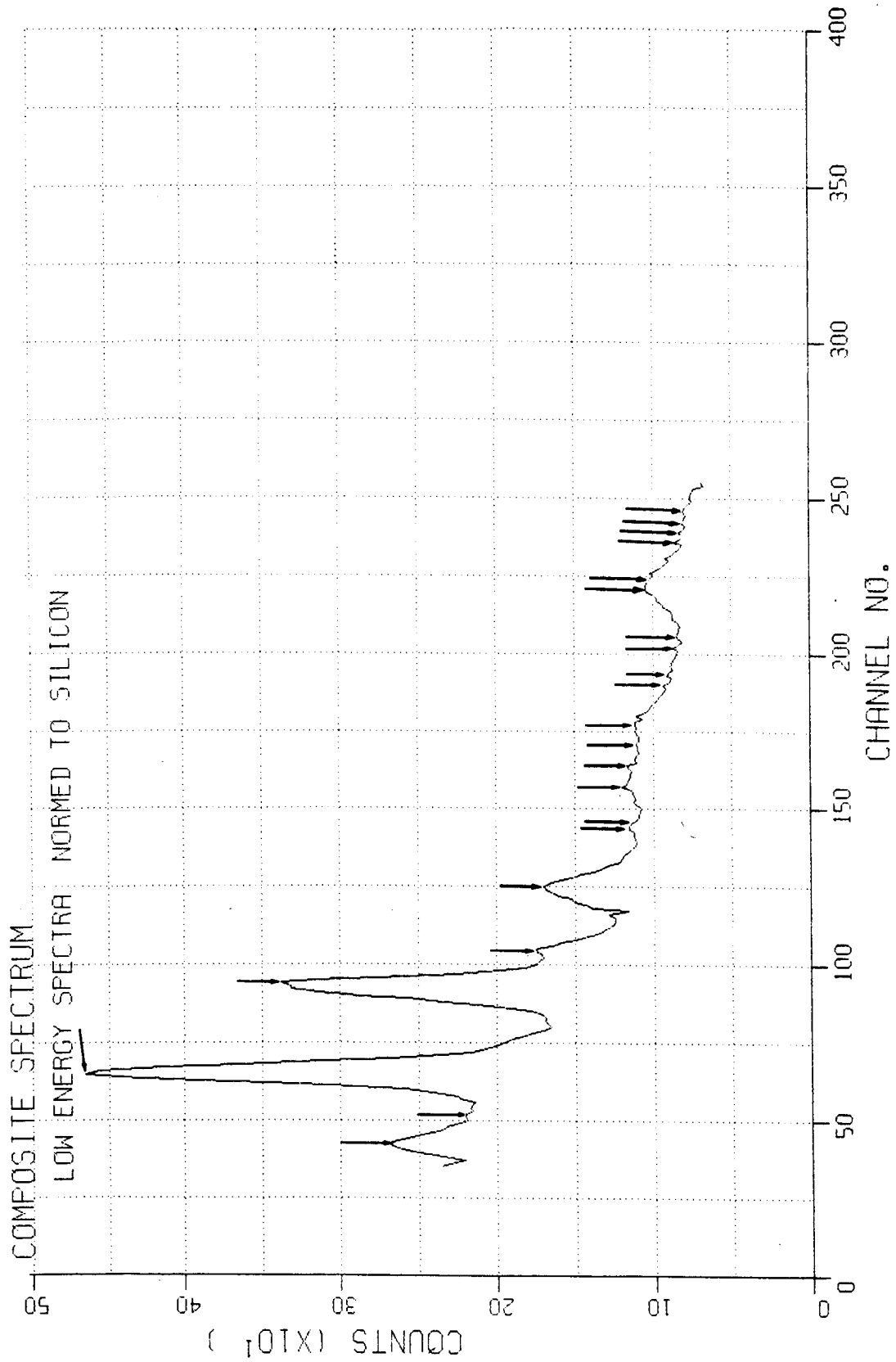


Figure 36 SPECTRAL PEAKS DETECTED BY PEAK-PICKING ALGORITHM

Next the MCA is purged, the unknown specimen is rotated into position and a background spectrum is recorded and stored for subsequent use during the measurement modes. Lastly the total background count is compared to a second threshold to determine efficaciousness of thermal activation analysis.

**Detection of Hydrogenous Materials** — — Subsequent to calibration, the existence of hydrogenous material is ascertained. The presence of such materials, which might thermalize neutrons from the generator, can be inferred by the presence of a strong energy peak in the vicinity of 2.2 MeV. The detection procedure is diagrammed in Figure 37. The unknown sample is positioned between the generator and detector and the MCA is purged. The generator is then activated and a thermal-capture spectrum is taken. The peak channel in the vicinity of the channel corresponding to 2.2 MeV is determined, the count from the corresponding channel of the stored background spectrum is subtracted and the difference is thresholded. If the difference is super-threshold, indicative of a thermalizing medium, the fast neutron spectral measurements are inhibited. Also irradiation and live-count times of the thermal mode could be adjusted.

**Measurement and Identification** — — Five separate measurements will be performed in order to gather the data required for analysis. These measurements, listed in the order in which they will be performed are:

- measurement of the capture spectrum in the thermal neutron mode,
- measurement of the activation spectrum in the thermal neutron mode,
- measurement of the prompt spectrum in the fast neutron mode,
- measurement of the activation spectrum in the fast neutron mode, and
- half-life measurements (from thermal and fast activation).

In the thermal neutron mode, a moderator is used to slow the incident neutrons to thermal velocities. No moderator is used in the fast neutron mode. No attempt will be made to measure the capture spectrum in the fast neutron mode, or the prompt spectrum in the thermal mode, for reasons explained in a previous section.

The capture spectrum must be measured in a pulsed mode. After each neutron source pulse, the Multi-Channel Analyzer (MCA) is gated on for two mutually exclusive time intervals, Figure 38. The first time interval,  $\tau_1$ , is coincident with the presence of capture gammas. During this time interval both activation and capture gammas are present. Therefore, the spectrum obtained by analyzing the pulses which occur during time intervals,  $\tau_1$ , is a composite spectrum generated by both activation and capture gammas. The second time interval,  $\tau_2$ , begins after the capture gammas have decayed. Therefore, the spectrum obtained by analyzing the pulses which occur during the second time interval is a pure activation spectrum. The two spectra can be stored in separate sections of the MCA's memory, and the activation spectrum can be subtracted from the composite spectrum in order to obtain the capture spectrum. Preferably, the

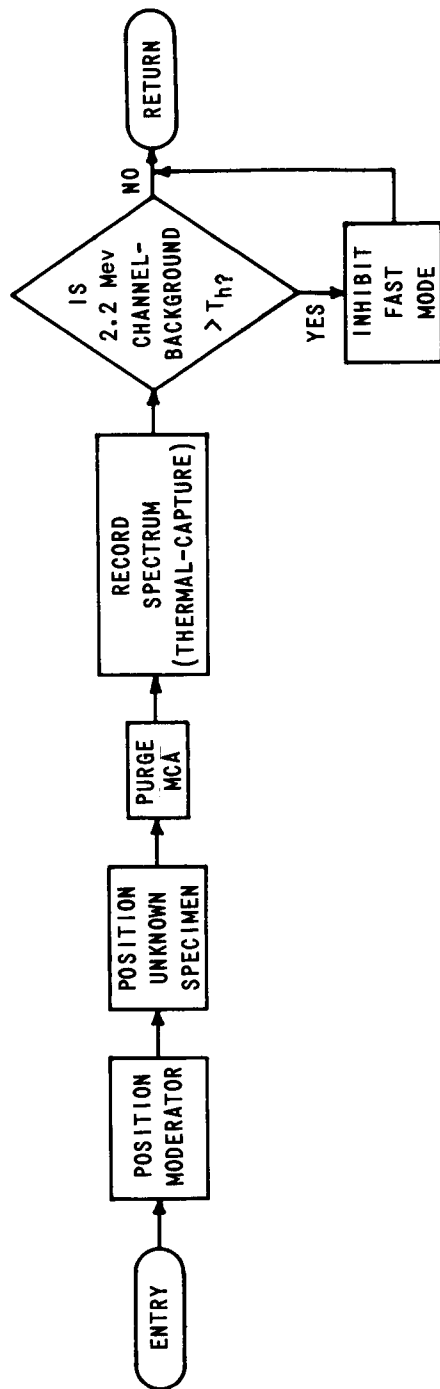


Figure 37 FUNCTIONAL FLOWGRAM OF TEST FOR PRESENCE OF HYDROGENOUS MATERIAL

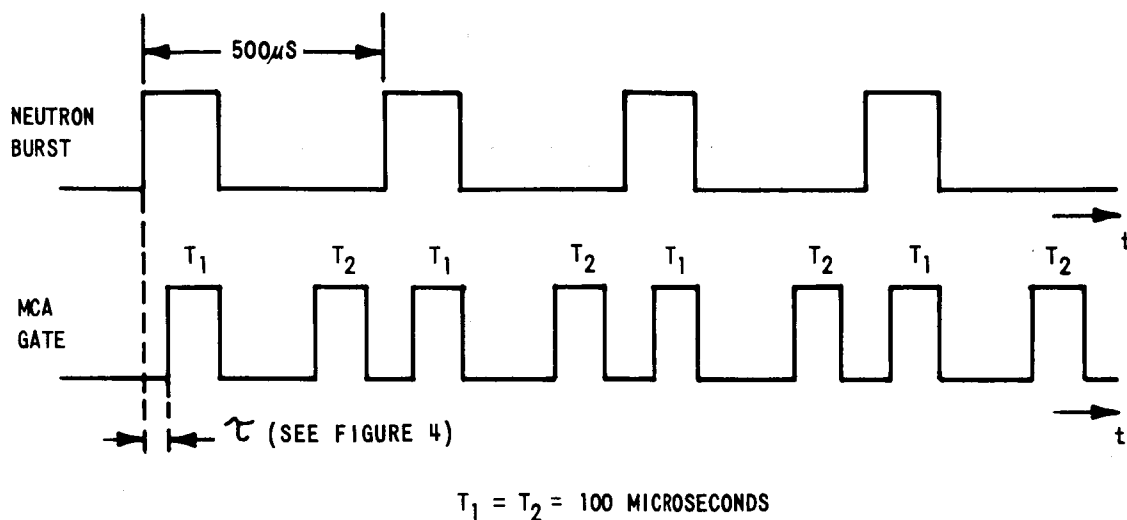


Figure 38 TIMING FOR THE MEASUREMENT OF THE CAPTURE SPECTRUM IN THE THERMAL MODE

subtraction could be performed by switching the MCA into its subtract mode during time intervals  $T_2$ . The activation gammas would then be subtracted on a pulse-to-pulse basis. This would eliminate the need for dividing the MCA's memory into two sections. The number of neutron source pulses would be counted in order to yield a measure of the total incident neutron flux.

The activation spectrum in the thermal neutron mode can be measured after the capture spectrum by simply gating the MCA on for a fixed length of time. Prior to the measurement, the sample would be further bombarded with neutrons if the number of pulses used to measure the capture spectrum did not raise the activity to a suitable level for measurement.

The fast neutron prompt spectrum must also be measured in a pulsed mode. Prompt gammas appear during the neutron pulse and decay rapidly after removal of the pulse. Therefore, when measuring the prompt spectrum, the MCA will be gated on for a short time interval which overlaps the neutron pulse, Figure 39. Activation gammas will also be present during this time interval, but their number should be small compared with the number of prompt gammas. The present plan is to ignore these activation gammas. If they prove to be a problem, the activation spectrum can be measured and subtracted from the composite spectrum as proposed for the capture spectrum measurement. Although a negligible number of prompt gammas are expected to occur after removal of the one microsecond neutron burst, a three microsecond MCA gate will be used in order to accommodate the finite resolution of the detector. Capture gammas are not expected to interfere with the measurement because their numbers do not become appreciable until about ten microseconds after the neutron burst.



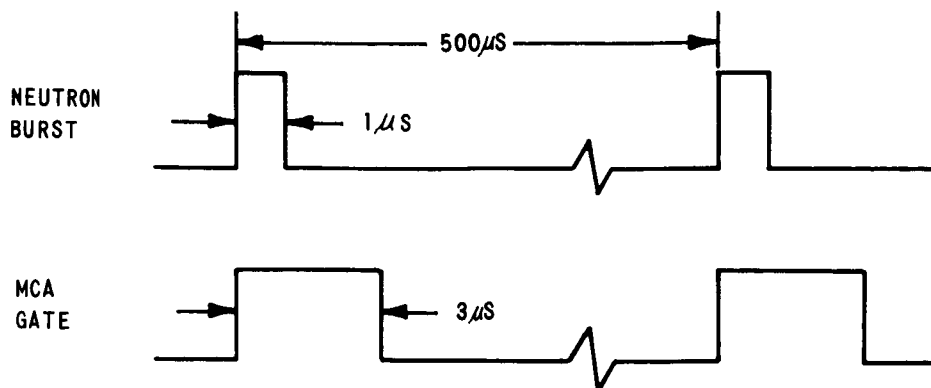


Figure 39 TIMING FOR THE MEASUREMENT OF THE PROMPT SPECTRUM IN THE FAST MODE

The fast neutron activation spectrum can be measured after the prompt spectrum by gating the MCA for a fixed length of time. It may be necessary to further irradiate the sample to increase its activity to measurable levels.

After each spectrum is measured, the background spectrum obtained during calibration will be subtracted from the measured spectrum. The resultant spectrum will then be analyzed. The analysis consists of locating the spectral lines, or peaks, in the spectrum. If a peak occurs at an energy characteristic of one of the elements being searched for, then this fact is tabulated within the memory of the control computer. An identification matrix, Table IX, is thereby developed which is a tabulation of which characteristic spectral lines were found in the measured spectra. Half-life measurements will also be made. Measured half-lives would also be tabulated as a further indication that the corresponding element is present. Each check mark in a particular column of the matrix is an indication that the particular element which heads that column is present. Each of these indicators will be assigned a numerical weight representative of the importance of the indicator in the identification process and the confidence with which it can be measured. The sum of the weights in a particular column will then be compared with a fixed threshold in order to perform the final identification. A superthreshold sum is indicative of the presence of the element with high confidence. The weights and thresholds have yet to be determined.

Table IX

## EXAMPLE OF AN IDENTIFICATION MATRIX

SPECTRUM	ENERGY (MeV)	Fe	Si	Al	Mg	O
THERMAL CAPTURE	2.82				X*	
	3.54		X			
	4.44		X			
	5.46	X				
	6.61	X				
	7.13	X				
	7.64	X				
	7.72				X*	
THERMAL ACTIVATION	0.834				X	
	1.015				X	
	1.782			X		
FAST PROMPT*	0.84	X				
	0.88				X	
	0.98		X			
	1.01			X		
	1.37				X	
	1.78		X			
	1.82				X	
	2.20			X		
	5.12					X
	5.63					X
6.14					X	
FAST ACTIVATION	0.58				X	
	0.834			X		
	1.78		X			
	6.13					X
HALF-LIFE CHECK		X	X	X	X	X
* FEASIBILITY OF IDENTIFICATION TENTATIVE - MORE INFORMATION NEEDED.						

The thermal neutron activation spectrum may prove to be of limited use. Calculations made in the previous section indicate that the number of activation gammas is extremely low except for Mg<sup>27</sup> and Al<sup>28</sup>. From thermal activation of equal masses of Fe, Si, Mg and Al, only Mg<sup>27</sup> and Al<sup>28</sup> were detected experimentally. Also, since half-life measurements are based upon the decay rate of spectral lines in the activation spectrum, it will be possible to measure only the half lives of Al and Mg in the thermal mode.

Half-life estimates will be made by measuring the decay rate of certain spectral lines in the activation spectra. As explained in a previous section, this can be done by using two activation spectra taken after two different cooling times. Half life can be estimated by measuring the decrement in count rate, at a given energy level, between two separated time intervals. Alternatively, a more refined measurement can be made by operating the MCA in its multiscalar mode.

In the multiscalar mode the MCA accumulates for a preset time all input pulses which have amplitudes within a preset energy window. The counts in successive time intervals are stored in successive channels. For a half-life measurement, the energy window would be set so that the MCA would accept only those activation gammas corresponding to the pertinent spectral line. The time base for counting would be small compared with the half-life of the element thought to be causing that spectral line. The resultant curve of counts versus channel number should then be an exponential decay, the decay constant of which can be computed. The decay constant,  $\lambda$ , is related to half life through the equation  $T_{1/2} = \frac{0.693}{\lambda}$  where  $T_{1/2}$  is half-life. This half life is uniquely related to the element causing the particular spectral line. In general, a different energy window and time base is required for each half-life measurement. Therefore, the measurements must be done in sequence. The measurements can be sequentially performed without neutron bombardment between measurements by measuring the shorter half-lives first.

Estimation of the mass of each constituent element in the sample can be made in two ways. One method uses a measurement of activation gammas while the other uses a measurement of capture gammas. The former and then the latter methods are explained below.

After neutron bombardment for some arbitrary time,  $t_b$ , the activity of the  $i^{th}$  constituent element is:

$$A_i(t) = \frac{\phi N \sigma_i m_i f_i}{w_i} \left(1 - e^{-\lambda_i t_b}\right) e^{-\lambda_i t} \quad (3.1)$$

where  $t$  is the time elapsed since the termination of neutron bombardment and

$\phi$  = neutron flux

$N$  = Avogadro's number

$\sigma_i$  = reaction cross section of  $i^{th}$  element

$m_i$  = mass of  $i^{th}$  element in target

$f_i$  = isotopic fraction of  $i^{th}$  target nuclide

$\lambda_i$  = decay constant of  $i^{th}$  nuclide

$w_i$  = atomic weight of  $i^{th}$  element

$N$ ,  $\sigma_i$ ,  $f_i$ ,  $\lambda_i$ , and  $w_i$  are known constants which are stored in memory. The activity,  $A_i(t)$ , is proportional to the sum of all the count rates in each spectral line:

$$A_i(t) = \frac{1}{K} \sum_{j=1}^M \left[ \frac{A_i^{(j)}(t)}{g(E_j)} \right] \quad (3.2)$$

where  $M$  is the number of different gamma energies released by element  $i$  and  $A_i^{(j)}(t)$  is the measured count rate, or average frequency of detection, of gammas with  $j$ th energy,  $E_j$ .  $A_i^{(j)}(t)/K g(E_j)$  is the count rate which would be measured if the detection process were 100 percent efficient.  $K g(E_j)$  is the efficiency of the process;  $K$  is a constant determined by geometry and  $g(E_j)$  expresses the functional dependence of efficiency upon energy which is introduced by the detector.

It is not necessary to measure the count rates at all of the spectral lines of a given element because the relative count rate at each of the spectral lines of a given element is known for those elements under consideration. Let  $K_i(E_j)$  be the fraction of the total number of gammas from element  $i$  which have energy,  $E_j$ . Then:

$$A_i(t) = \frac{A_i^{(j)}(t)}{K K_i(E_j) g(E_j)} \quad (3.3)$$

Equations (3.1) and (3.3) yield:

$$\frac{A_i^{(j)}(t)}{K K_i(E_j) g(E_j)} = \frac{\phi N \sigma_i m_i f_i}{w_i} (1 - e^{-\lambda_i t_b}) e^{-\lambda_i t} \quad (3.4)$$

$$m_i = \frac{1}{K \phi N} \left[ \frac{w_i e^{\lambda_i t}}{K_i(E_j) \sigma_i f_i (1 - e^{-\lambda_i t_b})} \right] \frac{A_i^{(j)}(t)}{g(E_j)}$$

The count rate  $A_i^{(j)}(t)$ , is measured at a unique energy peak,  $E_j$ , for element  $i$  at a particular time,  $t$ , after irradiation. Assuming that  $1/K \phi$  is known,  $m_i$  can be calculated from the above equation.  $K \phi$ , in turn, can be measured by irradiating a known mass of some reference element (such as the chromium reference used for calibration purposes) with the same flux for the same length of time as used to irradiate the unknown, and then measuring the count rate  $A_{ref}^{(j)}(t)$  at some time  $t$ .  $1/K \phi$  is then given by Equation (3.4) evaluated for the (chromium) reference. The necessary count rates can be measured by operating the MCA in its multiscalar mode or by examining the appropriate peaks in an activation spectrum taken for a short time duration relative to the half-lives of the elements being detected. It will probably be possible to use this technique only for the elements Mg, O and Al since only they have prominent spectral peaks in the composite thermal and fast activation spectra. If  $K \phi$  is not measured, relative masses for the pertinent elements can be determined via Equation (3.4).

The second method for measuring mass is basically the same as above except that the thermal capture spectrum, which is time independent, is used. The count rate at energy  $E_i$  due to capture gammas is:

$$A_i(E_i) = \frac{\kappa \phi N \sigma_i \rho_i g(E_i) m_i \kappa_i(E_i)}{w_i} \quad (3.5)$$

Hence the mass of element  $i$  is given by:

$$m_i = \frac{1}{\kappa \phi N} \left[ \frac{w_i}{\kappa_i(E_i) \sigma_i f_i} \right] \left[ \frac{A_i(E_i)}{g(E_i)} \right] \quad (3.6)$$

where  $E_i$  is the energy associated with the spectral line used for the  $i$ th element.  $A_i(E_i)$  is the count rate at energy  $E_i$ , and  $\kappa_i(E_i)$  is that fraction of all the capture gammas from element  $i$  which have energy  $E_i$ . The other constants are as defined earlier. Again,  $1/\kappa \phi$  can be measured by irradiating a known reference mass with the same flux and same number of neutron source pulses as used to irradiate the unknown, and then measuring the count rate  $A_{ref}(E)$  at an appropriate energy  $E$ . Once  $1/\kappa \phi$  and  $A_i(E_i)$  are measured, the mass  $m_i$  is computed from Equation (3.6). If  $\kappa \phi$  is not measured, relative masses for the pertinent elements can be determined via Equation (3.6).

Domination of spectral response by certain elements, e.g. iron, can be alleviated somewhat by spectrum stripping techniques. This technique involves subtracting from a measured spectrum, the pure spectrum, suitably scaled, of the offending element. Ideally the entire element's contribution would be subtracted, which presupposes knowledge of the relative amount of element present, whereas, practically, subtraction of arbitrary amounts tends to enhance detection of suppressed peaks. Of course, utilization of this technique requires storage of, at least, partial spectra of the dominating elements. Figures 40-45 illustrate results of stripping experiments utilizing composite capture spectral data

Figures 41 and 42 show the effect of subtracting various amounts of iron spectrum from the low energy composite capture spectrum. Figure 41 illustrates the best that can be achieved, i.e., an amount of iron was subtracted to yield a three element composite spectrum. Figure 42 illustrates the effect of subtracting only a portion of the iron contribution; one-half of the composite channel 65 activity was attributed to iron. Clearly totally eliminating a spectral component enhances detection of suppressed peaks, therefore elements; suboptimal stripping is also advantageous but to a lesser extent.

Figures 44 and 45 show the effect of subtracting the spectral contribution of iron from a high energy composite capture spectrum. The stripped spectrum of Figure 44 was obtained by attributing the activity of channel 168 of the composite spectrum, Figure 43, solely to iron, deducing the amount of iron, relative to

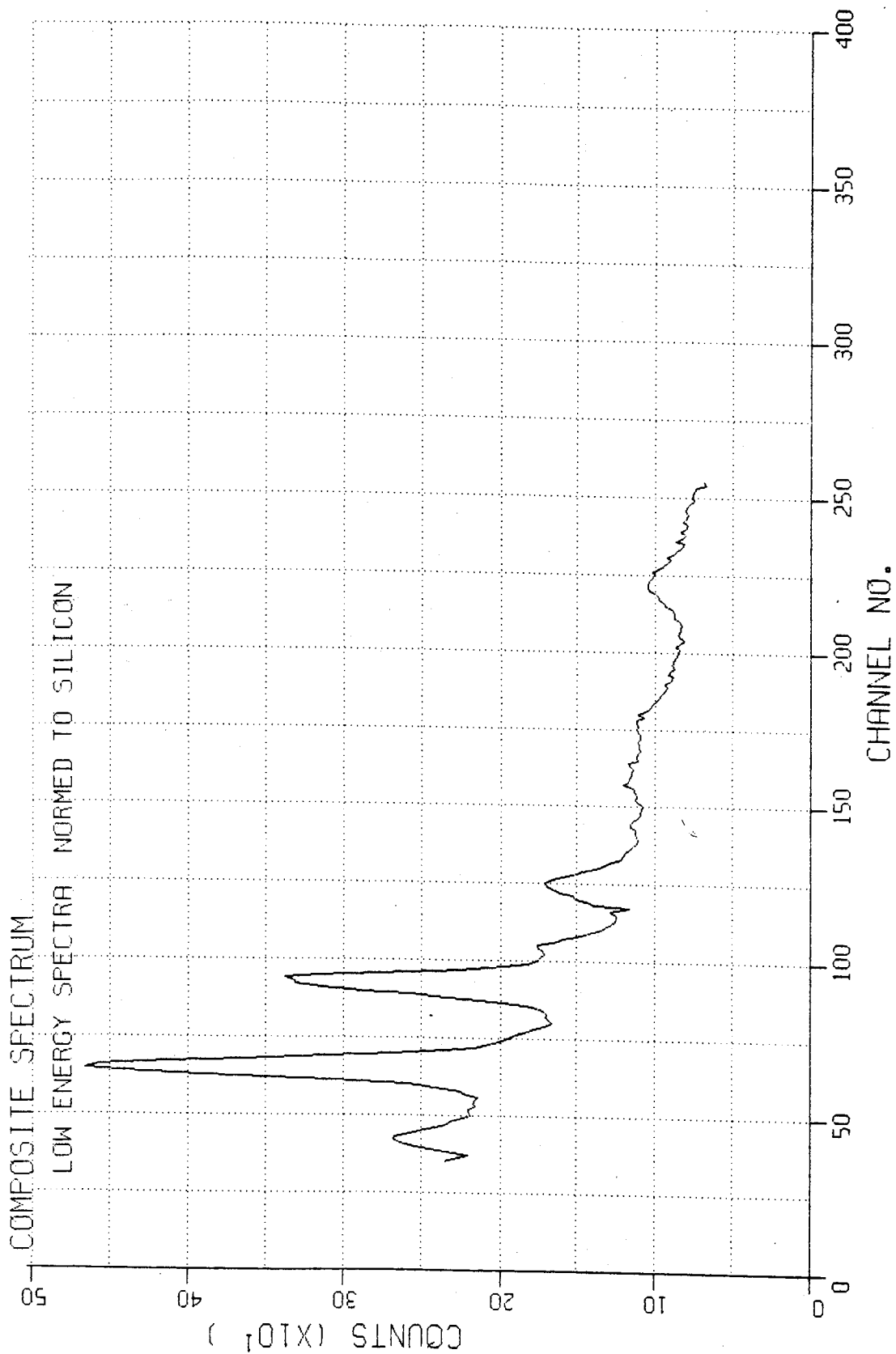


Figure 40 COMPOSITE LOW ENERGY GAMMA RAY SPECTRUM  
ELEMENT MASS: 1gm EACH Mg, Si, Al, Fe

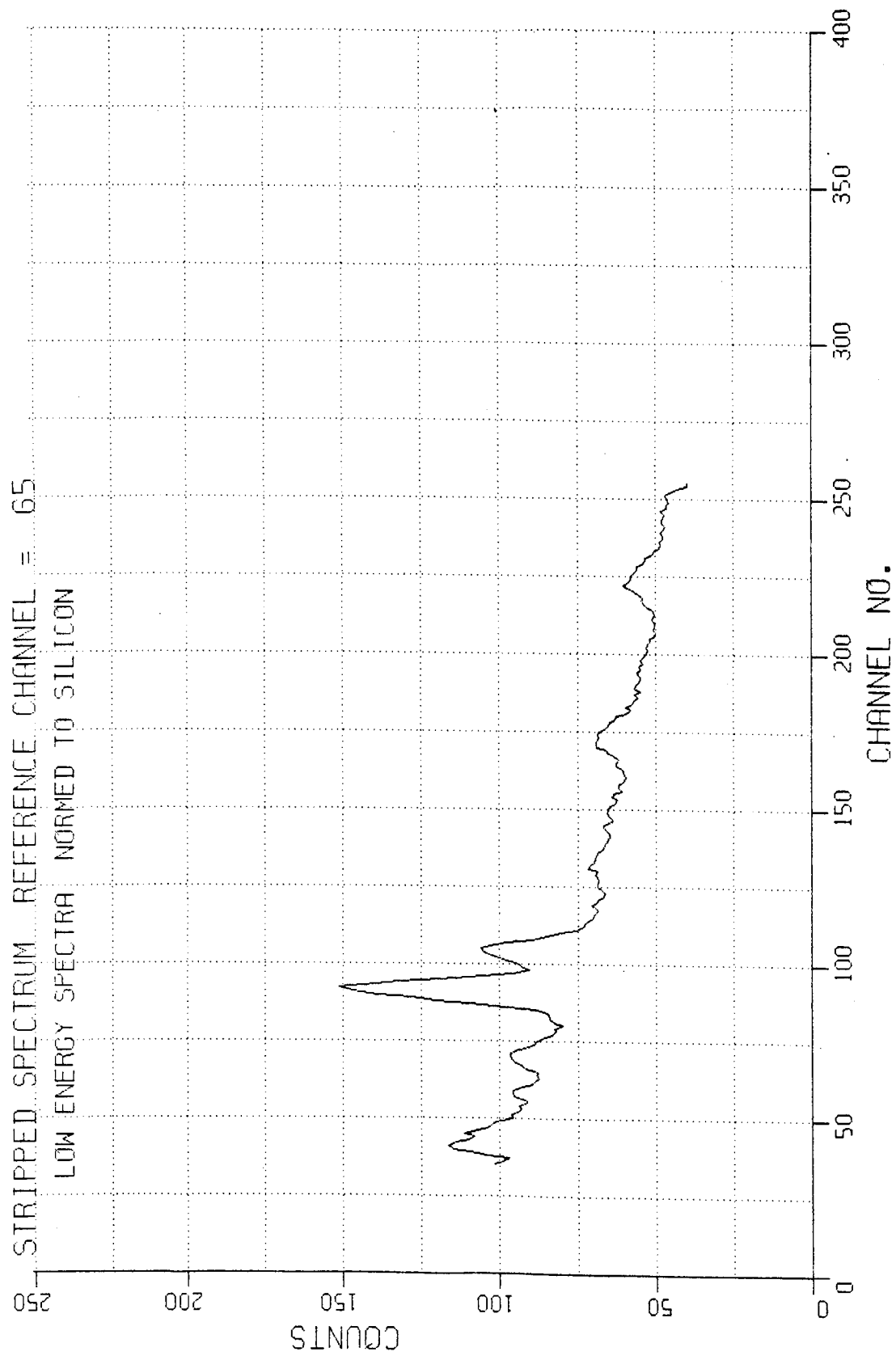


Figure 41 STRIPPED LOW ENERGY SPECTRUM IRON COMPLETELY REMOVED (1gm)

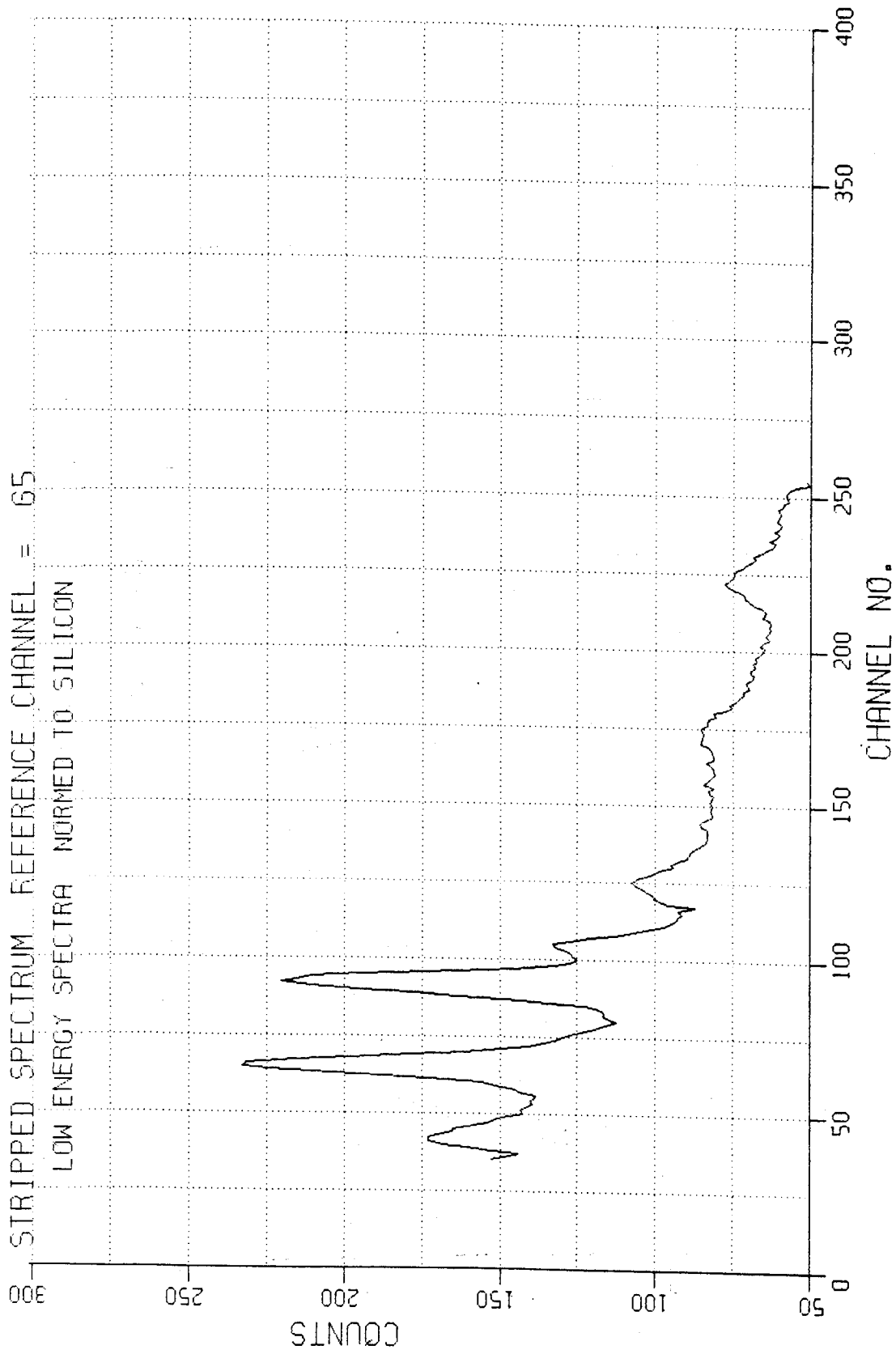


Figure 42 STRIPPED LOW ENERGY SPECTRUM IRON PARTIALLY REMOVED



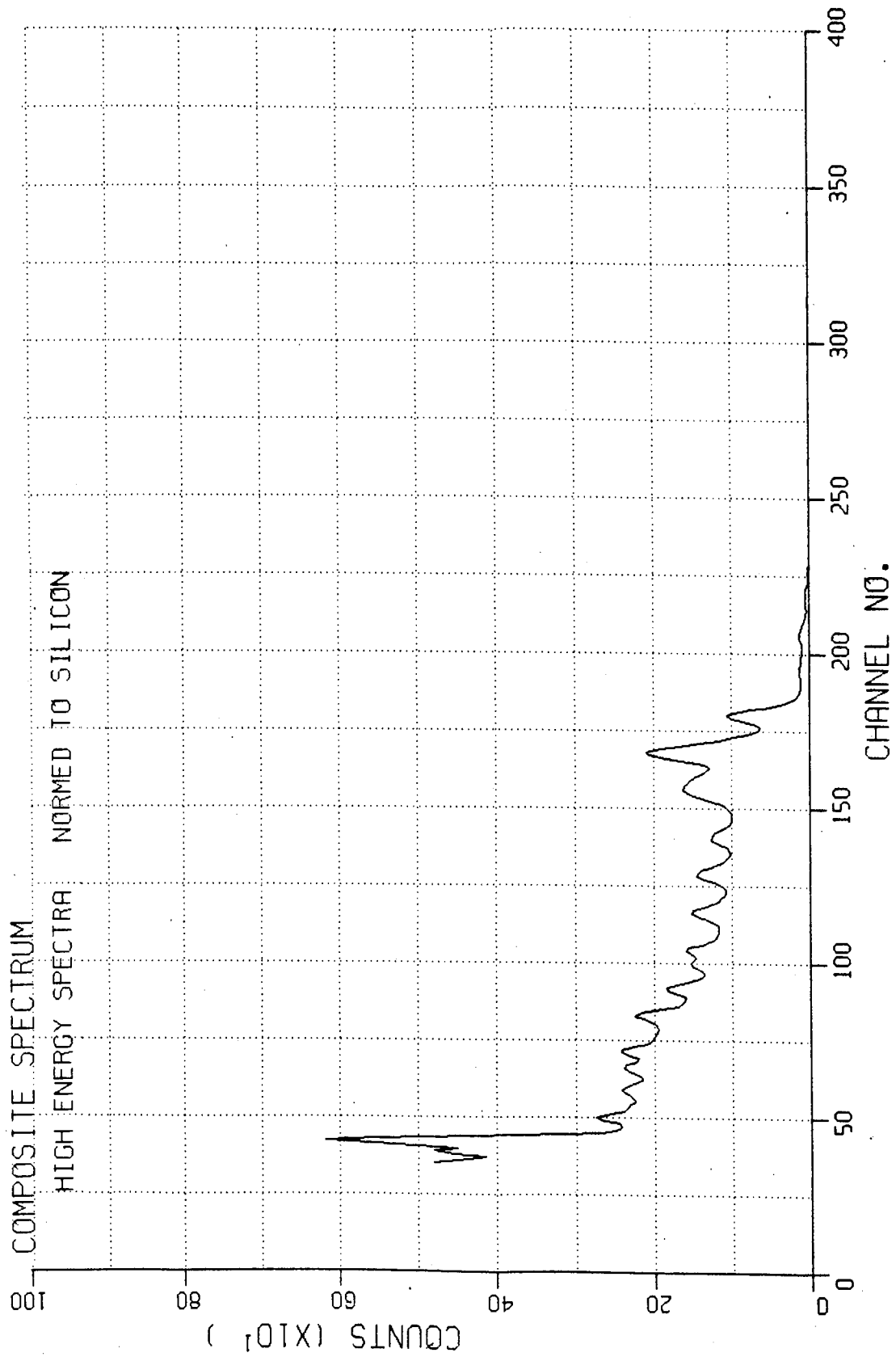


Figure 43 COMPOSITE HIGH ENERGY GAMMA RAY SPECTRUM  
ELEMENT MASS: 1 gm EACH Mg, Si, Al, Fe

STRIPPED SPECTRUM REFERENCE CHANNEL = 168  
 HIGH ENERGY SPECTRA NORMED TO SILICON

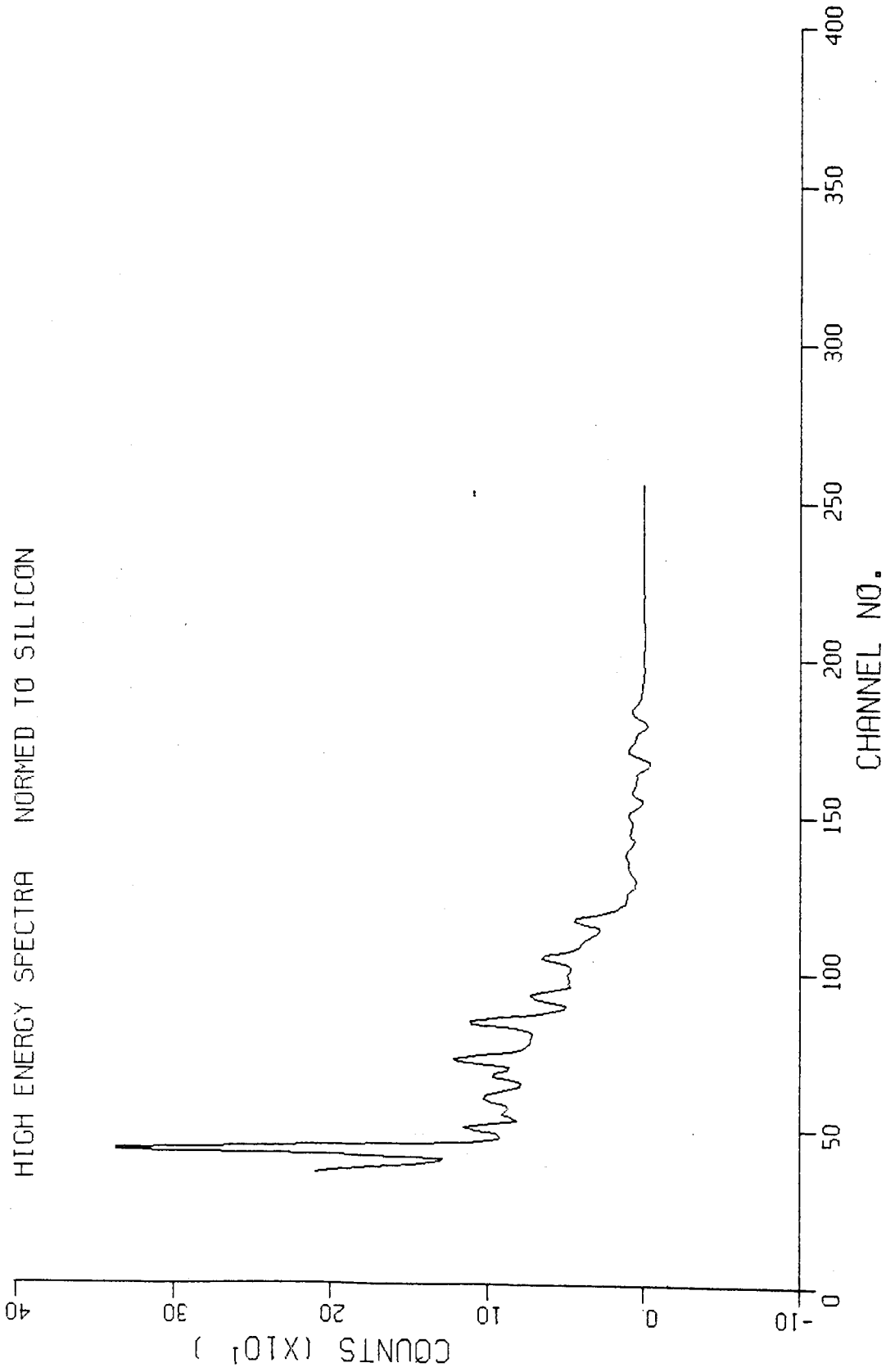


Figure 44 STRIPPED HIGH ENERGY SPECTRUM EXCESS IRON REMOVED

$$(1 \text{ gm } \frac{A_{\text{COMP}}(168)}{A_{\text{Fe}}(168)}) = 1 \frac{220}{188} = 1.17 \text{ gm}$$

STRIPPED SPECTRUM REFERENCE CHANNEL = 166  
 HIGH ENERGY SPECTRA NORMED TO 511 keV

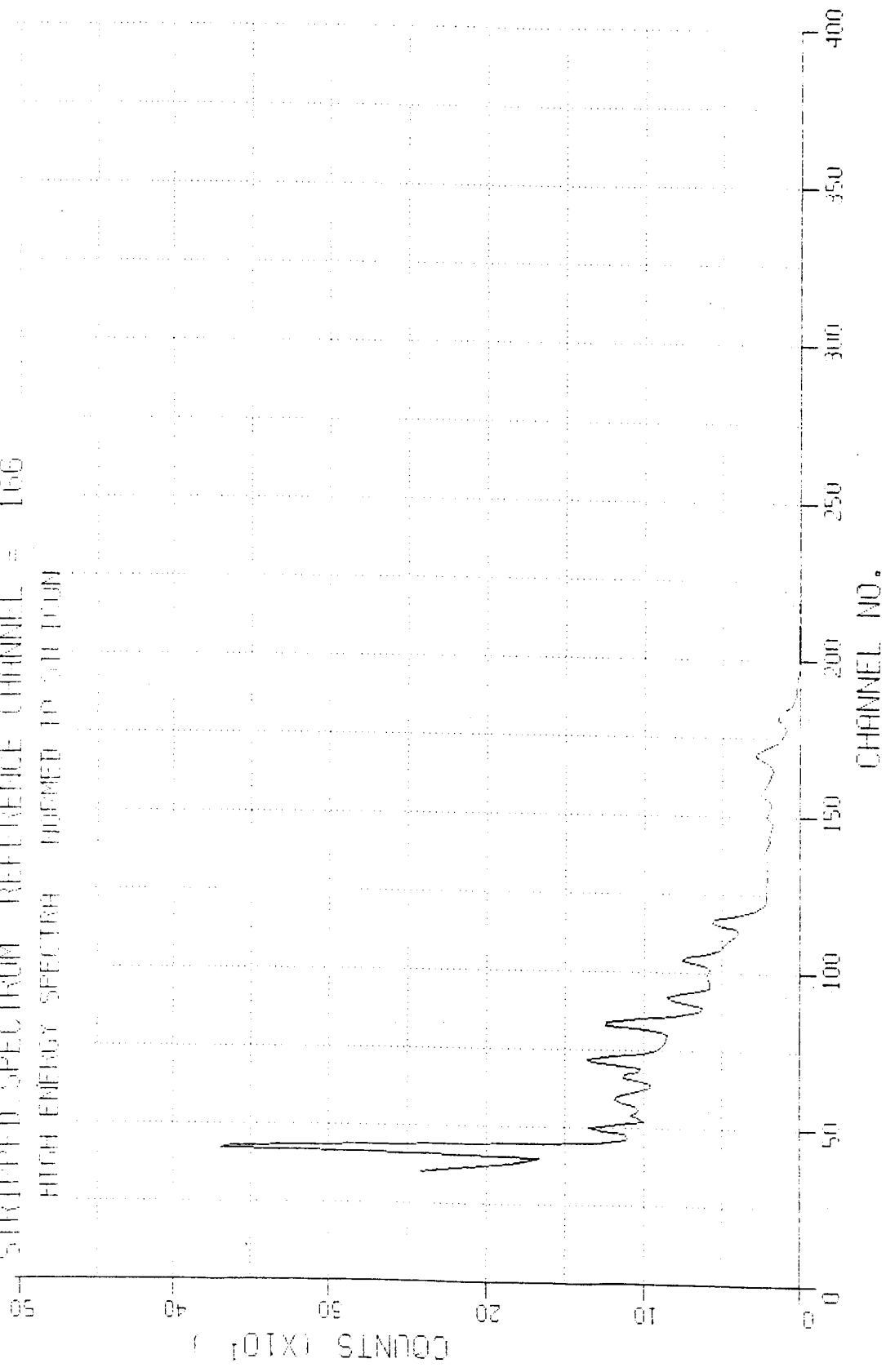


Figure 45 STRIPPED HIGH ENERGY SPECTRUM IRON PARTIALLY REMOVED

$$(1 \text{ gm } \frac{A_{\text{COMP}}(166)}{A_{\text{Fe}}(168)}) = 1 \frac{165}{188} = .88 \text{ gm}$$

one gram, necessary to produce the observed activity in the channel, scaling the one-gram iron spectrum accordingly and subtracting the scaled spectrum from the composite. The same procedure was employed to obtain Figure 45, except that the "wrong" composite channel was chosen to simulate the effect of erraneously determining the peak location. In the first case "too much" iron was subtracted as evidenced by the slightly negative channel activities. Suppressed peak enhancement is not especially dramatic in as much as iron peaks tend to appear above channel 150 whereas peaks of other elements tend to appear from channels 50 to 150. This stripping technique offers possibilities for adaptive element mass estimation wherein by iteration, element mass is estimated and the spectrum is stripped of this element. This adaptive procedure is not included in the model design, but could be fruitfully incorporated into a system in which considerable spectral ambiguity is anticipated.

The measurement and identification procedures are summarized in Figures 46 to 49.

**Post-Calibration** -- Upon completion of the measurement and identification modes, a post-calibration is performed to ascertain condition of the instrumentation, and thereby validate experiment outcomes. The procedure is diagrammed in Figure 30. The procedure is similar to pre-calibration except that background is not measured.

The moderator is removed from around the generator, the MCA is purged and the calibration sample is positioned between generator and detector. Then the "calibration with known sample" procedure is executed as diagrammed in Figure 34 and discussed in a previous section. When all calibration peaks have been found, their locations are compared with their locations at the conclusion of pre-calibration. If the discrepancies between peak channel locations for the several calibration peaks are tolerable, the experiment results are accepted and outputted. Otherwise the operator is signaled that pre- and post-calibrations fail to authenticate and the controller idles until commanded by the operator to terminate or return to pre-calibration.

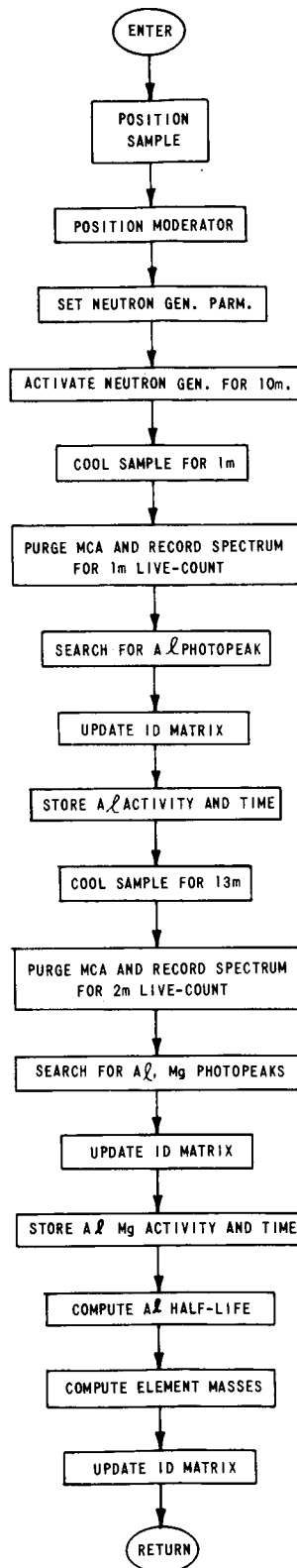


Figure 46 FUNCTIONAL FLOWGRAM FOR THERMAL-CAPTURE PROCEDURE

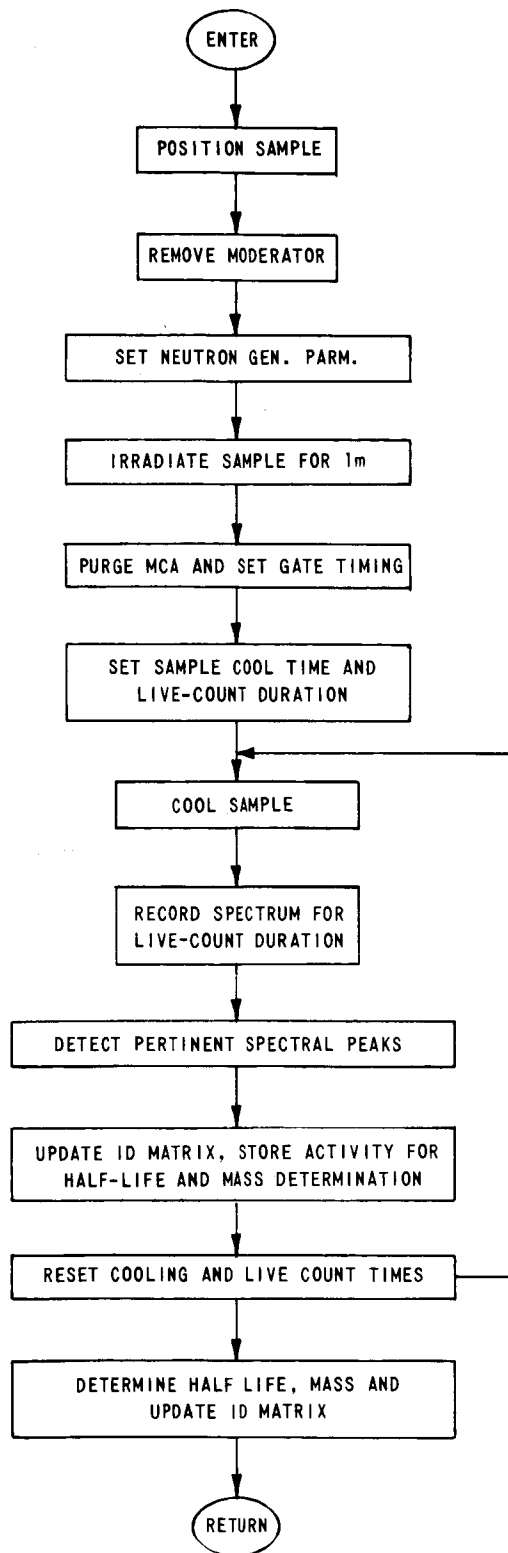


Figure 47 FUNCTIONAL FLOWGRAM FOR FAST-ACTIVATION PROCEDURE

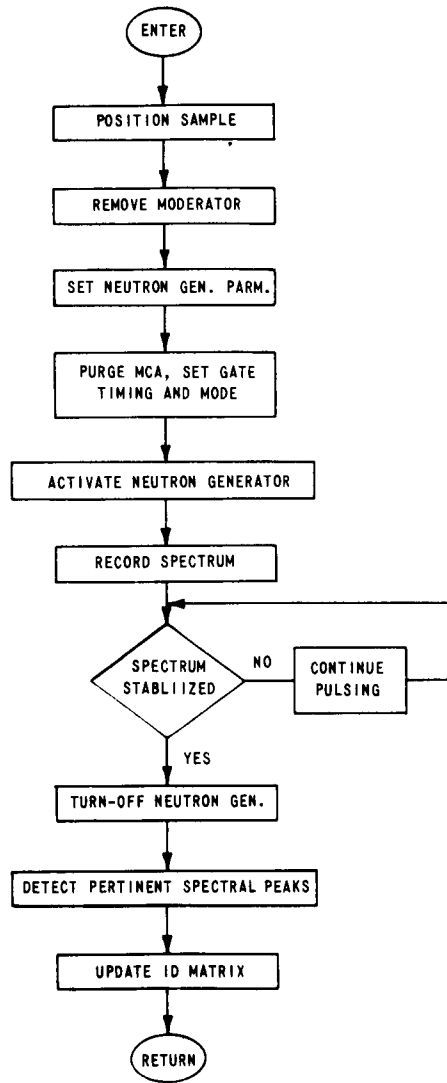


Figure 48 FUNCTIONAL FLOWGRAM OF FAST-PROMPT PROCEDURE

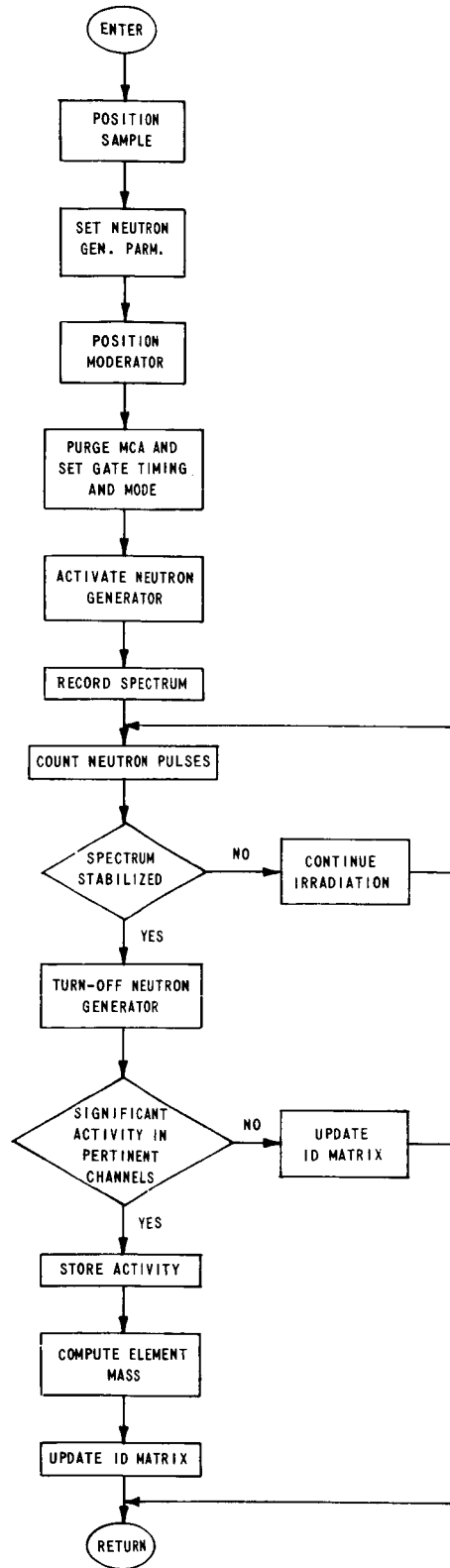


Figure 49 FUNCTIONAL FLOWGRAM FOR THERMAL-ACTIVATION PROCEDURE



Control Computer -- Based upon a brief market survey, two computers were selected as adequate for a laboratory demonstration model of the pulsed neutron excitation experiment. Their characteristics and costs are summarized in Tables X and XI. The factors considered in their selection, other than the obvious factor of low cost, are:

- Computing requirements for the neutron excitation experiment are quite minimal;
- Speed is not important;
- A twenty-four bit word length is desirable, but not necessary, to be compatible with the six decade BCD code of most pulse height analyzers. (Each channel of the pulse height analyzer could be stored in two twelve-bit words and operated upon with double precision arithmetic.);
- 2048 twenty-four bit words of memory, in addition to that required for control software and computing programs, is needed to accommodate four 512-channel reference spectra that may be used. (This memory is included in the computer cost estimates.);
- At least assembly language software should be available to facilitate programming the machine;
- A paper tape reader and keyboard input is considered essential to enter data and programs. In order to generate and modify program tapes and generate hard copy, a paper tape punch and teletype is needed. The Teletype Model 33, included in the cost estimates, provides the above functions at ten characters per second in either direction. Further study may reveal the need for higher speed paper tape input/output. A high speed paper tape reader and punch would cost about \$5000 extra.
- The computer must be capable of checking the status of peripheral equipment and accepting interrupts from them and, clearly, must be able to accept data from the pulse height analyzer.

The two machines described in the tables have the above capabilities.

Table X  
DESCRIPTION OF PDP-8/I COMPUTER

DESIGNATION	PDP-8/I
MANUFACTURER	DIGITAL EQUIPMENT CORPORATION 146 MAIN STREET MAYNARD, MASSACHUSETTS
WORD SIZE	12 BITS
CYCLE TIME	1.5 MICROSECONDS
INPUT/OUTPUT	64 DIFFERENT DEVICES WITH INTERRUPTS AND INTERROGATION

(a) BRIEF DESCRIPTION

BASE PRICE INCLUDING CABINET, 4096 WORD CORE MEMORY, ASR-33 TELEPRINTER (MODEL 33).	\$13,500
EXTRA 12 BIT, 4096 WORD CORE MEMORY WITH NECESSARY CONTROLS.	\$ 5,000
STANDARD SOFTWARE INCLUDES MACRO-8 SYMBOLIC ASSEMBLER, FORTRAN COMPILER, PAL-III ASSEMBLER, SYMBOLIC ON-LINE DEBUGGING PROGRAM, SYMBOLIC TAPE EDITOR, FLOATING POINT PACKAGE, MATHEMATICAL SUBROUTINES INCLUDING DOUBLE PRECISION ARITHMETIC, UTILITY AND MAINTENANCE PROGRAMS. ALL STANDARD SOFTWARE OPERATES WITH THE BASIC 4096 WORD CORE MEMORY.	NO CHARGE
TOTAL	\$18,500

(b) COST BREAKDOWN

Table XI  
DESCRIPTION OF SCC-655 COMPUTER

DESIGNATION	SCC-655
MANUFACTURER	SCIENTIFIC CONTROL CORPORATION 14008 DISTRIBUTION WAY DALLAS, TEXAS
WORD SIZE	24 BITS
CYCLE TIME	1.75 MICROSECONDS
INPUT/OUTPUT	1-64 PRIORITY INTERRUPT CHANNELS

(a) BRIEF DESCRIPTION

CENTRAL PROCESSING UNIT WITH CORE MEMORY ADAPTER AND 4096 WORD MEMORY	\$27,000
ASR-33 TELETYPE (MODEL 33)	\$ 5,500
STANDARD SOFTWARE INCLUDES A SYMBOLIC ASSEMBLER, UTILITY AND MATHEMATICAL SUBROUTINES, FORTRAN, DIAGNOSTIC ROUTINES	NO CHARGE
TOTAL	\$32,500

(b) COST BREAKDOWN

## SUMMARY OF SPACE RESEARCH AREAS SURVEY

This section contains capsule summaries of the experiments considered in the survey task. Investigations of individual experiments address the following:

- definition of the experiment and assessment of scientific interest;
- consideration of instrumentation including detectors and functional and physical characteristics;
- determination of feasibility and suitability of applying adaptive techniques to experiments, considering adaptive sensors, adaptive data compression and adaptable parameters unique to the experiment;
- determination of the feasibility of a laboratory demonstration model of the experimental adaptive system considering particularly availability of signal sources and instrumentation;
- estimation of the physical requirements of an experimental adaptive system with regard to scientific spacecraft payload capability.

By quantifying the results of these investigations, the experiments were rank-ordered and a subset recommended for design of the laboratory demonstration models.

The twelve experiments are divided into three groups according to their application to a planetary, solar, or interplanetary scientific mission. This grouping is not unique but is logical from a system design point of view wherein an adaptive system could be employed to optimize interexperiment performance of scientific spacecraft. However, for the most part, the adaptive systems considered in the survey are of the intraexperiment type, that is, optimization of an individual experiment constituted the design objective.

### Planetary Experiments

The planetary experiments considered are trapped radiation, pulsed neutron excitation analysis, X-ray fluorescence analysis, and magnetic field measurements.

Trapped Radiation -- The study of particles trapped within a planetary magnetic field is of considerable scientific interest because of the insight concerning magnetospheric structure and interplanetary radiation which can be gained thereby. A review of the literature pertaining to particle measurements reveals that many detectors have been arrangements of scintillation, proportional and Geiger-Mueller tubes and their associated electronics. Recently surface

barrier detectors have been utilized to circumvent the use of many detectors to determine parameters of interest and are included in the adaptive radiation experiment to determine particle type (electrons, protons, alphas, deuterons), energy of particles, and scalar and vector flux. Particle discrimination is accomplished by determining the energy loss of the particle in traversing a known thickness of silicon,  $\Delta E/\Delta X$ , and the total energy,  $E$ , of the particle stopped in a series of totally depleted detectors. The simultaneous mass-energy determination for charged particles is amongst state-of-the-art techniques using solid state detectors and earth-bound electronics. Figure 50 depicts a block diagram of the radiation experiment.

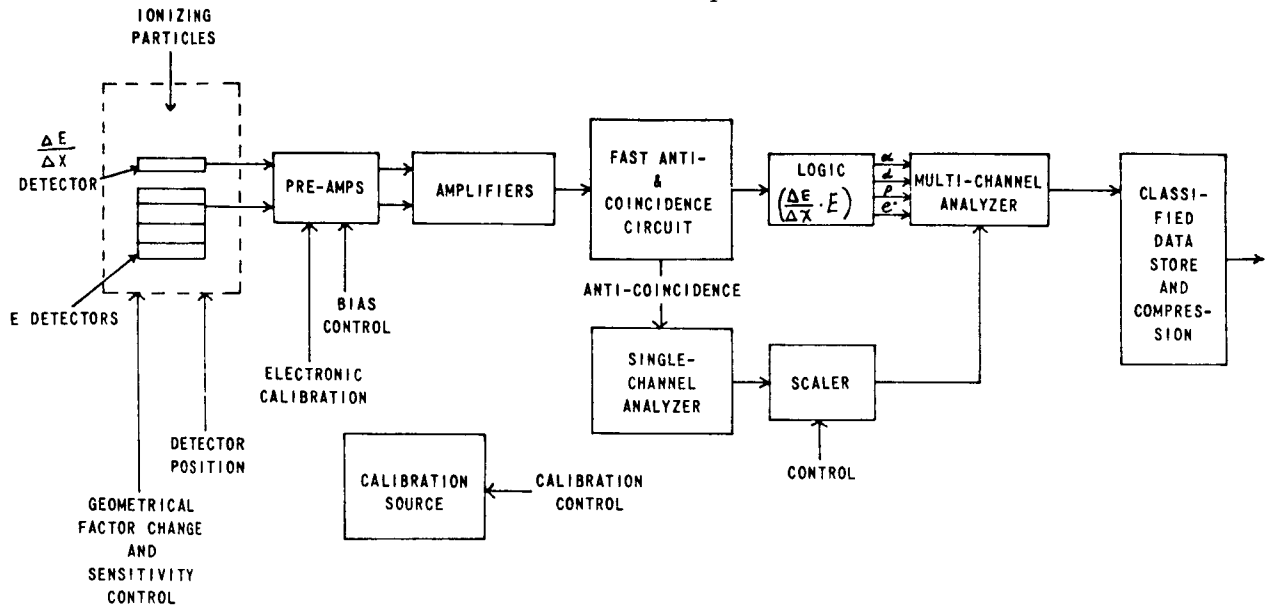


Figure 50 TRAPPED-RADIATION DETECTOR FUNCTIONAL SCHEMATIC-ADAPTIVE CONTROL SIGNALS INDICATED

Adaptive features pertinent to the trapped radiation experiment are:

- adaptation to high particle flux by adaptive positioning of the detector to minimize damage and/or pulse pile-up;
- adaptation to low particle flux by adaptive positioning of the detector to optimize particle reception;
- in-flight particle simulation and detector calibration to measure detector efficiency and malfunctioning;
- adaptive control of detector sensitivity by variation of depletion layer bias; and
- data compression to minimize telemetry requirements.

Feasibility of a laboratory model is contingent upon feasibility of providing sources of high-energy particles.

Pulsed Neutron Excitation Analysis — — Details of this experiment are contained in Sections 2 and 3 of this report.

X-ray Fluorescence Analysis — — X-ray fluorescence analysis (XRFA) is based upon the principle that when an atom is irradiated by a photon in the X-ray region, electrons are ejected from the inner orbits of the atom. Subsequent decay of outer electrons to the vacancies in the inner shells is then accompanied by emission of radiation in the X-ray region. Since the frequencies of these X-rays are characteristic of the atom involved, identification of the constituent elements is possible if the characteristic X-ray spectra can be identified. Laboratory use of XRFA is usually carried out utilizing a crystal spectrometer. The disadvantage of mechanical complexity and the possibility of order overlap in the crystal spectra indicate that this detection system is probably unsuited to a remote adaptive multimode system. Accordingly, lithium drifted silicon and germanium detectors are considered for the adaptive analysis experiment. Silicon detectors are primarily useful for the detection of K radiation for elements up to barium or for the L radiation of heavier elements, whereas germanium is preferable for the detection of radiation up to 120 keV. Figure 51 shows a block diagram of the XRFA experiment.

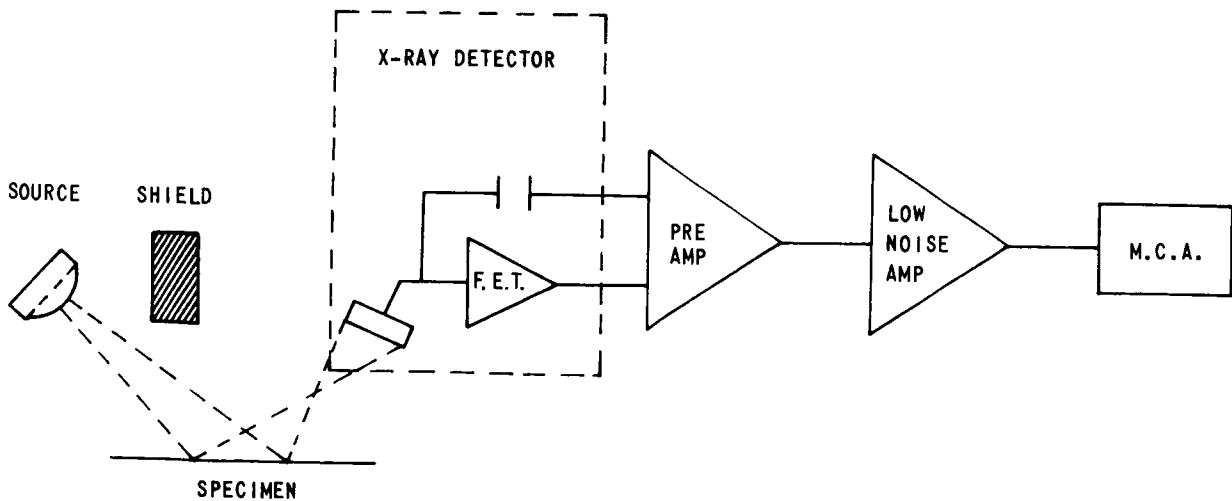


Figure 51 SCHEMATIC ARRANGEMENT FOR XRFA

Functions which the adaptive multimode controller could implement are:

- in flight calibration,
- dynamic resolution adjustment,
- selection of LDS or LDG detector
- characteristic spectral analysis, and
- background correction including attenuation of high background radiation by shielding or source modulation.

A laboratory demonstration model of an adaptive multimode X-ray fluorescence analysis experiment including sources and detectors with thermal-electric cooling is judged feasible using laboratory type instrumentation.

**Magnetic Field Experiment** -- The objective of the magnetic field experiment is to measure the magnitude and direction of planetary and/or interplanetary magnetostatic fields as a function of space-probe position and time. Such measurements are extremely important because despite its weakness, the magnetic field, rather than the electric or gravitation field, controls the motion of charged particles in space. Since the particulate matter ejected from the sun (or solar wind) is ionized, it is apparent that temporal variations in interplanetary fields considerably affect corona phenomena. The earth and other planets inside the orbit of Jupiter are thought to be within the corona of the sun. Hence, localized magnetic field measurements made in the vicinity of other planets and the sun, with a fly-by probe, can increase our knowledge regarding the nature of these bodies and the origin of the earth's magnetic field. Two types of magnetometers appear suitable for interplanetary, i.e., weak field, applications: component and optical pumping types. A combination of component type magnetometers (for direction measurement) and optical pumping magnetometers (for magnitude measurement) is commonly used for space probe magnetic field experiments. However, vector measurements can be made with an optical pumping magnetometer by sequentially applying known triaxial bias fields and component magnetometers can be calibrated to yield accurate magnitudes by using reference fields. Figure 52 shows two types of magnetometers.

Adaptive techniques which could be applied to the magnetometer instrumentation are:

- dynamic range switching,
- asynchronous calibration and sensitivity determination,
- sensor "flipping" to eliminate magnetic bias,
- alteration of processing mode to accommodate partial system malfunction,

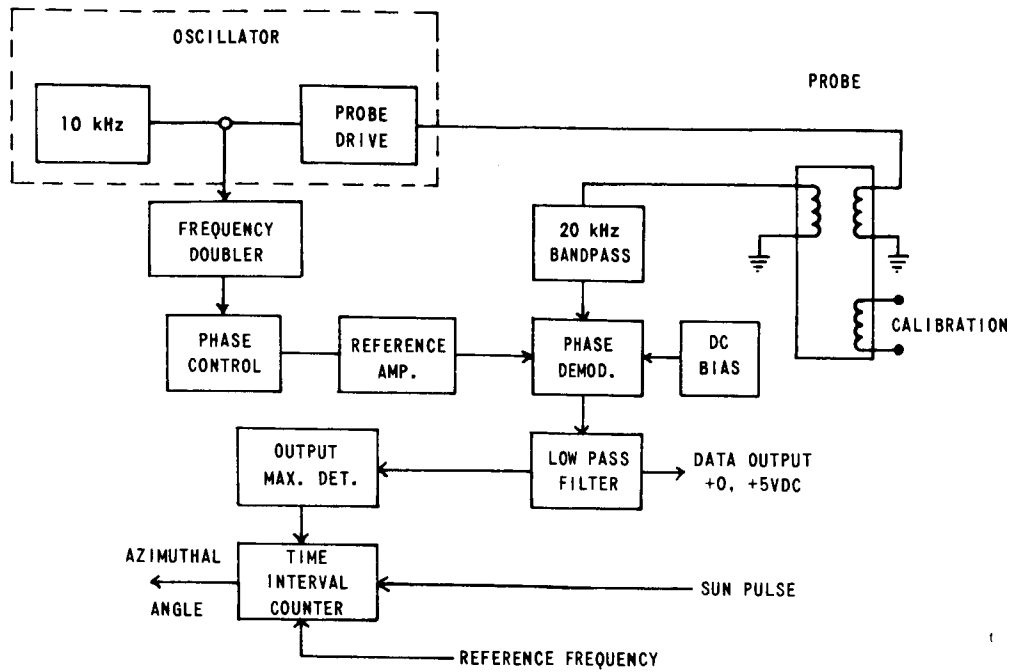


Figure 52(a) MONOAXIAL FLUX-GATE MAGNETOMETER SYSTEM USED ON IMP-1

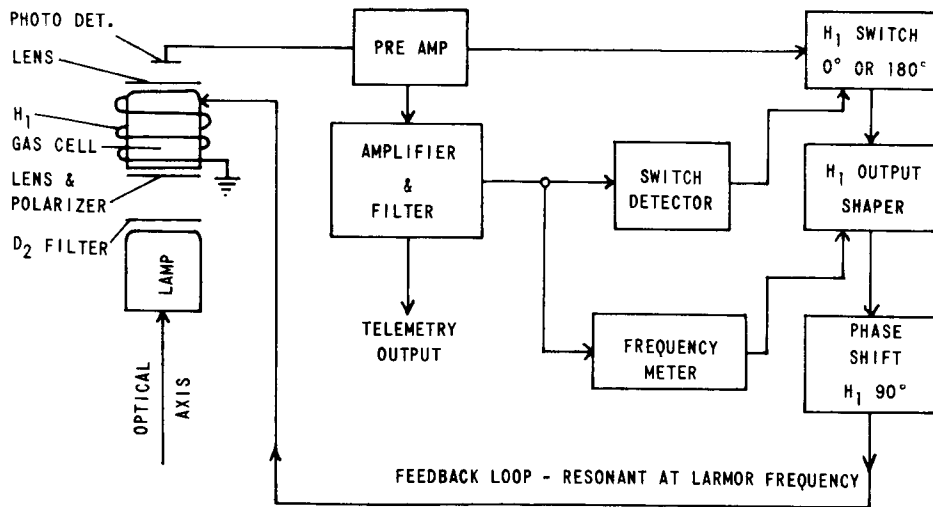


Figure 52(b) RUBIDIUM-VAPOR MAGNETOMETER USED ON IMP-1



- provision of pseudo aspect-reference signals for data demodulation, and
- application of dynamic fields to optimize system sensitivity.

The feasibility of a laboratory model of the adaptive magnetometer is contingent on the feasibility of simulating the requisite magnetic fields. Three alternative approaches exist which can be described as: simulation of a deep space magnetic environment, generation of a nonrealistic field which fully exercises the adaptive system and electronic simulation of the magnetic field sensor outputs. Choice of approach is dependent upon the factors of reality, cost and complexity.

### **Solar Flare Experiments**

Experiments which measure solar protons, cosmic rays, X-rays, and ultraviolet radiation are discussed here.

Geomagnetic phenomena occurring in the Earth's stratosphere are attributed to solar activity. The mechanism held directly responsible for this terrestrial activity, the solar flare, is of considerable scientific interest because of its strong influence upon the earth. Solar flares appear as sudden increases in brightness of an area on the solar surface and are sources of intense electromagnetic and corpuscular radiation. The occurrence of a flare is usually followed by geomagnetic storms caused by high-energy particles being propagated out of the solar atmosphere. In addition to X-rays, ultraviolet radiation, visible light, infrared light, and radio waves, the sun emits charged atomic particles such as protons and electrons. Determination of the directional characteristics, type of particles, particle intensities as function of particle energy, and temporal variations requires a multiparametric detector complex.

**Solar Proton Experiment** -- A relatively simple instrument capable of monitoring the frequency of occurrence and intensity of energetic protons emitted from the sun is available. Designed for inclusion in spacecraft, it could give continuous coverage over at least half a solar cycle and thus provide a crude measure of the proton energy spectrum. The experiment consists of an array of solid state detectors capable of measuring proton intensities in four distinct energy ranges from 1 to 60 MeV. Separate detectors are used for each energy range and a combination of discriminator levels and shielding thickness defines the energy response of each channel. This method permits accurate, absolute flux determination. Figure 53 shows a block diagram of the solar proton experiment.

**Cosmic Ray Experiment** -- The spectra of cosmic rays encompass a range extending in energy from the MeV to the GeV region and in charge from hydrogen through the very heavy nuclei group. For illustration the cosmic ray experiment aboard OGO-E is described and is shown in Figure 54. This experiment is divided into four subsystems which are detectors of high, medium and low energy coupled to an accumulator and readout operation. The integration of simultaneous

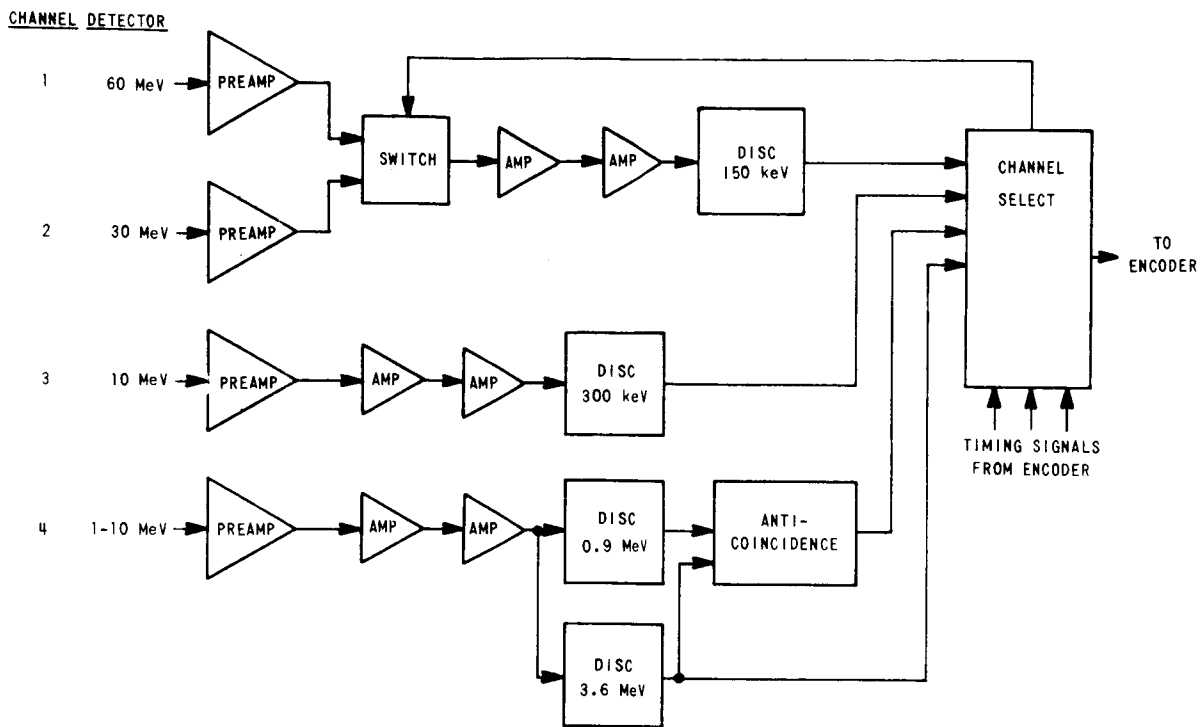


Figure 53 SOLAR PROTON MONITORING EXPERIMENT

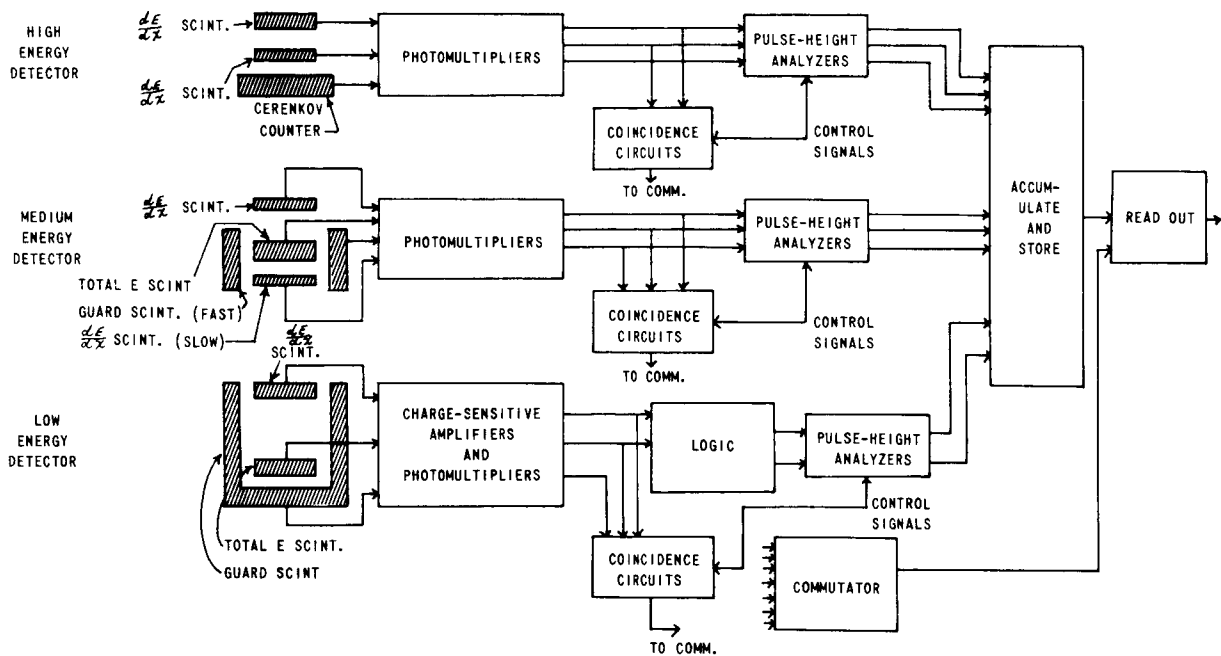


Figure 54 COSMIC-RAY EXPERIMENT

observations by all three detectors is intended to generate an apperception of the production, acceleration and modulation of solar cosmic rays. The high-energy detector is a double scintillator-Cerenkov telescope measuring charge and differential energy spectra over the range between 220 to 1000 MeV per nucleon and integral particle flux above 1000 MeV per nucleon. The rate of ionization loss is determined by two separate scintillation counters and coincidences between the two scintillators define the geometrical acceptance aperture of the telescope. Velocity independent scintillation measurements and Cerenkov-detector pulse heights identify the charge and energy of the incident particle.

The medium energy detector is a scintillator telescope which compares the total energy against the rate of ionization loss. It measures charge and differential energy spectra in the range between 20 to 80 MeV per nucleon, the intergral flux above 80 MeV per nucleon, and the electron spectrum from 1 to 10 MeV.

The low energy detector is composed of two large-area solid-state detectors and a guard scintillator. The guard scintillator reduces the background flux that arises from scattering and nuclear interactions in the spacecraft. Additionally, it detects particles that do not enter the aperture but penetrate the total energy detectors. Charge-sensitive preamplifiers are used with the two solid state detectors. Events occurring in the low energy detectors are analyzed to provide flux and energy information for particles having more energy than 0.4 MeV. This mode of operation is intended primarily for use during periods of very high counting rate that follows solar flares.

**Ultraviolet Experiment** -- The difficulty in obtaining reliable ultraviolet-radiation data during flare activity resides in the facts that: (a) increase in radiation is small compared to the continuous emission from the sun, and (b) the time required to scan the spectrum is long and limits resolution of spectral lines. For illustration the ultraviolet spectrometer designed for OSO-2 which measures solar ultraviolet radiation from 500 Å to 1500 Å is described. The spectrometer, shown in Figure 55, is operated in one of two different modes depending upon whether the spacecraft is stationary or scanning. While the instrument is pointed at the sun's center, a grating is rotated continuously at a rate of one step per 160 milliseconds resulting in a complete scan in 26.67 minutes. On command, the grating is turned at four times fixed scan rate and set to the nearest 0.4 Å; in this mode, the spectrometer becomes a monochromator. Under optimum conditions, a dozen pictures of the sun can be obtained in a period of one hour.

**X-ray Flux Experiment** -- The frequency of flares which emit X-rays, their unpredictability and the rapidity with which they develop require continuous observation over several weeks with time resolution of order one second. The long time duration is mandatory because active regions are a source of soft X-rays and evolve over a period of several days to a few weeks. Pertinent characteristics of solar X-ray emissions are, (a) X-ray flux is cyclic, hence, time dependent, (b) the quiet sun normally does not emit more than  $6 \times 10^{-4}$

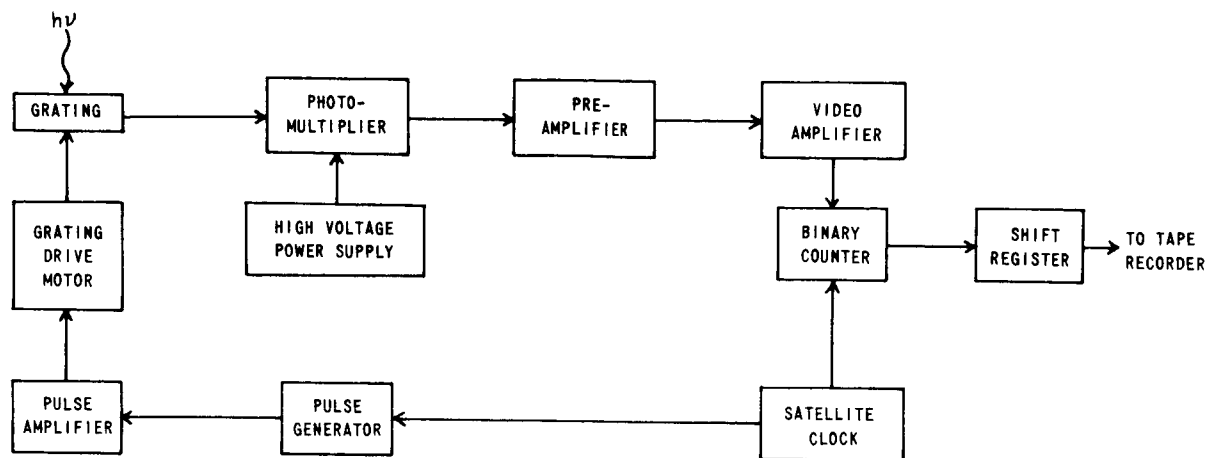


Figure 55 A BLOCK DIAGRAM OF THE UV SPECTROMETER

ergs/cm<sup>2</sup>/s below 8Å, (c) solar activity is usually visible when large X-ray flux is observed below 8Å, and (d) ionospheric effects are detectable when the X-ray flux below 8Å exceeds  $2 \times 10^{-3}$  ergs/cm<sup>2</sup>/s.

An instrument specifically designed to study these properties is the M5 detector. This detector: (1) provides continuous monitoring of the quiescent solar X-ray flux and solar X-ray flare events, (2) obtains information concerning hardening of the X-ray spectrum during X-ray flares, (3) searches for fast time-variations in the X-ray signal from both the quiet and active sun, and (4) studies intensity, spatial distribution, time variations, and energy spectra of electrons in the transition region and in the tail of the earth's magnetosphere.

**Adaptive Techniques** -- Because of similarity among the solar flare experiments, application of certain adaptive techniques is valid for all of these experiments. These include:

- calibration on a periodic and/or dynamic basis,
- data-acquisition mode such as stand-by and continuous, which can be implemented by adaptive control of system thresholds and dynamic ranges,
- data compression by adaptive quantile systems,
- directionality to optimize detection of individual particle types.

Adaptable features peculiar to individual experiments include the following:

- Solar Proton Experiment - The discriminator levels shown can be altered to vary the sensors' energy response in accordance with previously detected outputs by adjustment of detector bias.
- Cosmic Ray Experiment - Sensitivity to particle energy can be controlled by adjustment of bias levels of the solid-state detectors. System sensitivity and energy spectrum location and extent can be varied by adaptively controlling the pulse-height analyzers.
- Ultraviolet Experiment - Two scanning modes are possible with the ultraviolet detector: stationary and slowly-scanning. Choice of mode can be controlled by an adaptive system whose decision, based upon other experimental outcomes, optimizes the type of data acquired.
- X-Ray Flux Experiment - The X-ray detector, previously described, provides dynamic-range capability by discriminator level settings. Dynamic-range expansion or contraction can be executed upon command of an adaptive controller at onset of a flare. Further, the above X-ray detector can be desensitized to electrons by placing a solenoidal magnetic field at the "windows". Hence, two operating modes are possible: detection of X-rays and detection of X-rays and electrons. Appropriate adjustments within the pulse-height analyzer permit either one or both energy spectra to be displayed. System gain can be dynamically controlled by appropriately biasing photo-multiplier tubes.

Laboratory Demonstration Models -- Inasmuch as the instrumentation is available and in many cases has been test-flown, feasibility of laboratory demonstration models is contingent upon being able to provide sources of particles and energy flux of appropriate magnitudes and variability to satisfy the sensors and to exercise the adaptive systems. Many of these sources are either difficult to obtain or unfeasible for a demonstration model. An alternative solution is to simulate electronically, the signals at the output of the sensors for insertion into the following electronics. That is, the detectors could be removed from the instrumentation and replaced by electronically generated signals which duplicate the response of the detectors to the incident particles. In this configuration, the adaptive system would be exercised by preprogrammed electrical signal variations which simulate fluctuations in solar activity.

#### **Interplanetary Experiment**

The interplanetary experiment considered is the measurement of micrometeoroids.

Micrometeorite Experiment -- The purpose of the micrometeorite experiment is to directly measure the physical and dynamic properties of interplanetary dust particles, i.e., those with radii, less than 100 microns and mass less

than  $10^{-6}$  grams. Although numerous measurements of the near-earth micrometeoroid environment have been made by space probes and rockets, the experimental objective in most cases has been limited to evaluation of the hazardous affects of these high velocity particles on spacecraft surfaces. The nature of interplanetary material is of scientific interest for use in determining the formation of the planetary system and the evolution of comets.

Most spacecraft micrometeoroid experiments flown to date have utilized impact, penetration or abrasion type detectors, see Table XII. Of these only the impact detector, exemplified by the piezoelectric transducer or microphone, can be considered to be a scientific instrument. Unfortunately, the impact detector responds to particle momentum,\* hence, it must be used in conjunction with a detector of another type, e.g., velocity tube, Figure 56, if the individual parameters of mass and velocity are to be estimated.

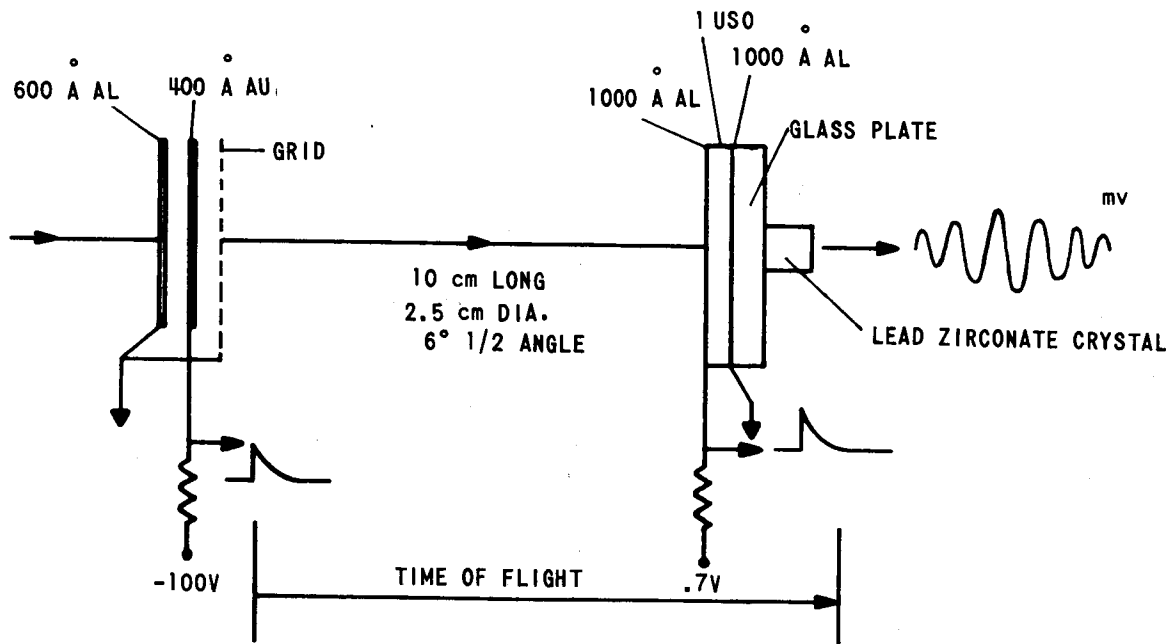


Figure 56 THE OGO-1 MICROMETEOROID SENSOR WHICH DETERMINES PARTICLE MASS AND VELOCITY

Direct measurements of the near-earth dust-particle environment made by microphone-detector equipped space probes, indicate that the impact rate fluctuates by one to two orders of magnitude in times of only a few hours. In addition, there is evidence of encounters with interplanetary streams lasting several hours to a few days, during which time the impact rate increases several orders of magnitude above the long term average. Although the spatial density of particles in interplanetary space may be about  $10^3$  times less than near to earth, similar impact-rate fluctuation can also be expected there. The extreme variability of the micrometeoroid environment makes adaptive techniques attractive, especially on-board data compression in the form of average and peak rate reporting or quantile recording.

\* Detector response to fast particles is proportional to  $mv^n$ ,  $1 \leq n \leq 2$ , in which  $n$  is related to particle speed.

Table XII  
SCIENTIFIC MICROMETEOROID SENSORS

SENSOR	STATUS	OPERATING PRINCIPLE	OUTPUT RESPONSE PROPORTIONAL TO
IMPACT TRANSDUCER, MOMENTUM DETECTOR	FLOWN ON EXPLORERS V-2 AND UP	IMPACT ON PIEZO-ELECTRIC ELEMENT PRODUCES VOLTAGE	$m(v)^n$
LANGLEY MICROPHONE AND SOUNDING BOARD	FLOWN ON EXPLORERS XIII, XVI	" "	$m(v)^n$
PHOTOMULTIPLIERS	FLOWN ON VARIOUS ROCKETS	LIGHT FLASH FROM PENETRATING PARTICLE	$mv^2$
VELOCITY TUBE	FLOWN ON OGO-1	TIME OF FLIGHT BETWEEN FOILS AND IMPACT TRANSDUCER	$v$ AND $m(v)^n$
MARINER CAGE	MARINER C	PIEZOELECTRIC MOMENTUM PLUS CAPACITOR FOR BOARD SIDE	$m(v)^n$
CERAMIC BEAM AND CADMIUM SULFIDE CELLS	QUALIFIED FOR PIQSY	IMPACT TRANSDUCER PLUS AREA EXPOSED TO SUN	$m(v)^n$ AND SIZE
BALLISTIC PENDULUM AND VELOCITY SENSOR	DEVELOPMENTAL (FOR OSO-F REQUIREMENTS)	TIME OF FLIGHT PLUS X-Y DEFLECTION OF MASS VIA ATTACHED LIGHT SOURCE	$v$ AND $m(v)^n$
<p>NOTES: <math>mv</math> = MASS TIMES VELOCITY (MOMENTUM)  <math>mv^2</math> = MASS TIMES VELOCITY SQUARED (ENERGY)  <math>v</math> = VELOCITY  <math>1 \leq n \leq 2</math>, <math>n</math> DEPENDS UPON PARTICLE SPEED</p>			

The relatively unsophisticated micrometeoroid sensors presently available, somewhat mitigate the advantages accruing to an experiment from application of adaptive techniques to the sensors. Hence, application of adaptive data-compression, at least in the immediate future, probably will afford greater gains in micrometeoroid experiment performance than adaptive sensors. Nonetheless, possibilities for applying adaptive techniques to present sensors does exist. These include:

- scale factor of the velocity meter could be adaptively varied to increase accuracy and precision;
- clock frequency could be adaptively selected, depending upon particle bearing, to keep the frequency counter output within range;
- threshold system within a momentum-type detector could be adaptively adjusted to maintain nearly constant pulse-rate input to the data-processing electronics.

Because instrumentation exists, the main consideration in a laboratory demonstration model is the need for a micrometeoroid accelerator to produce hypervelocity particles for calibration and test purposes. The accelerator must be variable to dynamically exercise the adaptive experiment. Such accelerators exist but their use would necessitate locating the demonstration model at the accelerator site and present some attendant inconveniences. An alternative approach is to generate electronically the signals which the actual sensors would output. The adaptive system would then be exercised by programmed variation of the electronic signals over ranges which encompass the variations expected in interplanetary space.

#### **Rank-Scoring of Experiments**

Based upon the results of the survey analyses, experiments were rank-ordered according to their suitability for adaptive control and feasibility of constructing a laboratory demonstration model. The rank-ordering was performed by a) ascribing to the several attributes of each experiment, numerical values which reflect the relative importance, suitability or feasibility of the associated attribute; b) assigning to each attribute a numerical weight which reflects the relative importance of that attribute to the program objective; and c) multiplying the two matrices, constructed from the above sets of numbers, to obtain a third matrix which numerically scores the experiments according to their overall suitability for adaptation and feasibility of laboratory design. The numerical values employed in this analysis are subjective and were supplied by the CAL project staff. The rank scoring of experiments is shown in Table XIII. According to the criteria employed in this analysis, the most suitable experiments for detail design are, in decreasing order, neutron excitation and X-ray fluorescence, solar ultraviolet and X-rays, and trapped electrons and alphas.



Table XIII  
**RANK-SCORING OF EXPERIMENTS**  
**ATTRIBUTE MATRIX**

ATTRIBUTE EXPERIMENT	SUITABILITY				LABORATORY MODEL FEASIBILITY				RANK SCORE
	SCIENTIFIC INTEREST	SUITABILITY FOR ADAPTATION	FEASIBILITY OF ADAPTING SENSORS	FEASIBILITY OF DATA COMPRESSION	CURRENTLY FLYABLE	AVAILABILITY OF REAL SOURCES	FEASIBILITY OF SIMULATING SOURCES	AVAILABILITY OF SPACE-QUALIFIED INSTRUMENTATION	
TRAPPED RADIATION	3	3	3	3	2	2	2	2	46
	3	3	3	3	2	1	2	2	42
	2	3	3	3	2	2	2	2	40
	2	3	3	3	2	1	2	2	40
ACTIVATION ANALYSIS	4	4	3	2	1	4	4	3	61
X-RAY FLUORESCENCE	4	2	3	2	1	4	4	2	54
MAGNETOMETER	3	2	2	2	3	1	3	3	38
SOLAR FLARES	3	3	3	3	3	1	2	3	44
	3	3	3	3	3	1	2	3	44
	3	3	3	3	3	2	2	3	52
	3	3	3	3	3	2	2	3	52
MICROMETEORITES	3	2	1	3	3	1	3	3	35

=

X

**WEIGHT MATRIX**

WEIGHT	2	3	3	2	1	4	2	1
--------	---	---	---	---	---	---	---	---

### Suitability of Neutron Excitation for AMS

The neutron excitation experiment is well suited to application of an adaptive multi-mode system (AMS) because it provides significant opportunity for data processing/reduction and adaptation to environmental factors. Advantages accruing to the experiment from application of adaptive control are: 1) the ability to cope with unforeseen environments in the guise of background activity and intervening media; and 2) the large reduction in data transmission time and capacity resulting from nearly complete onboard data processing. In addition, the onboard adaptive controller can monitor and modify experimental procedures eliminating the need for assistance, i.e., long earth-originated sensor command and control delays.

The fundamental functions of an adaptive system, i.e., estimation, and decision and modification, are exemplified in the neutron excitation experiment as:

- Estimation of background activity, presence of thermalizing medium, presence of saturating elements.
- Decisions regarding significance of the background, e.g. go-no-go, effect of thermalizing medium, and effect of dominant element upon detection of other elements.
- Modification to accommodate background to alter techniques and measurement durations, and to apply spectrum stripping techniques.

Data compression within the neutron excitation experiment is especially fruitful. The spectra collected by the instrumentation represent of the order of sixty thousand bits of data. In the absence of data compression this entire data base would necessarily be transmitted to earth via the spacecraft telemetry system. However by providing data compression capability in the form of onboard processing, the transmission load can be reduced to a few hundred bits or less.

## RESULTS AND RECOMMENDATIONS

### Results

The long term objective of this study is application of adaptive multimode systems research to future scientific spacecraft instrumentation. The specific objective of the contract was the design of a laboratory demonstration model of an experiment which demonstrates the feasibility of applying this concept. To satisfy these objectives, a laboratory model of a neutron excitation experiment was designed which would autonomously calibrate sensors, take measurements, process data, estimate critical parameters, and adapt the sensor system for optimum results in the face of a hostile environment. The principal results of the research performed in this study are:

- designation of a set of scientific spacecraft experiments amenable to application of adaptive multimode control;
- delineation of parameters, unique to these experiments, which are suitable for adaptation; and
- design of a laboratory model of a neutron excitation experiment which exhibits adaptive multimode behavior.

### Recommendations

It is recommended that the present adaptive multimode research program be extended to include more general and significant adaptive control applications than current ad hoc procedures now in use and under investigation. That is, the framework within which the present problem is cast should be expanded so the techniques of optimal adaptive control can be brought to bear. Specific questions which an expanded study should address are:

- Interpretation of adaptivity in the context of unmanned spacecraft experiments.
- Criteria for optimality in conducting a series of experiments.
- Methods for characterizing the adaptive experiment management problem.
- Description of experiment-control decision processes and mechanizations of adaptivity.
- Development of programs to verify the synthesized experiment control techniques.

Adaptivity in the spacecraft context could be interpreted as describing the extent to which experiment operation is made efficient and information is gathered in spite of unexpected events. Unpredictable factors which make adaptation desirable both from the viewpoints of efficiency and information gained are:

- unexpected experimental results;
- component or subsystem failure;
- unexpected environmental conditions effecting;
  - a) expected survival time of spacecraft,
  - b) power consumption,
  - c) capability for performance of specific experiments, and
- measurement noise or errors.

Criteria for optimality upon which an adaptive controller could be based, stem from very broad goals defined for the spacecraft by the cognizant agency. These goals might be economic, political, military, scientific, or more likely a combination of these. Nonetheless, it would appear feasible to quantify both the value of benefit of the possible actions designed into the spacecraft to meet these goals and the cost of taking such action. Benefit could be associated with either operation of an experiment regardless of its outcome or the occurrence of particular experiment outcomes. Cost for purposes of adaptive experiment control could be associated with energy, time, material, or computing capacity. Benefit/cost ratio, or some function thereof, could then be defined as an index of performance. Assuming the definition of a performance index (PI) the experiment complex would be modeled in terms of the PI. Thereupon, a control algorithm could be synthesized to dynamically, i.e., adaptively, optimize the index of performance. Finally, the synthesized adaptive controller could be studied through control system analysis and simulation techniques. Such studies would provide answers to questions of system stability, sensitivity, and responsiveness to changing conditions.

## REFERENCES

1. J.A. Waggoner and R.J. Knox, Elemental Analysis Using Neutron Inelastic Scattering, UCRL-14654-T, 1965.
2. R.L. Caldwell, W.R. Mills, et al., Combination Neutron Experiment for Remote Analysis, Science Vol. 151, No. 3721, pp 457-465, 1966.
3. T.H. Braid, Neutron-Capture Rays from Various Elements Physical Review, Vol. 102, No. 4 1956, p 1109-1123.
4. R.C. Greenwood, et al., Prompt Gamma Rays from Radiative Capture of Thermal Neutron, IIT Research Institute Report 1193-54, 1965, Vol. 1,2.
5. J.M. Freeman, Gamma Radiation from Neutron Inelastic Scattering, p 1559-1600, Part II, Experiments and Theory Fast Neutron Physics.
6. Texas A&MU University - Activation Research Laboratory.  
An Investigation of Computer-Coupled Automatic Remote Activation Analysis for a Lunar Surface Analysis, 1965.
7. A.E. Metzger TR-32-286 JPL.  
Some Calculations Bearing on Use of Neutron Activation for Remote Composition Analysis, 1962.
8. R.L. Heath, Detector Efficiency, Appendix II, Vol. 1, Scintillation Spectrometry.